

**UCSF**

**UC San Francisco Electronic Theses and Dissertations**

**Title**

Control of Gene Expression Noise in the Pheromone Response Pathway in *Saccharomyces cerevisiae*

**Permalink**

<https://escholarship.org/uc/item/0xc6895c>

**Author**

McCullagh, Emma

**Publication Date**

2010

Peer reviewed|Thesis/dissertation

Control of Gene Expression Noise in the Pheromone Response  
Pathway in *Saccharomyces cerevisiae*

by

Emma McCullagh

DISSERTATION

Submitted in partial satisfaction of the requirements for the degree of

DOCTOR OF PHILOSOPHY

in

Biochemistry and Biophysics

in the

GRADUATE DIVISION

Copyright 2010  
by  
Emma McCullagh

## Acknowledgments

I would like to thank my advisors Hiten Madhani and Hana El-Samad for their guidance, patience, enthusiasm and their confidence in me. Specifically, I would like to thank Hiten for allowing a fiercely independent student some autonomy, while providing direction when needed and/or warranted. I am grateful to Hana for her words of encouragement and for being generous with her time when I needed it.

I am indebted to Madhani lab members past and present for all of the scientific help and great times in and out of the lab. To the Weissman and El-Samad labs, who understand the trials and tribulations of working with the *Isr2*, thanks for the support and the late night conversations at the flow cytometers. To the Cox lab, of which I consider myself an honorary member, thanks for the frequent pick-me-ups!

I am lucky enough to have fabulous friends. They know how to have a great time and have been beyond patient with me and my crazy graduate student schedule. A huge THANKS and hugs to my Sunday dinner crew and my Delaware girls. Love you guys!

To my parents, Rosa and Peter, and siblings, Martin, Nuala and Ellen, thanks for keeping me grounded, encouraging me when I needed it and listening to me vent endlessly. I love you all. Shmoo!

Chapter 2 of this thesis is reprinted largely as it appears in press at *Nature Cell Biology*. The majority of the work in this chapter was carried out by Emma McCullagh. Anupama Seshan performed the mating assay. Hana El-Samad and Hiten Madhani supervised the research.

Chapter 3 of this thesis is reprinted largely as it appears in the following commentary in *Nature Chemical Biology*:

**McCullagh E, Farlow J, Fuller C, Girard J, Lipinski-Kruszka J, Lu D, Noriega T, Rollins G, Spitzer R, Todhunter M, El-Samad H** 2009 Not all quiet on the noise front *Nat Chem Biol* Oct;5(10):699-704.

Emma McCullagh and Hana El-Samad developed the reading list and directed discussions for the mini-course from which this commentary emerged. Emma McCullagh and Hana El-Samad wrote sections of and edited the manuscript as well as designed the figures. Justin Farlow, Christopher Fuller, Juliet Girard, Joanna Lipinski-Kruszka, Dan Lu, Thomas Noriega, Geoffrey Rollins, Russell Spitzer and Michael Todhunter participated in the mini-course and wrote sections of the manuscript.

The work performed by Emma McCullagh in these studies is comparable to a standard dissertation.

# Control of Gene Expression Noise in the Pheromone Response Pathway in *Saccharomyces cerevisiae*

## Abstract

Cells must integrate signals from their environment and respond accurately in order to grow and divide properly. However, the chemical reactions within single cells do not occur with deterministic certainty. Rather, they occur with a probability due, in part, to the abundance of molecular components and their rates of synthesis and degradation. Therefore, while an entire population of cells may respond appropriately to environmental cues, single cells may vary wildly in their output responses. This phenomenon is called biological noise, and increasingly has been reported to be an important determinant for population heterogeneity, fitness, and development. Although biological noise has been characterized in a variety of systems and cellular pathways, mechanisms that regulate cell-to-cell variability remain poorly understood. In this work, we investigated the role of biological noise in the transcriptional output of the mating pathway, a canonical MAP kinase pathway in *S. cerevisiae*. We identified a role in noise suppression for Dig1, a negative regulator of the transcription factor Ste12. The removal of Dig1 causes an increase in intrinsic and extrinsic noise in the expression of Ste12 target genes. In conjunction, Dig1 inhibits long-range interactions between Ste12 target genes *in vivo*. Finally, we demonstrate a link

between fitness defects and the increased gene expression noise in *dig1Δ* cell populations. These studies suggest that gene expression noise is an evolvable trait and that, when necessary, mechanisms can arise to modulate cell-to-cell variability.

## Table of Contents

|                   |  |      |
|-------------------|--|------|
| <b>Preface</b>    | Title Page   | i    |
|                   | Acknowledgements   | iii  |
|                   | Abstract   | v    |
|                   | Table of contents  | vii  |
|                   | List of figures and tables   | viii |
| <b>Chapter 1</b>  | Introduction   | 1    |
| <b>Chapter 2</b>  | Coordinate control of gene expression noise and interchromosomal interactions in a MAPK pathway  | 11   |
| <b>Chapter 3</b>  | Not all quiet on the noise front   | 88   |
| <b>Appendix A</b> | A genetic approach to understanding the mechanism of Ste12-focus formation in <i>dig1Δ</i> cells | 114  |



## List of figures and tables

|                   |                            |     |
|-------------------|----------------------------|-----|
| <b>Chapter 2</b>  | Figure 1 a-d               | 38  |
|                   | Figure 1 e                 | 39  |
|                   | Figure 2                   | 41  |
|                   | Figure 3                   | 43  |
|                   | Figure 4                   | 45  |
|                   | Figure 5 a                 | 47  |
|                   | Figure 5 b-d               | 48  |
|                   | Figure 6 a,b               | 50  |
|                   | Figure 6 c,d               | 51  |
|                   | Figure 7 a                 | 53  |
|                   | Figure 7 c-e               | 54  |
|                   | Figure 8 a                 | 56  |
|                   | Figure 8 b,c               | 57  |
|                   | Supplementary Figure 1 a,b | 59  |
|                   | Supplementary Figure 1 c,d | 60  |
|                   | Supplementary Figure 2     | 62  |
|                   | Supplementary Figure 3     | 64  |
|                   | Supplementary Figure 4 a,b | 66  |
|                   | Supplementary Figure 4 c-e | 67  |
|                   | Supplementary Figure 5 a   | 69  |
|                   | Supplementary Figure 5 b,c | 70  |
|                   | Supplementary Figure 6     | 72  |
|                   | Supplementary Figure 7 a   | 74  |
|                   | Supplementary Figure 7 b   | 75  |
|                   | Supplementary Figure 8     | 77  |
|                   | Supplementary Table 1      | 79  |
|                   | Supplementary Table 2      | 85  |
| <b>Chapter 3</b>  | Figure 1                   | 108 |
|                   | Figure 2                   | 110 |
|                   | Figure 3                   | 112 |
| <b>Appendix A</b> | Figure 1                   | 118 |
|                   | Figure 2                   | 120 |
|                   | Figure 3 a                 | 122 |
|                   | Figure 3 b                 | 123 |
|                   | Table 1                    | 125 |

# **CHAPTER 1**

## **Introduction**

Evidence for non-genetic individuality in cellular behaviors was reported in early studies of bacterial persistence during antibiotic treatment (1),  $\lambda$  phage burst size (2) and bacterial chemotactic behavior (3). Such phenotypic variability within a population has been termed “noise” and is thought to arise, in part, due to stochastic fluctuations in molecular reactions. Cellular reactions are probabilistic in nature. They involve discrete numbers of molecules and many depend on the rate of diffusion to bring reactant species together in space. Therefore, it is not surprising that fluctuations arise in the molecular input-output relationships of cellular processes. These fluctuations have been attributed to small numbers of molecules present in the cell, as well as probabilistic synthesis, degradation and catalysis/reaction rates (4-9).

### The regime of small numbers

Fluctuations in the average output of a process are greater when the average is small. Intuitively, we can think of the process of rolling a single fair die to understand why stochastic fluctuations have larger effects when the mean is small. Whether rolling a die once or 100 times, the expected value of the average die roll is  $\frac{1+2+3+4+5+6}{6} = 3.5$ . Since it is impossible to get 3.5 in a single roll, the value of one roll will be far from the expected value. However, in the case of 100 rolls, the average of all throws is likely to be close to the expected value. As the number of rolls increases, the average value of the rolls approaches the expected value of 3.5. In probability theory, this is called the law of large numbers. Many biological processes operate in the realm of small

numbers since both mRNA and proteins can be present at a few copies per cell (10, 11). Consequently, stochastic fluctuations in levels or activities of molecules within these processes might be expected to significantly affect pathway output. Indeed, experimental and theoretical evidence suggest that noise in biological systems does arise, in part, from small numbers of molecules (4-9, 12-14).

### Noise in gene expression

There has been great interest in recent years in understanding the origins of noise in gene expression as well as the mechanisms by which it is controlled. The development of a dual-reporter assay that decomposes gene expression noise into intrinsic and extrinsic components has aided in the identification of the origins of noise within this process (15). In this method, identical promoters are used to drive the expression of distinguishable fluorescent proteins in the same cell and measurements of the expression of each reporter gene are made at the single-cell level (15). The uncorrelated variation in expression of these two genes has been termed intrinsic noise and is thought to reflect stochastic fluctuations in the process of gene expression itself. In contrast, extrinsic noise is defined as the correlated variation in expression of the two genes and has been suggested to measure cell-to-cell variability in the global cellular state.

Simple models of prokaryotic gene expression account for rates of transcription, translation and degradation of mRNA and protein species and suggest that intrinsic noise arises due to small numbers of molecules produced by these processes (4, 5, 7, 9, 14). Specifically, these models predict that both

the rate of transcription and the translational burst size (the number of proteins produced from a single mRNA molecule) are important for determining intrinsic noise. Experimental evidence in *B. subtilis* supports the notion that increasing the translational efficiency, or burst size, results in increased intrinsic noise (5).

Intrinsic gene expression noise has also been studied in eukaryotic systems. As predicted from prokaryotic models, proteome-wide studies illustrate that, in general, intrinsic gene expression noise in eukaryotes is greater when the mean expression is small (12, 13). Using a two-reporter system, Raser and O'Shea investigated the source(s) of intrinsic gene expression noise for three genes in *S. cerevisiae*. The intrinsic noise of two genes, *GAL1* and *PHO84*, behaves as predicted by models of prokaryotic gene expression. In contrast, intrinsic noise in *PHO5* expression appears to originate from transcription-independent chromatin remodeling during promoter activation. By using mutants that affect the rate of chromatin remodeling at the *PHO5* promoter, the authors were able to modulate the levels of intrinsic noise in *PHO5* expression. They conclude that promoter activation through chromatin remodeling may be an important source of intrinsic noise for some eukaryotic genes.

Extrinsic gene expression noise is thought to arise in general cellular processes that affect the expression of all genes. However, the origins of extrinsic noise are not well understood. Studies in yeast have established that cell cycle-dependent differences in cells contribute significantly to extrinsic gene expression noise, although the molecular nature of this effect has not been parsed (12, 16, 17). Additionally, it has been suggested, but not proven, that

variable levels of general cellular factors such as RNA polymerase or ribosomes also give rise to extrinsic gene expression noise (18) as they impact the general expression capacity of the cell.

### Biological impact of noise

Phenotypic diversity produced by noise in gene expression has the potential to be important for fitness. Theoretical evidence from stochastic models suggest that population growth in fluctuating environments can achieve higher rates when the population is dynamically heterogeneous (19). The theory of bet-hedging offers a framework within which we can consider how noise can confer selective advantage to a population. A bet-hedging strategy is one in which the production of phenotypically diverse offspring increases the probability that at least one offspring will survive in a given environment. Such a strategy only proves advantageous in an unpredictably fluctuating environment since organisms cannot foresee what environmental stresses will present themselves. Phenotypic diversity usually does not benefit individual organisms under all environmental conditions, but instead bestows a growth advantage to the population as a whole under fluctuating conditions. For example, heterogeneity may increase the likelihood that, in the event of environmental stress, some cells are poised to survive (20-22). Bacterial persistence (1, 23) as well as sporulation and competence in *B. subtilis* (24-26), are reported to reflect such bet-hedging strategies.

Bacterial persistence during antibiotic stress was first reported in the 1940s (1). It was observed that a small number of bacteria cells within a population stochastically switch to a persistent state in which they do not grow or divide (1, 23). Under ideal conditions, the persistent state does not benefit individual persister cells, since these cells do not divide. However, the existence of a persistent population could prove advantageous during environmental stress with antibiotics since these cells survive and can stochastically switch out of the persistent state and repopulate after the sensitive cells die.

Competence for DNA uptake and sporulation in *B. subtilis* are cellular differentiation programs initiated during harsh environmental conditions. These processes appear to utilize bet-hedging mechanisms to maximize growth while ensuring population survival in fluctuating environments (24-26). While growing exponentially, *B. subtilis* cells are not competent to take up DNA from the environment. However, upon entering stationary phase, a small proportion of the population becomes competent and can acquire foreign DNA.

Intrinsic fluctuations in the levels of a key pathway regulator ComK result in a small fraction of cells being driven into the competent state (25, 26). While it is plausible that populations of cells harness noise in gene expression to generate phenotypic diversity in order to increase fitness, this notion is quite difficult to prove. These examples of systems in which a small proportion of the population adopts a fate in preparation for a stressful environment are enticing. However, it will be crucial to prove that the fitness of a population depends on phenotypic variability and the proportion of individuals that switch to the resistant state.

Gene expression noise has also been reported to be disadvantageous and to prove costly for cellular processes. Pathways in which fidelity is required to maintain cellular housekeeping or to make crucial developmental decisions have been described to lack output variability (27). Consistent with this, in a genome-wide study of gene expression noise, variability in the expression of genes involved in homeostasis, such as ribosomal protein genes, was lower than average (12). More recently, it has been reported that increasing noise in a transcriptional network that specifies intestinal development in *C. elegans* results in significant phenotypic heterogeneity (28). The authors found that increased noise in this network resulted in the failure of some worm embryos to develop intestinal cells, while other embryos developed normally. The authors hypothesize that noise in gene expression may account for the incomplete penetrance of some mutant phenotypes in multicellular organisms (28).

#### Noise in the yeast mating pathway

The pheromone-response pathway in *S. cerevisiae* has classically been used to study eukaryotic signal transduction and gene expression, but recently has been exploited to investigate noise in signaling cascades (16, 29). The pathway contains a canonical MAPK cascade that transmits the signal produced by the presence of extracellular mating pheromone (a-Factor or  $\alpha$ -Factor) from a G-protein coupled receptor to the nucleus to control transcription. Unstimulated cells maintain a basal level of signaling through this pathway, perhaps through the dissociation of the heterotrimeric G-protein. Upon activation by pheromone,



cells arrest in the G1 phase of the cell cycle and up-regulate transcription of target genes by relieving the inhibition of the transcription factor Ste12 by the redundant negative regulators Dig1 and Dig2.

Cell-to-cell variability in signaling through the mating pathway was recently investigated by Colman-Lerner *et al* (16). To measure cell-to-cell variability in the output of the mating pathway, the authors constructed dual-reporter strains in which distinguishable fluorophores YFP and CFP were driven by identical pheromone-inducible promoters. To distinguish noise specific to signaling through the mating pathway from that originating in the expression of the fluorophores, the authors also constructed strains in which YFP was driven by a pheromone-inducible gene and CFP was driven by a pheromone-independent promoter. The authors found that cell-to-cell variability in signaling was dominated by extrinsic sources, specifically the cell cycle stage. Interestingly, the total noise in the output of the mating pathway was unchanged when crucial redundant signaling components Fus3 and Kss1 were removed. This suggests that noise in the mating pathway may be highly buffered and that systems may have evolved to constrain variability so that cells can function properly.

The goal of this study was to investigate whether there are, indeed, mechanisms in place in the yeast mating pathway to reduce cell-to-cell variability in the pathway output. Curiously, transcriptional activation by the transcription factor Ste12 is inhibited by redundant negative regulators Dig1 and Dig2 (30). These two proteins bind to distinct regions on Ste12; Dig1 to the activation domain and Dig2 to the DNA binding domain (31, 32). Given that both Dig1 and

Dig2 are individually capable of inhibiting Ste12 activity, it is unclear why both proteins have been retained during evolution. As previous studies of Dig1 and Dig2 have examined their roles on population-averaged phenotypes, it is possible that differential roles of Dig1 and Dig2 in quantitatively modulating pathway dynamics could have been missed. This work describes the results of single-cell studies that reveal a distinct role for Dig1 in the control of noise in the transcriptional output of, and in preventing long-range physical associations between, Ste12 target genes. Finally, by taking advantage of the biological consequences of disrupting the output of the mating pathway, we demonstrated a link between the increased noise phenotype displayed by *dig1* $\Delta$  cell populations and quantitative defects in growth and mating fitness.

## References

1. J. W. Bigger, *Lancet* **1944**, 497 (1944).
2. M. Delbruck, *J Bacteriol* **50**, 131 (Aug, 1945).
3. J. L. Spudich, D. E. Koshland, Jr., *Nature* **262**, 467 (Aug 5, 1976).
4. H. H. McAdams, A. Arkin, *Proc Natl Acad Sci U S A* **94**, 814 (Feb 4, 1997).
5. E. M. Ozbudak, M. Thattai, I. Kurtser, A. D. Grossman, A. van Oudenaarden, *Nat Genet* **31**, 69 (May, 2002).
6. M. S. Ko, *J Theor Biol* **153**, 181 (Nov 21, 1991).
7. W. J. Blake, K. A. M. C. R. Cantor, J. J. Collins, *Nature* **422**, 633 (Apr 10, 2003).
8. J. Paulsson, *Nature* **427**, 415 (Jan 29, 2004).
9. M. Thattai, A. van Oudenaarden, *Proc Natl Acad Sci U S A* **98**, 8614 (Jul 17, 2001).
10. V. E. Velculescu *et al.*, *Cell* **88**, 243 (Jan 24, 1997).
11. S. Ghaemmaghami *et al.*, *Nature* **425**, 737 (Oct 16, 2003).
12. J. R. Newman *et al.*, *Nature* **441**, 840 (Jun 15, 2006).
13. A. Bar-Even *et al.*, *Nat Genet* **38**, 636 (Jun, 2006).
14. A. Becskei, B. B. Kaufmann, A. van Oudenaarden, *Nat Genet* **37**, 937 (Sep, 2005).
15. M. B. Elowitz, A. J. Levine, E. D. Siggia, P. S. Swain, *Science* **297**, 1183 (Aug 16, 2002).
16. A. Colman-Lerner *et al.*, *Nature* **437**, 699 (Sep 29, 2005).
17. J. M. Raser, E. K. O'Shea, *Science* **304**, 1811 (Jun 18, 2004).
18. D. Volfson *et al.*, *Nature* **439**, 861 (Feb 16, 2006).
19. M. Thattai, A. van Oudenaarden, *Genetics* **167**, 523 (May, 2004).
20. T. M. Neildez-Nguyen *et al.*, *Differentiation* **76**, 33 (Jan, 2008).
21. W. J. Blake *et al.*, *Mol Cell* **24**, 853 (Dec 28, 2006).
22. T. S. Bayer, K. G. Hoff, C. L. Beisel, J. J. Lee, C. D. Smolke, *J Biol Eng* **3**, 1 (2009).
23. N. Q. Balaban, J. Merrin, R. Chait, L. Kowalik, S. Leibler, *Science* **305**, 1622 (Sep 10, 2004).
24. J. W. Veening, W. K. Smits, L. W. Hamoen, O. P. Kuipers, *J Appl Microbiol* **101**, 531 (Sep, 2006).
25. H. Maamar, A. Raj, D. Dubnau, *Science* **317**, 526 (Jul 27, 2007).
26. G. M. Suel, J. Garcia-Ojalvo, L. M. Liberman, M. B. Elowitz, *Nature* **440**, 545 (Mar 23, 2006).
27. T. Bollenbach *et al.*, *Development* **135**, 1137 (Mar, 2008).
28. A. Raj, S. A. Rifkin, E. Andersen, A. van Oudenaarden, *Nature* **463**, 913 (Feb 18, 2010).
29. R. C. Yu *et al.*, *Nature* **456**, 755 (Dec 11, 2008).
30. K. Tedford, S. Kim, D. Sa, K. Stevens, M. Tyers, *Curr Biol* **7**, 228 (Apr 1, 1997).
31. K. A. Olson *et al.*, *Mol Cell Biol* **20**, 4199 (Jun, 2000).
32. L. Bardwell, J. G. Cook, J. X. Zhu-Shimoni, D. Voora, J. Thorner, *Proc Natl Acad Sci U S A* **95**, 15400 (Dec 22, 1998).

## **CHAPTER 2**

**Coordinate control of gene expression noise and interchromosomal interactions in a MAPK pathway**

## ABSTRACT

In the *Saccharomyces cerevisiae* pheromone-response pathway, the transcription factor Ste12 is inhibited by two MAP kinase-responsive regulators, Dig1 and Dig2. These two related proteins bind to distinct regions of Ste12 but are redundant in their inhibition of Ste12-dependent gene expression. Here we describe three unexpected functions for Dig1 that are non-redundant with those of Dig2. First, the removal of Dig1 results in a specific increase in intrinsic and extrinsic noise in the transcriptional outputs of the mating pathway. Second, in *dig1* $\Delta$  cells, Ste12 relocates from the nucleoplasmic distribution seen in wild-type cells into discrete subnuclear foci. Third, genome-wide iChIP studies revealed that Ste12-dependent genes display increased interchromosomal interactions in *dig1* $\Delta$  cells. These findings suggest that the regulation of gene expression through long-range gene interactions, a widely-observed phenomenon, comes at the cost of increased noise. Consequently, cells may have evolved mechanisms to suppress noise by controlling these interactions.

## INTRODUCTION

Cells respond to environmental fluctuations by transducing signals to networks of DNA-binding proteins. Numerous transcriptional regulators, including p53<sup>1</sup>, E2Fs<sup>2</sup> and Smads<sup>3, 4</sup>, are subject to overlapping inhibitory mechanisms, yet the logic underlying these potential circuit redundancies remains poorly understood. A well-defined example of such regulatory architecture occurs in the *S. cerevisiae* mating pathway in which the transcription factor Ste12 is inhibited by two MAP kinase-responsive regulators, Dig1 and Dig2. These related proteins are redundant in their suppression of Ste12 activity since the removal from cells of both proteins is required to de-repress pathway activity<sup>5, 6</sup>. Despite this redundancy Dig1 and Dig2 bind to distinct regions of Ste12; Dig1 to the activation domain and Dig2 to the DNA-binding domain<sup>7, 8</sup>.

Ste12 lies at the terminus of a signal transduction pathway that is initiated by the binding of extracellular pheromones to a G-protein coupled receptor. This ligand-sensing event triggers the activation of a MAP kinase (MAPK) cascade, which initiates a cytoplasmic response and transmits the mating signal to the nucleus to activate the transcription factor Ste12 (Fig. 1a). Ste12 regulates the expression of a network of genes whose products are required for the process of mating. Unstimulated cells display a basal level of signalling that increases upon stimulation with pheromone. This system has been utilized recently as a model to measure variability, or noise, in a signal transduction cascade and to ascertain whether such noise is controlled<sup>9, 10</sup>. Interestingly, it was found that removal of either of the MAPKs, Fus3 or Kss1, did not affect total output variability,

suggesting that this natural system may have evolved overlapping mechanisms that buffer against noise<sup>9</sup>. Since the regulation of gene expression noise has been suggested to be important for appropriate input-output responses<sup>11-13</sup>, we reasoned that the investigation of noise in the output of the mating pathway might reveal mechanisms that underlie the redundant regulatory architecture controlling Ste12 activity.

## RESULTS

### Noise in Ste12-dependent gene expression outputs is limited by Dig1

We constructed two Ste12-dependent reporter genes, *pAGA1-YFP* and *pFUS1-YFP*. Their output distributions in wild-type and *dig1Δ* cells overlapped less than 5% with the background autofluorescence of yeast (Supplementary Information, Fig. S1). The mean output of *dig1Δ* strains increased 1.4-fold over wild-type, while mean fluorescence levels in *dig2Δ* did not change measurably (Fig. 1b), confirming that Dig1 and Dig2 appear redundant in their inhibition of average Ste12-dependent transcription<sup>5, 6</sup> when assayed in this manner. As expected, deleting *DIG1* and *DIG2* resulted in a 19-fold and 9-fold increase in mean expression for *pAGA1-YFP* and *pFUS1-YFP*, respectively (Fig. 1b). The mean output of a Ste12-independent reporter, *pPMP1-GFP*, was unaffected by deletion of *DIG1* or *DIG2* (Fig. 1b).

In contrast, examination of the single-cell output distributions of the Ste12-dependent reporters revealed a non-redundant role for Dig1 that is distinct from

Dig2. Deletion of *DIG1*, but not *DIG2*, significantly increased the variability as measured quantitatively by the coefficient of variation or CV (Fig. 1c), and qualitatively by the spread of the *pAGA1-YFP* and *pFUS1-YFP* distributions (Fig. 1d). The CVs of the *pFUS1-YFP dig1Δ* and *pAGA1-YFP dig1Δ* output distributions were 29.6% ( $P = 0.0003$ ) and 12.5% ( $P = 0.0014$ ) higher, respectively, than those of wild-type and *dig2Δ* (Fig. 1c,d). Cell sorting experiments indicated that a cell population isolated from the middle of the *dig1Δ* output distribution could regenerate the entire distribution within 1-2 cell cycles (Fig. 2). Thus, while the steady-state fraction of cells experiencing the high-expression state at any given time point in the *dig1Δ* mutant is modest, the entire population of *dig1Δ* cells is likely to dynamically experience inappropriately high-expression states over time. The larger CV of *dig1Δ* output distributions was unexpected, and all the more significant, because the slight increase in mean output in *dig1Δ* cells might be predicted to generate a decrease, rather than an increase, in noise<sup>14</sup>. Furthermore, the increase in noise in *dig1Δ* cell populations was independent of forward scatter and side scatter, flow cytometric surrogate measures of cell size and shape (Fig. 1e, see Methods). As expected from the rise in mean expression, *dig1Δdig2Δ* double mutants displayed less variability than wild-type in mating pathway outputs (Fig. 1c). The effect of deleting *DIG1* on noise is specific to outputs of the mating pathway, as the deletion of *DIG1* or *DIG2* did not affect the variability in three Ste12-independent reporters, *pPMP1-GFP*, *pYEF3-GFP* and *pAGP1-GFP* (Fig. 1c,d, Supplementary Information, Fig.



S2). Furthermore, the changes in noise cannot merely be due to changes in the mean expression or growth rate since the analysis of several additional mutants illustrate that increased mean output and decreased growth rate do not result in increased noise (Supplementary Information, Fig. S3).

### **Both intrinsic and extrinsic noise increase in *dig1*Δ cell populations**

Gene expression noise can be decomposed into intrinsic and extrinsic components using a two-colour reporter gene system in which distinct fluorescent proteins are expressed from identical promoters in the same cell<sup>15</sup>. Intrinsic noise is defined as the uncorrelated cell-to-cell variation in levels of these two fluorescent proteins and is thought to reflect stochastic fluctuations in gene expression itself<sup>16-19</sup>. Extrinsic noise is defined as the correlated variation in the levels of the two proteins. Although extrinsic noise is thought to be impacted by cell-to-cell variability in the global cellular state, its origins and effectors are considerably less well-understood<sup>9, 11, 14</sup>.

Using a two-colour assay with strains containing GFP and mCherry driven by *pAGA1* (Fig. 3a), we observed that both intrinsic and extrinsic noise increased in *dig1*Δ cell populations as compared to wild-type and *dig2*Δ cell populations. This result can be seen qualitatively by the reduced density of cells in the centre of the scatter plot of the data for the *dig1*Δ mutant relative to wild-type and *dig2*Δ (Fig. 3b), indicating an increased spread in fluorescence values. Quantitative calculations also reveal increases in the CV measurements (Fig. 3c, Supplementary Information, Fig. S4). The extrinsic noise ( $\eta_{\text{ext}}$ ) was 22.8% ( $P =$

0.035) greater in magnitude in *dig1Δ* cells as compared to wild-type, while the intrinsic noise ( $\eta_{\text{int}}$ ) was 14.9% ( $P = 0.009$ ) higher (Fig. 3c). These patterns of increased intrinsic and extrinsic noise in *dig1Δ* populations were independent of cell size and shape and were specific to Ste12-dependent outputs (Fig. 3d-f, Supplementary Information, Fig. S4d,e).

### **Dig1 prevents formation of subnuclear foci of Ste12-GFP molecules**

The increased extrinsic noise in *dig1Δ* cell populations could result from the breakdown of a mechanism in which Dig1 limits fluctuations in the levels of the transcription factor Ste12 through an autoregulatory feedback loop at the Ste12 promoter<sup>20-22</sup>. However, this was not the case since replacing the Ste12-dependent Ste12 promoter had no effect on noise (Fig. 4). This posed the possibility that the mechanism by which Dig1 acts on Ste12-dependent genes to limit extrinsic noise is beyond correlations in upstream factors. Extrinsic noise is typically measured by quantifying the correlated variability in the expression from two identical promoters, in this case *pAGA1*. However, more generally, correlated or extrinsic noise in *pAGA1* output would be expected to increase in *dig1Δ* cells if Dig1 limited the correlated expression of all Ste12 outputs in the cell. One way for this to occur would be if Ste12 target genes co-localized in space in the absence of Dig1. If this were the case, the spatial proximity of these genes could increase the dependence of the expression of one Ste12 target gene on the expression of another, perhaps due to increased local concentration of activators. For example, if Ste12 target genes co-localized in space, the

induction of one gene could stimulate the induction of a neighbouring Ste12 target gene. Thus, it would be expected that the expression of such co-localized genes would be more correlated, in turn resulting in an increase in extrinsic noise. Given that Ste12 has many known interacting partners and exhibits self-cooperativity<sup>5, 6, 23-27</sup>, Dig1 may function to shield protein-protein interaction domains on Ste12 that would otherwise cause Ste12 to homo-dimerize or bind to other proteins. Therefore, the loss of Dig1 might allow DNA-bound Ste12 proteins to enable long-range interchromosomal interactions between Ste12 target genes.

Consistent with this possibility, Ste12-GFP molecules localized to subnuclear foci in *dig1Δ* cells (Fig. 5a, white arrowheads), while Ste12-GFP displayed granular nucleoplasmic staining in both wild-type and *dig2Δ* cells (Fig. 5a). Approximately 65% of *dig1Δ* cells showed one or more Ste12-GFP foci (Fig. 5b). These foci did not co-localize with the nucleolus (Supplementary Information, Fig. S5a) and focus formation could not be explained by changes in total Ste12 protein levels since these levels were unaltered in *dig1Δ* and *dig2Δ* cells, as measured by quantitative immunoblotting (Supplementary Information, Fig. S5b). *dig1Δdig2Δ* double mutants also exhibited Ste12-GFP foci, but a slightly higher nucleoplasmic accumulation of Ste12-GFP protein precluded accurate assessment and quantification (Supplementary Information, Fig. S5c). Focus formation in *dig1Δ* cells was specific to Ste12 as the transcription factor

Reb1-GFP displayed nucleoplasmic staining in wild-type, *dig1* $\Delta$  and *dig2* $\Delta$  cells (Fig. 5a).

### **Focus-suppressing function of Dig1 is not controlled by MAPK signaling**

In wild-type cells, stimulation with pheromone does not induce formation of Ste12-GFP foci (Fig. 5c), indicating that an increase in signalling and transcriptional output is not sufficient to induce their formation. While it has been suggested that mating signalling inactivates Dig1<sup>5, 6</sup>, we found that this protein remains physically associated with target genes (presumably via Ste12) in cells treated with pheromone (Fig. 5d). Thus, consistent with our finding that Ste12-GFP foci do not form in wild-type cells upon pheromone stimulation, not all activities of Dig1 are eliminated by signalling.

### **Increased long-range interactions between Ste12-target genes in *dig1* $\Delta$ cells**

Using a genome-wide adaptation of the single-locus iChIP technique<sup>28</sup>, we examined interactions between the Ste12 target locus, *pFUS1*, and the rest of the genome in wild-type and *dig1* $\Delta$  cells (see Methods). The locus efficiently immunoprecipitated as seen by the large peak centred on the *FUS1* promoter on the left arm of Chromosome III (Fig. 6a). No enrichment was observed at the *pFUS1* locus in the absence of Lacl (Supplementary Information, Fig. S6). The 5% of genes (269 genes) whose promoters displayed the largest differences in ChIP-chip signals between *dig1* $\Delta$  cells and wild-type were analyzed

(Supplementary Information, Table S1). Remarkably, of the 203 gene regulators for which genome-wide localization data are available<sup>21</sup>, only targets of Ste12 and Tec1 displayed a statistically significant increase in interactions with the *FUS1* locus in *dig1Δ* cells (Fig. 6b, similar results obtained for 1%, 3% and 10% cutoffs). Moreover, these physical interactions were dependent on the presence of Ste12 (Fig. 6c, Supplementary Information, Table S1). Tec1 and Ste12 are known to interact and are found at promoters of genes involved in both mating and filamentous growth<sup>22, 27</sup>. Well-studied genes implicated in these processes were prominently featured among those that displayed increased physical interactions with the *FUS1* locus in *dig1Δ* cells (Fig. 6d). We constructed promoter-YFP fusions for 11 of these Ste12-target genes and found that the mean expression increased for seven upon deletion of *DIG1* (Supplementary Information, Fig. S7a). Rigorous analysis of the changes in noise for these genes is complicated by the fact that the means increase significantly and the relationships between the means and CVs are unknown. However, we note that the removal of Dig1 induces a broadening of the output distributions that is highly reminiscent of trends seen with the *pFUS1-YFP* and *pAGA1-YFP* reporter stains (Supplementary Information, Fig. S7b).

### **Nonredundant roles for Dig1 in growth, mating, and gene induction kinetics**

Under basal conditions, the mating pathway must appropriately balance the level of signalling to avoid cell cycle arrest and mating projection formation induced by pathway activation with a requirement for maintaining basal signalling

to express key pathway components<sup>29</sup>. This balance might be expected to be disrupted in *dig1Δ* cells, with repercussions for growth under basal conditions and mating in the presence of a pheromone signal. Therefore, cell-to-cell variability in outputs of the mating pathway could influence fitness. We found that *dig1Δ* cells grow more poorly than wild-type or *dig2Δ* cells and this defect is rescued by the deletion of *STE12* (Fig. 7a,b). Additionally, *dig1Δ* cells display a kinetic defect in cell-cell fusion compared to wild-type and *dig2Δ*, as measured quantitatively using a fluorescent-based assay in which the accumulation of double-positive fluorescent cells was scored (Fig. 7c-e, Supplementary Information, Fig. S8, see Methods). This defect is unlikely to be due to the slight increase in mean pathway output in *dig1Δ* cells since previous studies found that even large increases in basal signalling does not reduce mating efficiency<sup>30</sup>. The defect in fusion between mating partners is mirrored by two quantitative changes in the induction of pheromone-inducible genes in *dig1Δ* cells (Fig. 8a). First, *dig1Δ* cells display a larger proportion of cells that do not induce *pAGA1-YFP* or *pFUS1YFP* reporter genes in response to pheromone treatment (Fig. 8b). Second, the population of *dig1Δ* cells that does respond to pheromone displays a reduced dynamic range in the induction of pheromone inducible gene expression (Fig. 8c).

## DISCUSSION

Recent work has shown that *DIG1* and *DIG2* were derived from a single parental gene that existed prior to the whole-genome duplication (WGD) that occurred in the ancestor of *S. cerevisiae* 100-200 million years ago<sup>31</sup>. Their continued presence in the genome suggests that their maintenance has an adaptive role. Indeed, previous work indicates that Dig1 and Dig2 inhibit Ste12 by interacting with distinct domains of the transcription factor, implying biochemical specialization<sup>7, 8</sup>. However, their genetic redundancy for inhibiting Ste12 was puzzling. Studies presented here revealed three functions of Dig1 that are not redundant with those of Dig2: 1) control of gene expression noise, 2) regulation of the intranuclear distribution of Ste12, and 3) the control of long-range interactions between Ste12-target genes. We discuss below how these three functions may be related and the broader implications of these findings.

Dig1 is a well-studied regulatory protein that functions specifically in the pheromone response pathway and has only one reported biochemical function: to bind to a domain of Ste12 involved in protein-protein interactions<sup>5-8, 32, 33</sup>. The loss of Dig1 is, therefore, expected solely to unshield protein-protein interaction domains on the Ste12 transcription factor. Although indirect mechanisms are always difficult to rule out, we propose that this unshielding induces aggregation of Ste12 molecules and target genes, which results in increased cell-to-cell variability in the basal output of the pheromone response pathway. Dig2, which binds the distinct DNA-binding domain of Ste12<sup>7, 8</sup>, does not share these functions. The aggregation of Ste12 molecules into one or two foci may create a domain within the nucleus where the transcription of Ste12-target genes can be

activated. Our model suggests that the transcription of Ste12-target genes within the focus is more coordinated such that if one gene in the focus is transcribed, the others are, in turn, more likely to be expressed. Thus, such correlated expression within a single cell would be expected to yield increased correlated cell-to-cell variability in the transcriptional output of the pathway.

Transcriptional regulation that involves looping of DNA between distant sites via protein-protein interactions has been observed the *lac* operon<sup>34-38</sup> and  $\lambda$  phage<sup>39, 40</sup>. In the context of the results described here, it is notable that computational models of the *lac* system suggest that gene regulation by DNA looping can affect fluctuations in transcription<sup>41</sup>. These models predict that for transcriptional activators, DNA looping should increase noise in transcriptional outputs. Our model for the function of Dig1 is consistent with these theoretical predictions.

Recently, inter- and intrachromosomal interactions have been detected in other systems<sup>42-45</sup>. In erythroid cells, for example, Klf1-regulated genes, including *Hba* and *Hbb* globin genes, display long-range inter- and intrachromosomal interactions<sup>42</sup>. Although such interactions tend to correlate with transcriptional regulation and sites of active transcription, their precise functions remain a matter of considerable debate. Our observations suggest that while these long-range interactions could be important for gene expression, they may come at the cost of increased variability. This notion is in concordance with an emerging view that, in some cases, such gene interactions can be deleterious and even mutagenic<sup>46</sup>. It will be interesting to explore whether mechanisms of



noise regulation are pervasive among regulatory circuits that involve long-range DNA interactions and the extent to which gene localization is balanced with a need for limiting noise.

While establishing the generality of the effect of aggregate formation on output variability will require further investigation, we note that subcellular protein and DNA aggregation is not uncommon in biology. DNA replication and gene activation can occur in “factories” located at the nuclear periphery<sup>47-51</sup>. Sites of DNA damage along with proteins that respond to DNA damage form nuclear foci in yeast<sup>52, 53</sup>. Telomeres are also known to cluster in the nucleus<sup>54</sup>. Cytoplasmic P-bodies are foci of proteins involved in mRNA degradation and translational inhibition<sup>55-57</sup>. Given our data, these foci may serve, in some cases, to promote simultaneity in cellular transactions. The development of assays that can distinguish between correlated and uncorrelated noise in these systems would allow the testing of such concepts.

## **Methods**

### Strains

All yeast strains used are derived from BY4743, of the s288c background, and are described in Supplementary Information, Table S2. Yeast knockouts were generated by conventional lithium acetate and polyethylene glycerol procedures. YFP, eGFP (from pFA6a-EGFP-HIS3MX) and mCherry (from pFA6a-mCherry-HIS3MX or pFA6a-GFPtomCherry-URA3MX from J.S. Weissman) reporters for the mating pathway were constructed using methods as described<sup>58</sup>, while

*pPMP1*-fluorophore fusions were constructed using plasmids pFA6a-EGFP-HIS3MX6 and pFA6a-GFP<sub>tomCherry</sub>-URA3MX from J.S. Weissman.

#### Growth and fluorescence measurements by flow cytometry

Single fluorescent strains used: YM1968, YM2091, YM2100, YM2105, YM2109, YM2112, YM3550, YM3593, YM3594, YM3760, YM3762, YM3763, YM3764, YM3766, YM3767, YM3769, YM3770, YM3771, YM3772, YM3773, YM3776-YM3782 YM3804-YM3814. Dual fluorescent strains used: YM2636, YM2871, YM2876 and YM3132. Cells were grown in 1 mL cultures for 36 hr in 96-well deep pocket plates (Costar). OD<sub>600</sub> measurements were taken and cultures were diluted to an OD<sub>600</sub> = 0.08 and grown for 10 hr. A Becton Dickinson LSR-II flow cytometer was used, along with an autosampler device (HTS) controlled by custom software, to collect data over a sampling time of 7 sec<sup>11</sup>. YFP and GFP were excited at 488 nm and fluorescence was collected through a 505-nm long-pass filter and HQ530/30 and HQ515/20 band-pass filters (Chroma Technology), respectively. mCherry was excited at 532 nm and fluorescence collected through 600-nm long-pass filter and 610/20 band-pass filters (Chroma Technology).

#### Data analysis

All data analysis was done using custom MATLAB software. Raw cytometry data were filtered to eliminate errors due to uneven sampling time and negative fluorescence readings. Bulk calculations were done on these processed data. To control for cell aggregates, as well as cell size and shape, forward and side

scatter (FSC and SSC) data were expressed on orthogonal axes and subpopulations of cells were selected using circular gates of increasing radii centred on the median FSC and SSC values<sup>11</sup>. Nineteen circular bins were created with radii of 6000, 9000,  $10^4$ ,  $2 \cdot 10^4$ ,  $3 \cdot 10^4$ , ...,  $17 \cdot 10^4$  arbitrary units were used. Results are shown for data in bin 5, with a radius of  $3 \cdot 10^4$ . Data were used if at least 5000 cells were in this bin, but on average between 20,000-40,000 cells had FSC and SSC values within this gate. The coefficient of variation (CV) was used as a measure of total noise, while intrinsic/uncorrelated and extrinsic/correlated noise were calculated as described<sup>15</sup> using GFP and mCherry dual-colour strains (Supplementary Information, Table S2). T-tests were used to calculate level of significance for increases in noise in the *dig1Δ* mutant strains.

#### FACS sorting and expression dynamics

YM2105 (*pAGA1-YFP dig1Δ*) were grown to mid-log phase. The fluorescence distribution was determined. A narrow gate centered on the middle of this distribution was created and cells with expression levels within this gate were sorted using a Becton Dickinson FACSAria cell sorter. Cells were spun down, resuspended in YPAD and grown at 30 C. Aliquots were removed and the fluorescence distributions determined for 30,000 cells using a Becton Dickinson LSR-II flow cytometer. Data was analyzed as described above.

#### Microscopy

YM2910, YM3102, YM3103, YM3104, YM3722, YM3723, YM3724, YM3774 and YM3775 were grown overnight to saturation in YPAD. Cultures were diluted back to an OD<sub>600</sub> of 0.1 in YPAD and grown for 4 hr. Microscopy was performed using a DeltaVision deconvolution microscope, which was outfitted with Olympus Plan Apo 60- and 100-X objectives. Z-stacks were taken with 0.3 μm steps. DeltaVision deconvolution software was used to deconvolve and analyze these images. For Ste12-GFP, a 1 s exposure was used and for Nup188-mCh, a 0.5 s exposure was used. For Reb1-GFP, a 1.0 s exposure was used. For the Ste12-GFP and Nop7-mCherry co-localization experiments, a 0.5 s exposure was used for the FITC channel and a 0.2 s exposure was used for the rhodamine channel.

#### Quantitative immunoblotting

YM1953, YM2101, YM2315, and YM2102 were grown to log phase in YPAD and 3 OD<sub>600</sub> were collected by centrifugation and snap-freezing. Pellets were re-suspended in 100 μl 2X protein loading buffer and 1:100 Sigma phosphatase inhibitor cocktails 1 and 2 and 1:260 Sigma protease inhibitor cocktail. Samples were boiled for 2 min and 50 μl Zirconia/silica beads (Biospec Products) were added. Samples were then vortexed on a platform vortex for 2 min. Samples were again boiled for 2 min and centrifuged at 14,000 x g for 10 min to remove cell debris. The supernatants were pulled off, boiled for 3 min and resolved on a 10% SDS-PAGE gel. Proteins were then transferred to nitrocellulose and immunoblotting was performed as described in the Li-COR Odyssey manual

using  $\alpha$ Ste12 (1:1000, a gift from Ira Herskowitz),  $\alpha$ Tubulin (1:3000, AbCam),  $\alpha$ Rabbit-IR<sub>800</sub> (1:1000) and  $\alpha$ Rat-IR<sub>680</sub> (1:1000).

### Growth rate

YM1953, YM2101, YM2315, YM2643, YM2248, YM3776, YM3777 and YM3778 were grown to log phase overnight in YPAD. These cultures were then diluted back to an OD<sub>600</sub> = 0.2 (YM1953, YM2101, YM2315 and YM2643) or OD<sub>600</sub> = 0.05 (YM2248, YM3776, YM3777 and YM3778) at t=0 and OD<sub>600</sub> measurements were taken every hour. To avoid cultures reaching saturation and entering stationary phase, cultures were diluted periodically. This dilution was accounted for in the subsequent OD<sub>600</sub> calculations. OD<sub>600</sub> measurements at later time points were normalized to the OD<sub>600</sub> at time = 0 min. Best-fit lines were calculated using DeltaGraph 5 graphing software.

### Flow cytometry-based cell-cell fusion assay

A *MATa* strain (YM2901) containing at the *TRP1* locus a construct consisting of the N-terminus (AA 1-158) of *eGFP* fused to a leucine zipper dimerization domain<sup>59</sup> was constructed. *MAT $\alpha$*  strains (YM2903, YM3085, YM3086 and YM3087) containing at the *LEU2* locus a construct consisting of the C-terminus (AA 159-240) of *eGFP* fused to a leucine zipper dimerization domain<sup>59</sup> as well as an *mCherry* marker driven by *pTEF2* integrated at the *LYS1* locus were also constructed. Strains were grown overnight to saturation. The cultures were diluted to an OD<sub>600</sub> of 0.07 and collected after a 5.5 hr outgrowth to perform the

mating assay. At time 0, each *MAT $\alpha$*  strain was mixed in 10-fold excess with a *MAT $\alpha$*  strain to a final OD<sub>600</sub> of 1.0. 750 ml were removed from each mating mix as the zero time point. The rest of the mating culture was dispensed (200 ml/well) into a 96-well Millipore Multi-screen Filter plate and spun in a Beckman centrifuge at 1700 rpm for 5 min to bind the cells onto the filter. The filter plate was then placed on a pre-warmed Nunc OmniTray YPAD plate and incubated at 30°C. Samples were collected at the indicated time points in triplicate by adding TE to the well to resuspend the cells. The samples were left at room temperature in TE overnight before flow cytometric analysis to ensure complete folding of any GFP molecules present in each sample. Flow cytometry was done as described above in the two-colour assay and between 3,000 and 10,000 cells were analyzed for each time point. Data analysis was performed using FlowJo 8.7.1 using quadrants based on the zero time point. Diploids were visualized as GFP+/mCherry+ cells. To determine mating efficiency, the fraction of diploid cells (GFP+/mCherry+) divided by the total number of mCherry+ cells (GFP+/-) was calculated for each time point in each mating experiment. The average and standard deviation for the three replicates was then calculated for each time point (with the exception of the zero time point).

#### Pheromone time-course assay

YM1968, YM2091, YM2100 and YM2105 were grown into log phase over night in YPAD. Cultures were diluted back to an OD<sub>600</sub> = 0.4 and 50 nM  $\alpha$ -Factor was added. 1 mL aliquots were removed at t = 0, 15, 30, 60, 90, 120, 150, 180 and

240 min, washed with water, resuspended in 1 mL TE pH = 8 and fluorescence distributions were measured by flow cytometry. Data were analyzed as described above.

### ChIP

Dig1-GFP ChIP was performed as described<sup>60, 61</sup> with strains YM1731 and YM3747 using an anti-GFP antibody from AbCam (Ab290). 5  $\mu$ M  $\alpha$ -Factor was added to log phase cultures for 1 hr.

### Modified ChIP-chip method

An 11 kb construct consisting of 240 tandem arrays of Lac operators<sup>62</sup> and an associated *HIS3MX* marker was inserted 331bp upstream of the *FUS1* ATG in strains containing a mCherry-LacI plasmid (BHM1336 adapted from pJH212, strains: YM3587, YM3588 and YM3687). Cultures were prepared for ChIP-chip by overnight growth to saturation in –Ura medium. Cultures were then diluted to an OD<sub>600</sub> of 0.01 and grown for 4 hr in –Ura medium. These cells were again diluted to an OD<sub>600</sub> of 0.01 in YPAD and collected 4 hr later. Chromatin immunoprecipitation was performed as described<sup>60, 61</sup>. However, the protein crosslinker ethylene glycolbis (succinimidylsuccinate) (EGS) was added to a final concentration of 1.5 mM for 30 min before the addition of formaldehyde. Additionally, DNA was lightly sonicated in a Diagenode Bioruptor for 2x5 min on the low setting with 1 s on/ 0.5 s off pulses. To immunoprecipitate mCherry-LacI, a polyclonal anti-DsRed antibody from Clontech (catalogue number 632496) was

used at a 1:100 dilution. Following ChIP, strand displacement amplification and labelling were performed as described to generate DNA probes with incorporated aminoallyl-dUTP<sup>63</sup>. Probes representing mCherry-LacI immunoprecipitates and whole cell extracts were differentially labelled with Cy fluorescent dyes and hybridized on Agilent yeast whole-genome tiling microarrays (G4491A). Hybridization and array washing were performed as described by Agilent Technologies (Version 9.2). In addition, after the acetonitrile wash, slides were rinsed in Agilent Stabilization and Drying Solution (5185-5979). Microarrays were scanned at 5 µm resolution on a GenePix 4000B scanner (Molecular Devices) using GenePixPro 6.0 software. Microarray analysis was done using in-house software as described<sup>64</sup>. For each strain (wild-type, *dig1Δ* and *dig1Δste12Δ*) data from four arrays were averaged by calculating the geometric mean of the intensities of each probe. Averaged data were then smoothed using a moving average window over 11 probes and difference maps were constructed by subtracting the log<sub>2</sub> values for each WT (YM3587) probe from the corresponding probe in *dig1Δ* (YM3588) and *dig1Δ ste12Δ* (YM3687) datasets. Given the broad peak (due to light sonication) centred on the *FUS1* locus on the left arm of Chr. III, data from this region were removed from further analysis. We extracted 500 bp of sequence upstream of each gene and subdivided these segments into 20 bins, each of which represented 25 bp of sequence. Data from microarray probes were then assigned to the appropriate bin based on the genomic coordinate of the centre of a probe. These gene promoter segments were then ordered relative to one another based on the median value of all the



probes in a segment. The top 5% (269 genes) of differences from each *dig1Δ* - wild-type or *dig1Δste12Δ* - wild-type dataset were analyzed for enrichment of target genes for 203 transcription factors<sup>21</sup>. Similar results were obtained using 1%, 3% and 10% cutoffs. A list of target genes for the 203 transcription factors was compiled from ChIP-chip data ( $P < 0.05$ ) from Harbison and colleagues<sup>21</sup>. Next, we performed hypergeometric testing to determine whether the enrichment of transcription factor target genes in the top 5% of our datasets was statistically significant below a Bonferroni corrected P value of 0.05 (Supplementary Information, Table S1). We also compiled a list of genes bound by Ste12 or Tec1 in the presence or absence of pheromone ( $P < 0.05$ )<sup>21</sup>. We analyzed our list of genes with the top 5% of differences for an enrichment of these genes and calculated a P value using hypergeometric testing.

### **Acknowledgments**

We are grateful to J.S. Weissman, E.K. O'Shea, J.E. Haber, W.A. Lim, A.D. Johnson and D.J. Sherratt for plasmids and protocols. We thank C.D. Chun and P.D. Hartley for help in conducting and analyzing the ChIP-chip experiments and W.F. Marshall and K. Wemmer for assistance with microscopy. We are especially grateful to A.D. Johnson, S. Komili, W.F. Marshall and S. Shankar for helpful comments on the manuscript. This work was supported by a Genentech Fellowship and an NSF Predoctoral Fellowship to E.M., an NIH Ruth L. Kirschstein National Research Service Award to A.S., as well as funding from the

UCSF Program for Breakthrough Biomedical Research and an NIH grant (GSE17583) to H.D.M. and H.E-S.

### **Author Contributions**

E.M. constructed all strains and performed and analyzed all experiments except for the FACS-based mating assay. A.S. constructed strains for and performed the FACS-based mating assay. H.E-S. and E.M. wrote custom MATLAB software and conducted data analyses for the FACS assays. E.M., H. E-S. and H.D.M. wrote the manuscript.

### **Competing Financial Interests**

The authors declare no competing financial interests.

## References

1. Marine, J.C. *et al.* Keeping p53 in check: essential and synergistic functions of Mdm2 and Mdm4. *Cell Death Differ* **13**, 927-934 (2006).
2. DeGregori, J. & Johnson, D.G. Distinct and Overlapping Roles for E2F Family Members in Transcription, Proliferation and Apoptosis. *Curr Mol Med* **6**, 739-748 (2006).
3. Moustakas, A. & Heldin, C.H. The regulation of TGFbeta signal transduction. *Development* **136**, 3699-3714 (2009).
4. Xu, L. Regulation of Smad activities. *Biochim Biophys Acta* **1759**, 503-513 (2006).
5. Tedford, K., Kim, S., Sa, D., Stevens, K. & Tyers, M. Regulation of the mating pheromone and invasive growth responses in yeast by two MAP kinase substrates. *Curr Biol* **7**, 228-238 (1997).
6. Cook, J.G., Bardwell, L., Kron, S.J. & Thorner, J. Two novel targets of the MAP kinase Kss1 are negative regulators of invasive growth in the yeast *Saccharomyces cerevisiae*. *Genes Dev* **10**, 2831-2848 (1996).
7. Bardwell, L., Cook, J.G., Zhu-Shimoni, J.X., Voora, D. & Thorner, J. Differential regulation of transcription: repression by unactivated mitogen-activated protein kinase Kss1 requires the Dig1 and Dig2 proteins. *Proc Natl Acad Sci U S A* **95**, 15400-15405 (1998).
8. Olson, K.A. *et al.* Two regulators of Ste12p inhibit pheromone-responsive transcription by separate mechanisms. *Mol Cell Biol* **20**, 4199-4209 (2000).
9. Colman-Lerner, A. *et al.* Regulated cell-to-cell variation in a cell-fate decision system. *Nature* **437**, 699-706 (2005).
10. Yu, R.C. *et al.* Negative feedback that improves information transmission in yeast signalling. *Nature* **456**, 755-761 (2008).
11. Newman, J.R. *et al.* Single-cell proteomic analysis of *S. cerevisiae* reveals the architecture of biological noise. *Nature* **441**, 840-846 (2006).
12. Cagatay, T., Turcotte, M., Elowitz, M.B., Garcia-Ojalvo, J. & Suel, G.M. Architecture-dependent noise discriminates functionally analogous differentiation circuits. *Cell* **139**, 512-522 (2009).
13. Bollenbach, T. *et al.* Precision of the Dpp gradient. *Development* **135**, 1137-1146 (2008).
14. Volfson, D. *et al.* Origins of extrinsic variability in eukaryotic gene expression. *Nature* **439**, 861-864 (2006).
15. Elowitz, M.B., Levine, A.J., Siggia, E.D. & Swain, P.S. Stochastic gene expression in a single cell. *Science* **297**, 1183-1186 (2002).
16. McAdams, H.H. & Arkin, A. Stochastic mechanisms in gene expression. *Proc Natl Acad Sci U S A* **94**, 814-819 (1997).
17. Becskei, A., Kaufmann, B.B. & van Oudenaarden, A. Contributions of low molecule number and chromosomal positioning to stochastic gene expression. *Nat Genet* **37**, 937-944 (2005).
18. Raser, J.M. & O'Shea, E.K. Control of stochasticity in eukaryotic gene expression. *Science* **304**, 1811-1814 (2004).

19. Blake, W.J., M, K.A., Cantor, C.R. & Collins, J.J. Noise in eukaryotic gene expression. *Nature* **422**, 633-637 (2003).
20. Ren, B. *et al.* Genome-wide location and function of DNA binding proteins. *Science* **290**, 2306-2309 (2000).
21. Harbison, C.T. *et al.* Transcriptional regulatory code of a eukaryotic genome. *Nature* **431**, 99-104 (2004).
22. Zeitlinger, J. *et al.* Program-specific distribution of a transcription factor dependent on partner transcription factor and MAPK signaling. *Cell* **113**, 395-404 (2003).
23. Dolan, J.W. & Fields, S. Overproduction of the yeast STE12 protein leads to constitutive transcriptional induction. *Genes Dev* **4**, 492-502 (1990).
24. Yuan, Y.L. & Fields, S. Properties of the DNA-binding domain of the *Saccharomyces cerevisiae* STE12 protein. *Mol Cell Biol* **11**, 5910-5918 (1991).
25. Baur, M., Esch, R.K. & Errede, B. Cooperative binding interactions required for function of the Ty1 sterile responsive element. *Mol Cell Biol* **17**, 4330-4337 (1997).
26. Errede, B. & Ammerer, G. STE12, a protein involved in cell-type-specific transcription and signal transduction in yeast, is part of protein-DNA complexes. *Genes Dev* **3**, 1349-1361 (1989).
27. Madhani, H.D. & Fink, G.R. Combinatorial control required for the specificity of yeast MAPK signaling. *Science* **275**, 1314-1317 (1997).
28. Hoshino, A. & Fujii, H. Insertional chromatin immunoprecipitation: a method for isolating specific genomic regions. *J Biosci Bioeng* **108**, 446-449 (2009).
29. Fields, S., Chaleff, D.T. & Sprague, G.F., Jr. Yeast STE7, STE11, and STE12 genes are required for expression of cell-type-specific genes. *Mol Cell Biol* **8**, 551-556 (1988).
30. Stevenson, B.J., Rhodes, N., Errede, B. & Sprague, G.F., Jr. Constitutive mutants of the protein kinase STE11 activate the yeast pheromone response pathway in the absence of the G protein. *Genes Dev* **6**, 1293-1304 (1992).
31. Gordon, J.L., Byrne, K.P. & Wolfe, K.H. Additions, losses, and rearrangements on the evolutionary route from a reconstructed ancestor to the modern *Saccharomyces cerevisiae* genome. *PLoS Genet* **5**, e1000485 (2009).
32. Pi, H., Chien, C.T. & Fields, S. Transcriptional activation upon pheromone stimulation mediated by a small domain of *Saccharomyces cerevisiae* Ste12p. *Mol Cell Biol* **17**, 6410-6418 (1997).
33. Chou, S., Lane, S. & Liu, H. Regulation of mating and filamentation genes by two distinct Ste12 complexes in *Saccharomyces cerevisiae*. *Mol Cell Biol* **26**, 4794-4805 (2006).
34. Kramer, H. *et al.* lac repressor forms loops with linear DNA carrying two suitably spaced lac operators. *EMBO J* **6**, 1481-1491 (1987).

35. Whitson, P.A., Hsieh, W.T., Wells, R.D. & Matthews, K.S. Influence of supercoiling and sequence context on operator DNA binding with lac repressor. *J Biol Chem* **262**, 14592-14599 (1987).
36. Whitson, P.A., Hsieh, W.T., Wells, R.D. & Matthews, K.S. Supercoiling facilitates lac operator-repressor-pseudooperator interactions. *J Biol Chem* **262**, 4943-4946 (1987).
37. Eismann, E., von Wilcken-Bergmann, B. & Muller-Hill, B. Specific destruction of the second lac operator decreases repression of the lac operon in Escherichia coli fivefold. *J Mol Biol* **195**, 949-952 (1987).
38. Mossing, M.C. & Record, M.T., Jr. Thermodynamic origins of specificity in the lac repressor-operator interaction. Adaptability in the recognition of mutant operator sites. *J Mol Biol* **186**, 295-305 (1985).
39. Dodd, I.B., Perkins, A.J., Tsemitsidis, D. & Egan, J.B. Octamerization of lambda CI repressor is needed for effective repression of P(RM) and efficient switching from lysogeny. *Genes Dev* **15**, 3013-3022 (2001).
40. Revet, B., von Wilcken-Bergmann, B., Bessert, H., Barker, A. & Muller-Hill, B. Four dimers of lambda repressor bound to two suitably spaced pairs of lambda operators form octamers and DNA loops over large distances. *Curr Biol* **9**, 151-154 (1999).
41. Vilar, J.M. & Leibler, S. DNA looping and physical constraints on transcription regulation. *J Mol Biol* **331**, 981-989 (2003).
42. Schoenfelder, S. *et al.* Preferential associations between co-regulated genes reveal a transcriptional interactome in erythroid cells. *Nat Genet* (2009).
43. Spilianakis, C.G., Lalioti, M.D., Town, T., Lee, G.R. & Flavell, R.A. Interchromosomal associations between alternatively expressed loci. *Nature* **435**, 637-645 (2005).
44. Zhao, Z. *et al.* Circular chromosome conformation capture (4C) uncovers extensive networks of epigenetically regulated intra- and interchromosomal interactions. *Nat Genet* **38**, 1341-1347 (2006).
45. Apostolou, E. & Thanos, D. Virus Infection Induces NF-kappaB-dependent interchromosomal associations mediating monoallelic IFN-beta gene expression. *Cell* **134**, 85-96 (2008).
46. Lin, C. *et al.* Nuclear receptor-induced chromosomal proximity and DNA breaks underlie specific translocations in cancer. *Cell* **139**, 1069-1083 (2009).
47. Brickner, J.H. & Walter, P. Gene recruitment of the activated INO1 locus to the nuclear membrane. *PLoS Biol* **2**, e342 (2004).
48. Kitamura, E., Blow, J.J. & Tanaka, T.U. Live-cell imaging reveals replication of individual replicons in eukaryotic replication factories. *Cell* **125**, 1297-1308 (2006).
49. Meister, P., Taddei, A. & Gasser, S.M. In and out of the replication factory. *Cell* **125**, 1233-1235 (2006).
50. Taddei, A. *et al.* Nuclear pore association confers optimal expression levels for an inducible yeast gene. *Nature* **441**, 774-778 (2006).

51. Branco, M.R. & Pombo, A. Intermingling of chromosome territories in interphase suggests role in translocations and transcription-dependent associations. *PLoS Biol* **4**, e138 (2006).
52. Lisby, M., Mortensen, U.H. & Rothstein, R. Colocalization of multiple DNA double-strand breaks at a single Rad52 repair centre. *Nat Cell Biol* **5**, 572-577 (2003).
53. Bishop, D.K. RecA homologs Dmc1 and Rad51 interact to form multiple nuclear complexes prior to meiotic chromosome synapsis. *Cell* **79**, 1081-1092 (1994).
54. Cockell, M. & Gasser, S.M. Nuclear compartments and gene regulation. *Curr Opin Genet Dev* **9**, 199-205 (1999).
55. Parker, R. & Sheth, U. P bodies and the control of mRNA translation and degradation. *Mol Cell* **25**, 635-646 (2007).
56. Sheth, U. & Parker, R. Decapping and decay of messenger RNA occur in cytoplasmic processing bodies. *Science* **300**, 805-808 (2003).
57. Cougot, N., Babajko, S. & Seraphin, B. Cytoplasmic foci are sites of mRNA decay in human cells. *J Cell Biol* **165**, 31-40 (2004).
58. Storici, F., Durham, C.L., Gordenin, D.A. & Resnick, M.A. Chromosomal site-specific double-strand breaks are efficiently targeted for repair by oligonucleotides in yeast. *Proc Natl Acad Sci U S A* **100**, 14994-14999 (2003).
59. Magliery, T.J. *et al.* Detecting protein-protein interactions with a green fluorescent protein fragment reassembly trap: scope and mechanism. *J Am Chem Soc* **127**, 146-157 (2005).
60. Meneghini, M.D., Wu, M. & Madhani, H.D. Conserved histone variant H2A.Z protects euchromatin from the ectopic spread of silent heterochromatin. *Cell* **112**, 725-736 (2003).
61. Raisner, R.M. *et al.* Histone variant H2A.Z marks the 5' ends of both active and inactive genes in euchromatin. *Cell* **123**, 233-248 (2005).
62. Lau, I.F. *et al.* Spatial and temporal organization of replicating *Escherichia coli* chromosomes. *Mol Microbiol* **49**, 731-743 (2003).
63. Nobile, C.J. *et al.* Biofilm matrix regulation by *Candida albicans* Zap1. *PLoS Biol* **7**, e1000133 (2009).
64. Hartley, P.D. & Madhani, H.D. Mechanisms that specify promoter nucleosome location and identity. *Cell* **137**, 445-458 (2009).

# Figures and Tables

Figure 1 a-d

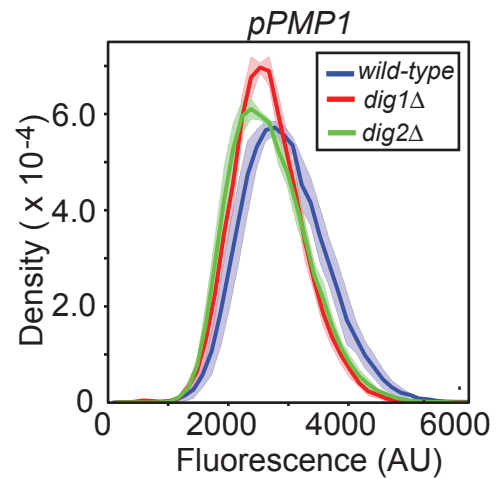
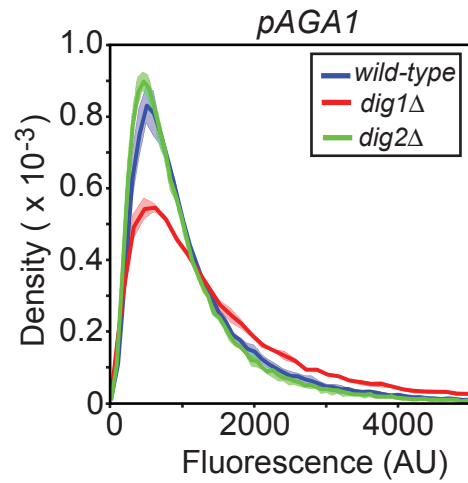
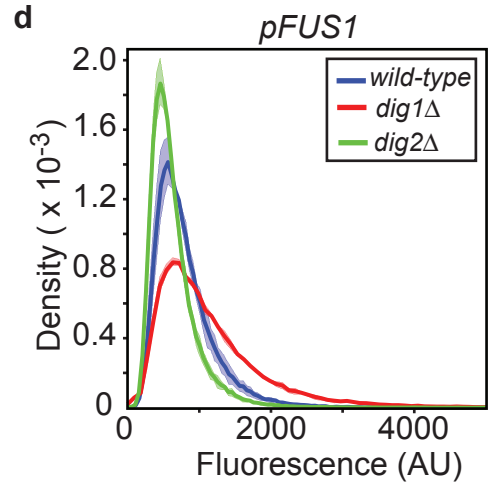
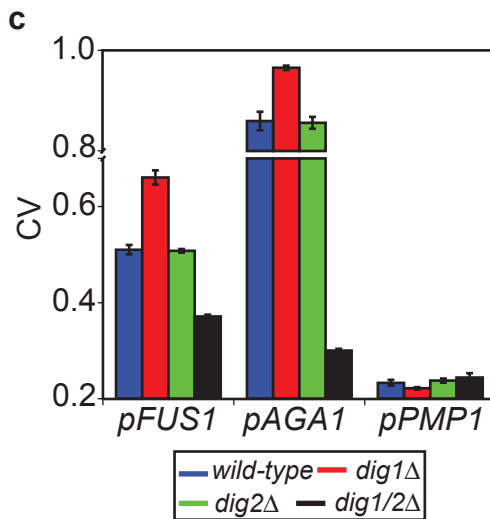
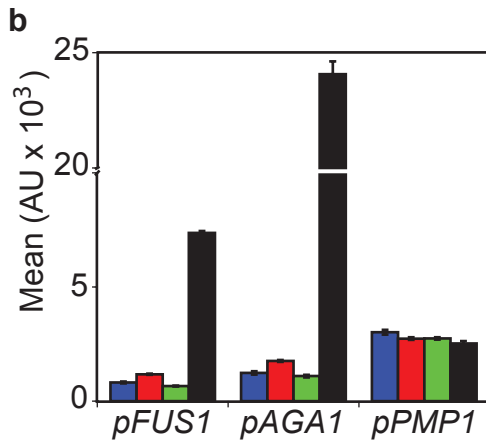
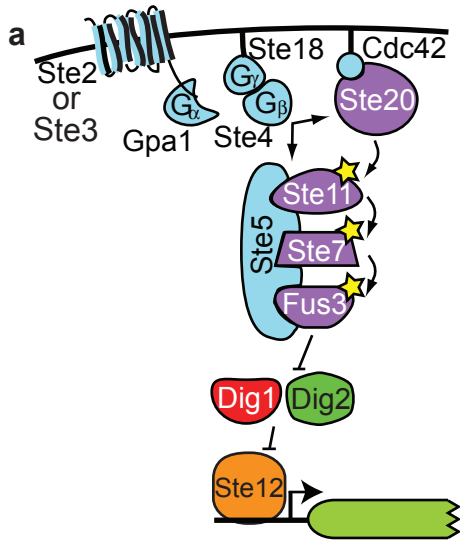
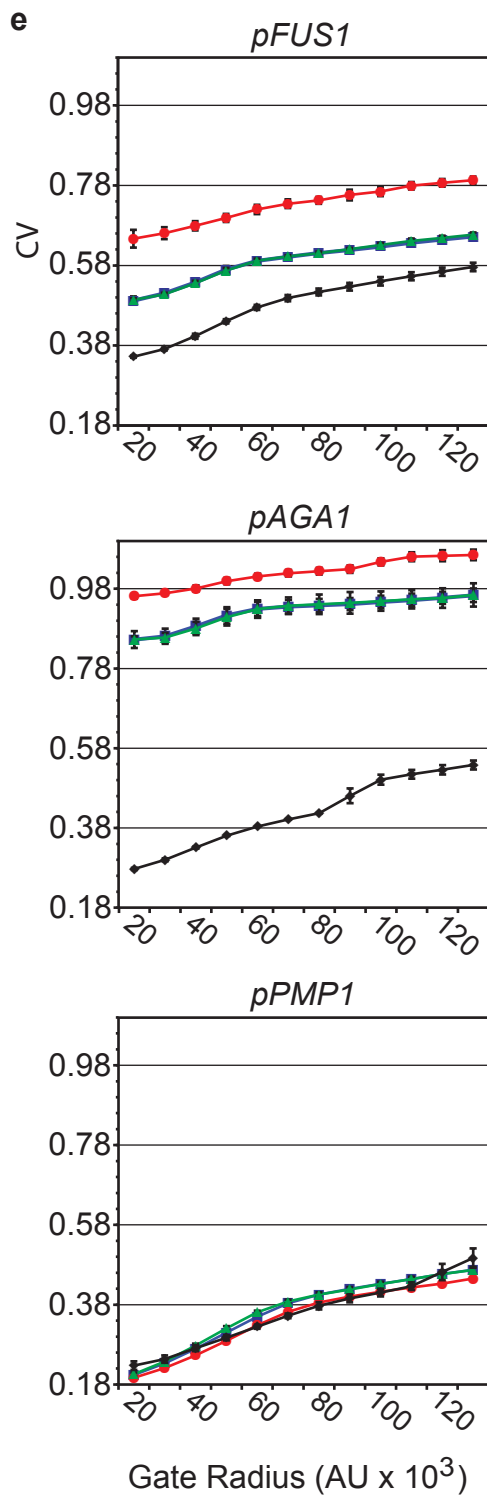


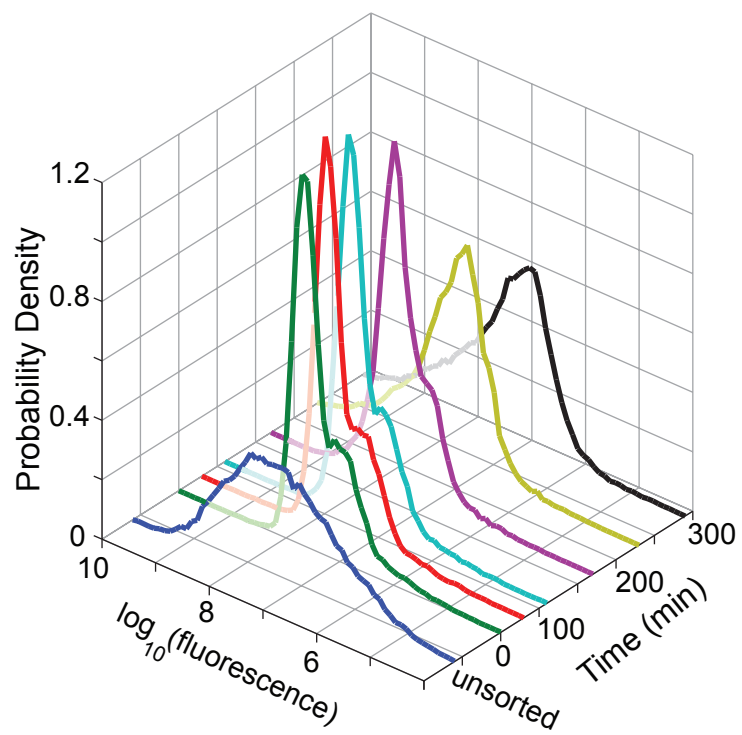
Figure 1 e





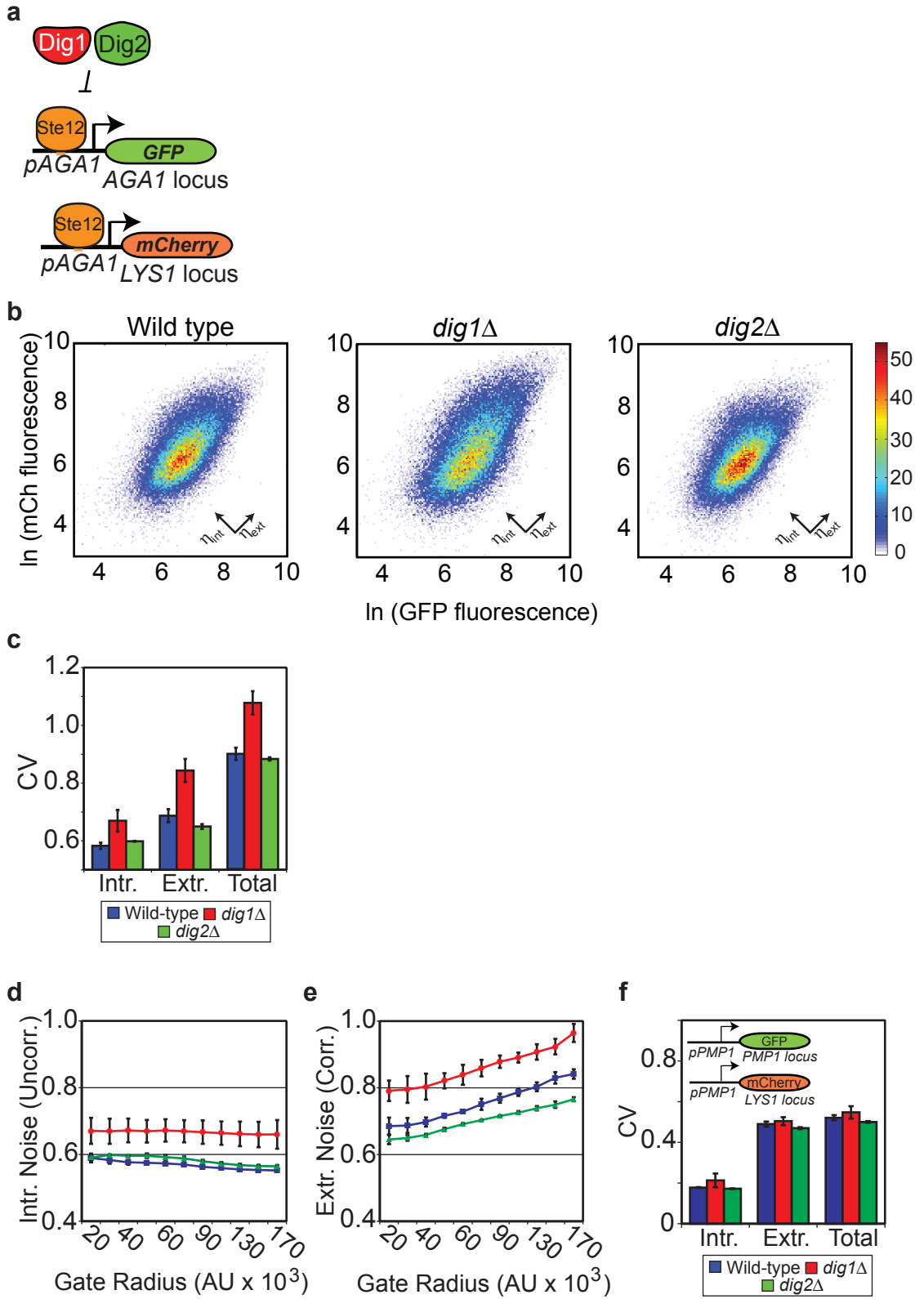
**Figure 1:** *dig1* $\Delta$ , but not *dig2* $\Delta$ , cells display increased noise in yeast mating pathway outputs. **a.** Schematic of the yeast mating MAPK pathway. Note: for simplicity the Ste12-target gene is illustrated as having one Ste12-binding site. **b.** Mean output for *pFUS1-YFP*, *pAGA1-YFP*, and *pPMP1-GFP* in wild-type (blue), *dig1* $\Delta$  (red), *dig2* $\Delta$  (green), and *dig1* $\Delta*dig2* $\Delta$  (black) mutants in absence of  $\alpha$ -Factor. Error bars indicate the standard deviation of three replicate experiments. The Y-axis is broken between 10,000 and 20,000 AU. **c.** Bar graphs illustrating the coefficient of variation (CV) for each strain as in **b.** The Y-axis is broken between 0.7 and 0.8. T-test was used to calculate  $P = 0.0003$  for difference between *pAGA1-YFP* and *pAGA1-YFP dig1* $\Delta$  and  $P = 0.0014$  for difference between *pFUS1-YFP* and *pFUS1-YFP dig1* $\Delta$ . **d.** Probability density functions (PDFs) of wild-type (blue) *dig1* $\Delta$  (red) and *dig2* $\Delta$  (green) for each reporter: *pFUS1-YFP* (left), *pAGA1-YFP* (middle) and *pPMP1-GFP* (right). Solid lines represent the average PDF for three replicates while the envelope indicates the standard deviation. (**b-d.** Data shown is for gate 5, see Methods.) **e.** CV vs. gate radius for *pFUS1-YFP* strains (left), *pAGA1-YFP* strains (middle) and *pPMP1-GFP* strains (right). **b-e.** See Methods for gate sizes and numbers of cells analyzed. Error bars represent the standard deviation of three replicate experiments.$

Figure 2



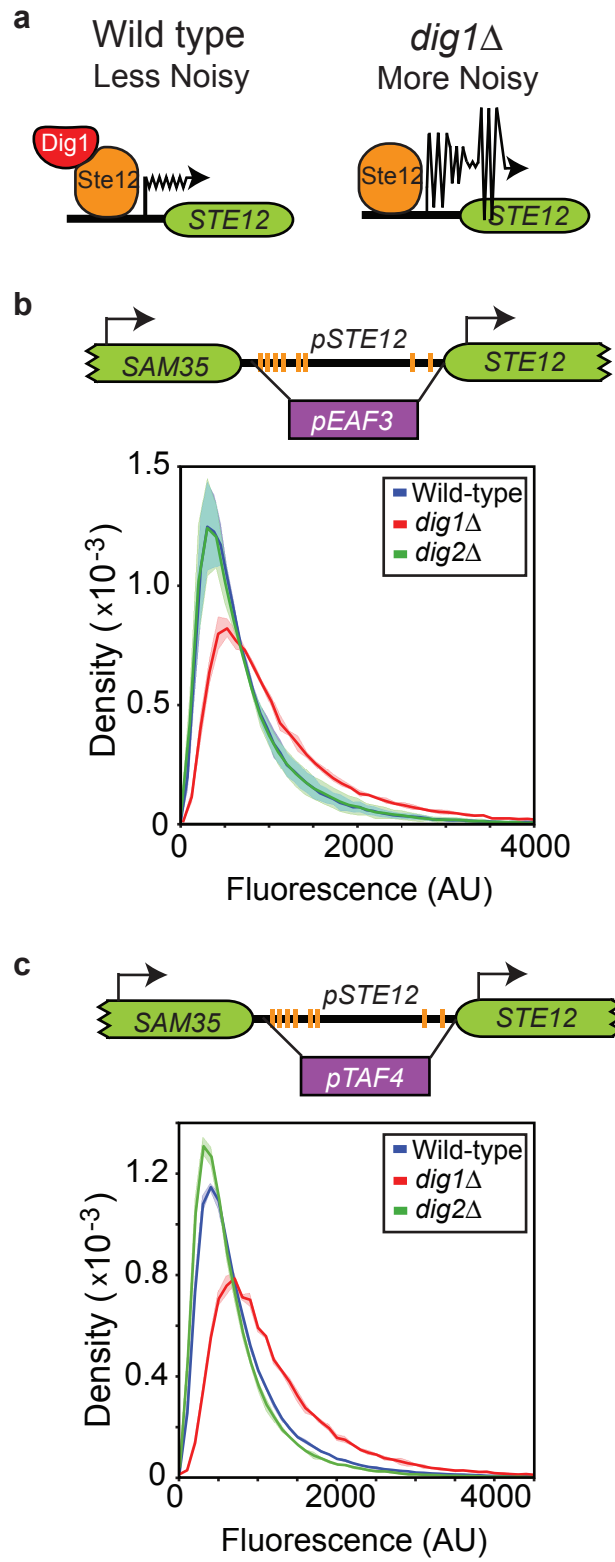
**Figure 2:** Sorted *dig1* $\Delta$  cells can regenerate the entire *pAGA1-YFP* output distribution. *dig1* $\Delta$  cells expressing mean levels of *pAGA1-YFP* were sorted and re-grown over time. At t = 0, 60, 120, 180, 240 and 300 min, cells were removed and the fluorescence distribution was determined.

Figure 3



**Figure 3:** Extrinsic and intrinsic noise in output of mating pathway increase in *dig1Δ* cell populations. **A.** Schematic of two-colour experiment. *pAGA1-GFP* is in the endogenous *AGA1* locus, while *pAGA1-mCherry-AGA1 3'UTR* is inserted into the *LYS1* locus. **B.** Density plots of wild-type (left), *dig1Δ* (middle) and *dig2Δ* (right). **c.** Quantification of intrinsic, extrinsic and total noise of wild-type (blue), *dig1Δ* (red), *dig2Δ* (green) populations. Each value is the mean of three replicates and error bars indicate the standard deviation. T-test was used to calculate  $P = 0.035$  for increase in intrinsic noise and  $P = 0.009$  for increase in extrinsic noise in *dig1Δ* mutant. Total noise was calculated as  $\eta_{tot} = \sqrt{\eta_{ext}^2 + \eta_{int}^2}$ . **d,e.** Plots of intrinsic (**d**) and extrinsic (**e**) noise vs. gate radius to control for cell size and shape. Error bars indicate the standard deviation of three replicates. **f.** Quantification of intrinsic, extrinsic and total noise in Ste12-independent reporter strain in which two fluorophores are driven by *pPMP1* (inset).

Figure 4



**Figure 4:** Increased noise in mating pathway outputs in *dig1Δ* cells is not due to feedback at the *STE12* promoter. **a.** Model for the increased noise in the mating pathway in *dig1Δ* cells. **b.** *pSTE12* was replaced with the Ste12-independent promoter *pEAF3* (above). PDFs of *pAGA1-YFP* strains containing *pEAF3-STE12* (below). **c.** *pSTE12* was replaced with the Ste12-independent promoter *pTAF4* (above). PDFs of *pste12::pTAF4* strains (below). **b,c.** wild-type in blue, *dig1Δ* in red and *dig2Δ* in green. Solid line is the mean of three replicate experiments and the envelope reflects standard deviation of three replicates.

Figure 5 a

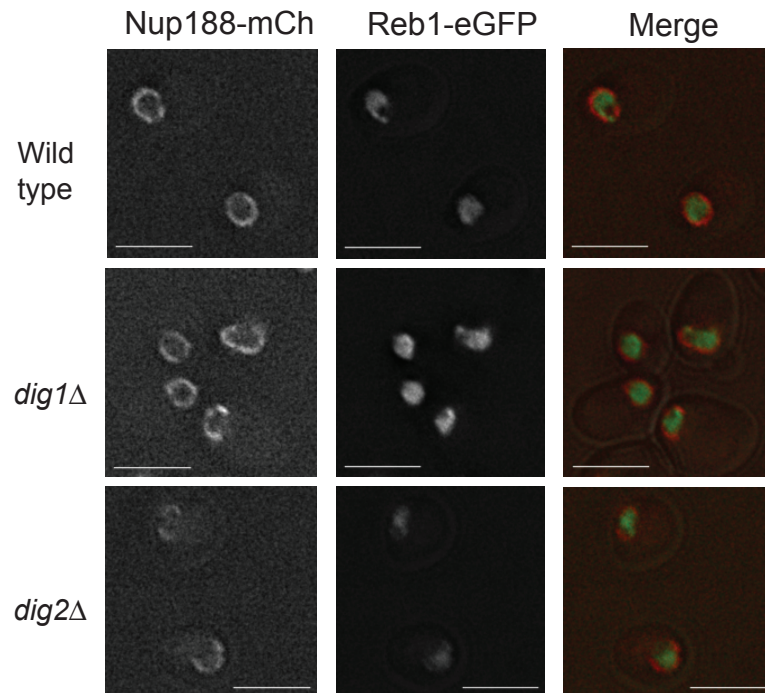
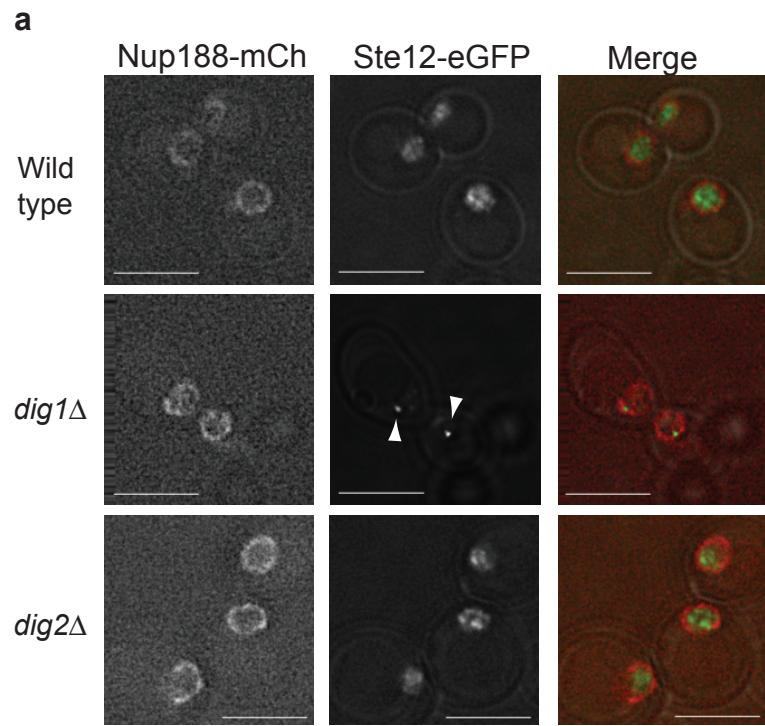




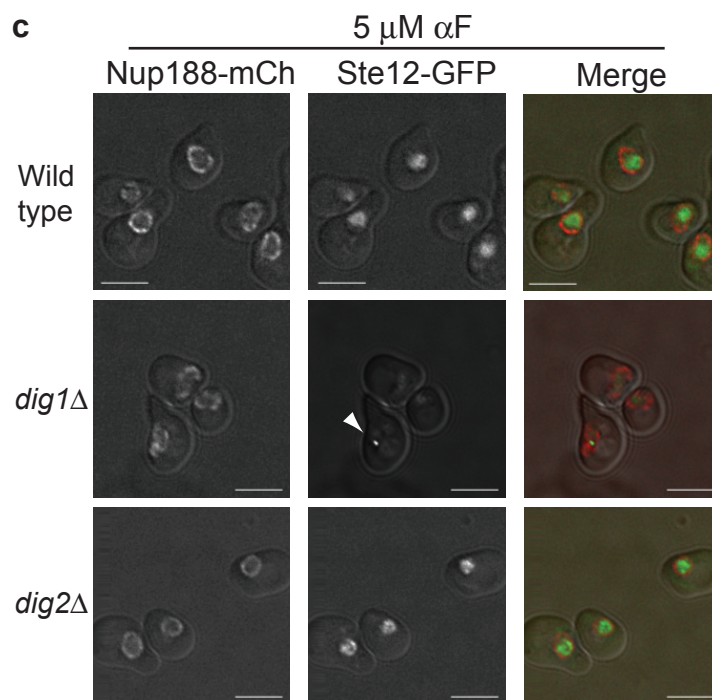
Figure 5 b-d

**b**

|                        | Percentage of Cells with Foci |      |      |    |
|------------------------|-------------------------------|------|------|----|
|                        | 0                             | 1    | 2    | >2 |
| Ste12-GFP              | 100                           | 0    | 0    | 0  |
| <i>dig1</i> $\Delta$ * | 35.3                          | 51.7 | 12.9 | 0  |
| <i>dig2</i> $\Delta$   | 97.9                          | 2.1  | 0    | 0  |

\*  $P < 0.001$

**c**



**d**

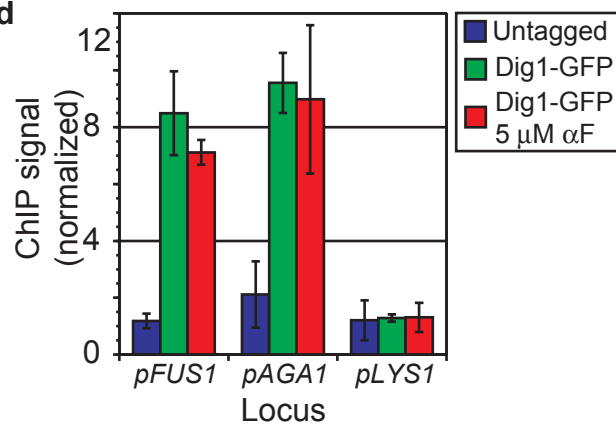


**Figure 5:** Ste12-GFP forms nuclear foci in *dig1Δ* cells. **a.** Fluorescence microscopy images of Ste12-GFP/Nup188-mCherry (left) and Reb1-GFP/Nup188-mCherry (right) from top to bottom: wild-type, *dig1Δ*, and *dig2Δ*. Ste12-GFP forms nuclear foci in *dig1Δ* (see white arrow heads). **b.** Quantification of foci seen in **(a)** n = 100 (wt), n = 116 (*dig1Δ*), n = 95 (*dig2Δ*). Distributions of foci in all mutants were compared to wild-type by the Chi-square test and only the distribution of foci in *dig1Δ* was statistically significant ( $P < 0.001$ ). **c.** Ste12-GFP localization upon addition of 5  $\mu\text{M}$   $\alpha$ -Factor for 1 hr. **d.** Normalized ChIP signal of Dig1-GFP at *AGA1*, *FUS1* and *LYS1* promoters in absence and presence of 5  $\mu\text{M}$  pheromone. Scale bar for all images is 5  $\mu\text{m}$ .

Figure 6 a,b

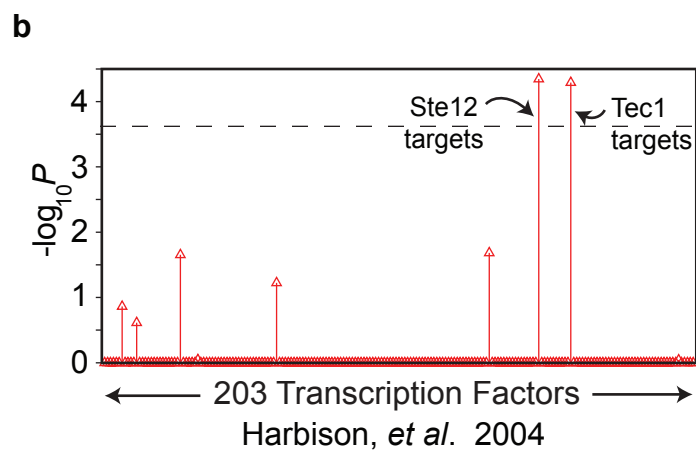
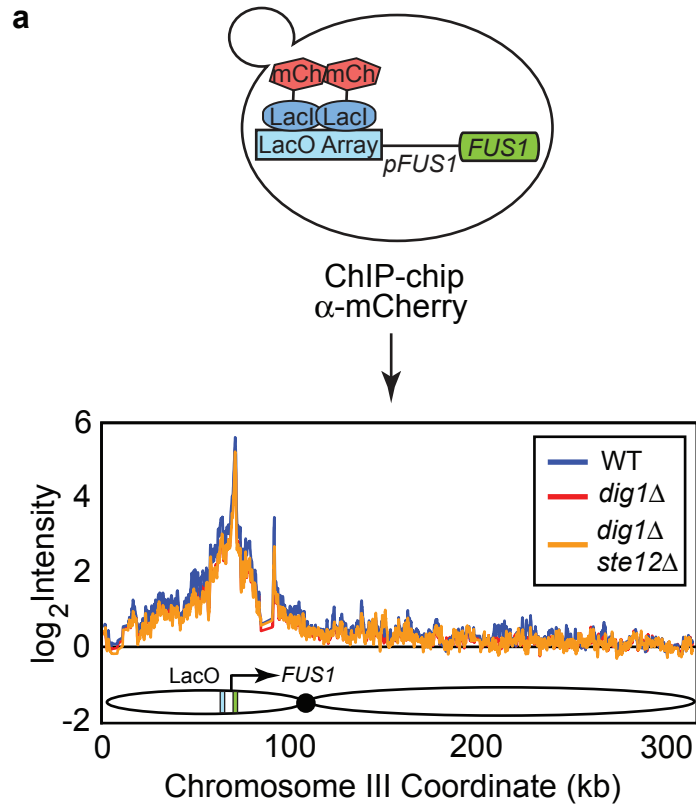
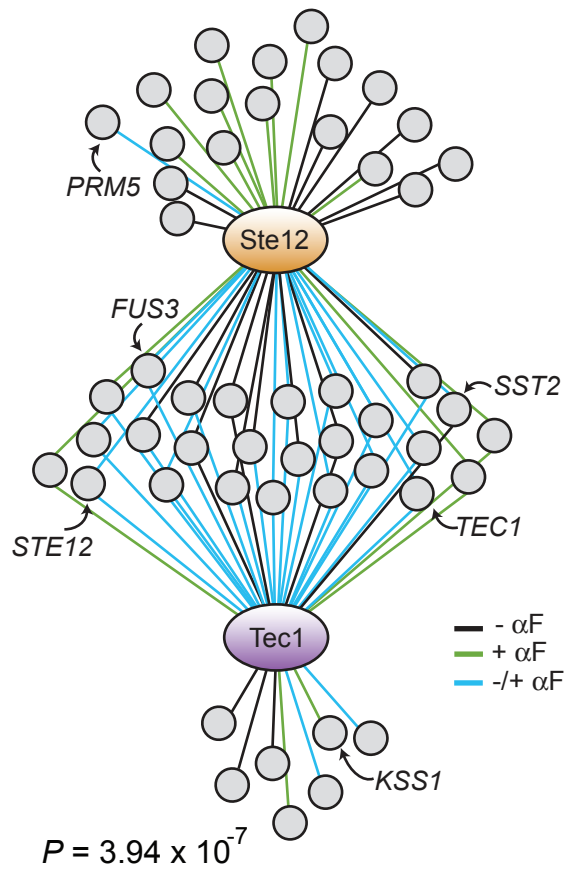


Figure 6 c,d

**c**

| Transcription Factor | Hypergeometric <i>P</i> -val |                        |
|----------------------|------------------------------|------------------------|
|                      | <i>dig1Δ</i> /wt             | <i>dig1Δste12Δ</i> /wt |
| Ste12                | $4.52 \times 10^{-5}$        | 1.0                    |
| Tec1                 | $5.12 \times 10^{-5}$        | 1.0                    |

**d**



**Figure 6:** ChIP-chip of Ste12-target locus reveals long-range interactions with other Ste12-target genes. **a.** Experimental set-up. LacI-mCherry was immunoprecipitated from cells and the *FUS1* locus (green), marked with an array of Lac operators (light blue), was efficiently pulled down (see peaks centred on Lac operators in graph below) in wild-type (blue), *dig1Δ* (red) and *dig1Δste12Δ* (orange) cells. The graph below illustrates the ChIP-chip signal along chromosome 3, where the array of Lac operators is inserted. See Methods for experimental details. **b.** Difference maps were calculated and genes were aligned by increasing median value of the region spanning -500bp to 0bp, with respect to the translation start site. The top 5% of differences (269 genes, Supplementary Information, Table S1) were analyzed for enrichment of target genes of 203 transcription factors<sup>21</sup>. The dashed line indicates the Bonferroni-corrected *P* value of 0.05. **c.** Bonferroni-corrected *P* values for enrichment of Ste12- and Tec1-target genes in the top 5% of genes with the greatest differences in *dig1Δ* vs. WT and *dig1Δste12Δ* vs. WT (Supplementary Information, Table S1). **d.** Ste12- and Tec1 target genes (in presence and absence of pheromone<sup>21</sup>) found in the list of 5% of genes with the largest differences in *dig1Δ* vs. WT datasets. *P* values calculated by hypergeometric testing.

Figure 7 a,b

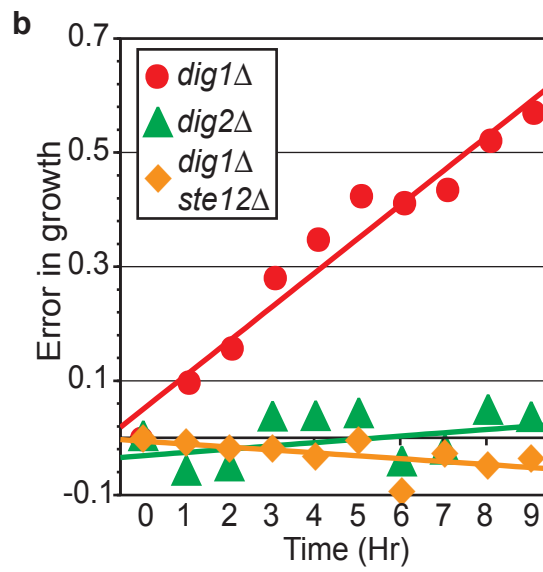
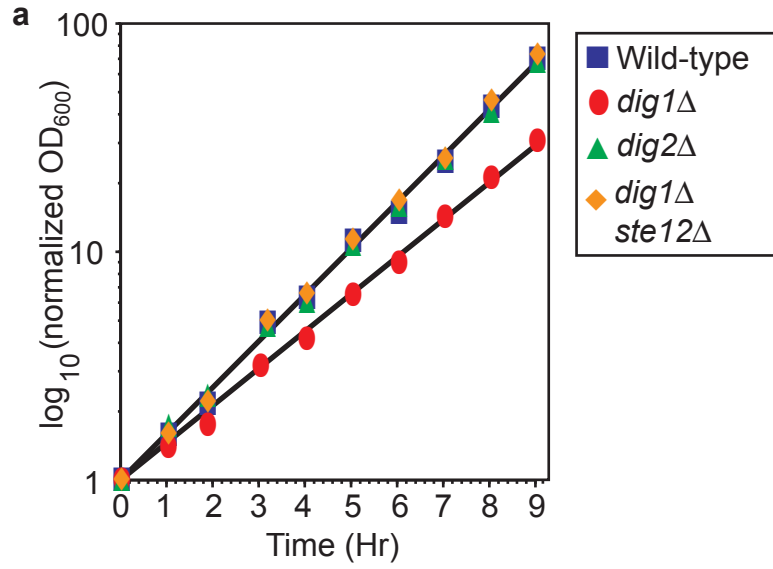
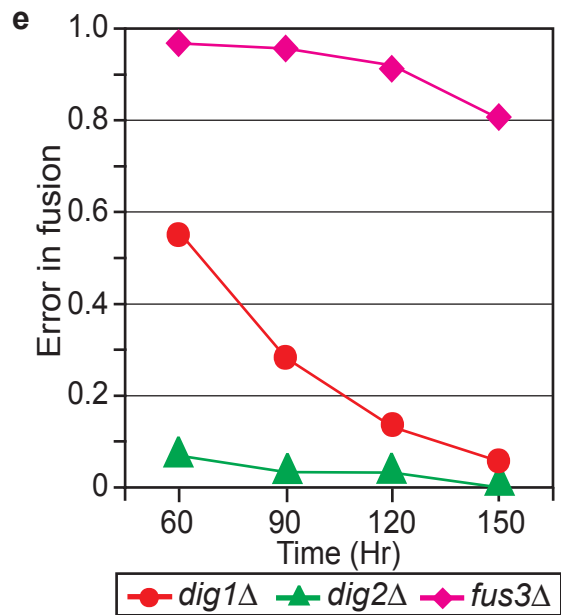
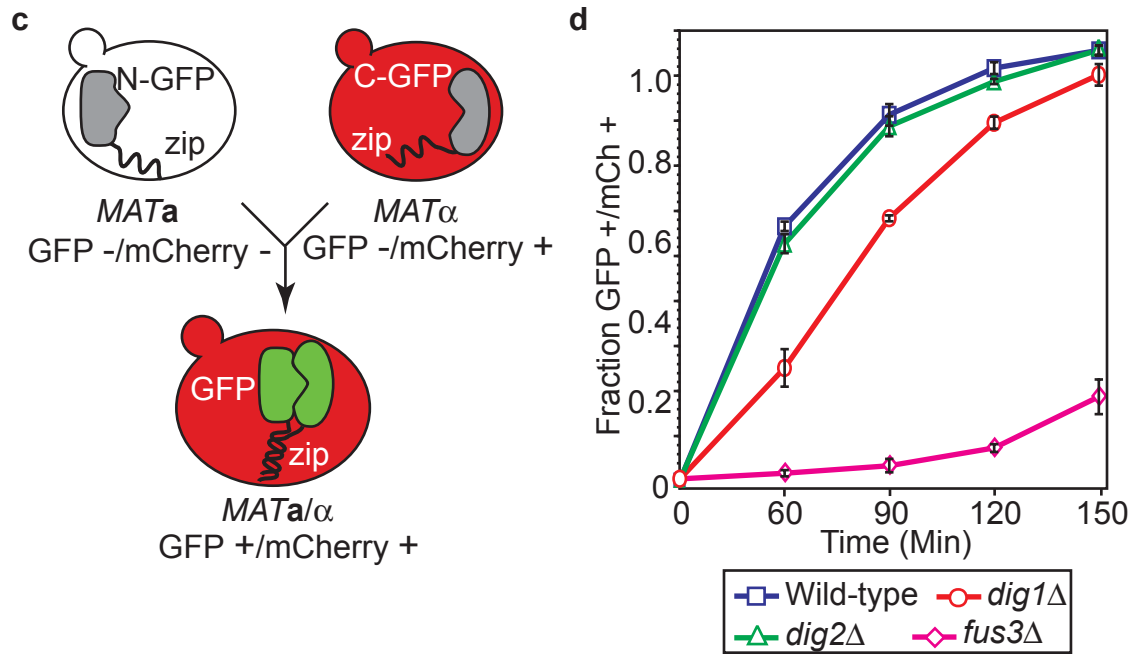


Figure 7 c-e



**Figure 7:** *dig1Δ* cells display defects in growth and cell-cell fusion. **a.** Log phase wild-type (blue squares), *dig1Δ* (red circles), *dig2Δ* (green triangles) and *dig1Δste12Δ* (orange diamonds) cells were grown for 9 hrs and OD<sub>600</sub> was measured every hour. **b.** Error in growth. OD<sub>600</sub> of mutant (*dig1Δ* in red, *dig2Δ* in green and *dig1Δste12Δ* in orange) was compared to that of wild type by calculating:  $1 - [\text{OD}_{600}(\text{mutant})]/\text{OD}_{600}(\text{wild-type})$ . **c.** Schematic for FACS-based cell fusion assay. See Methods for details. **d.** Fraction of GFP+/mCherry+ cells over time for wild-type (blue), *dig1Δ* (red), *dig2Δ* (green) and *fus3Δ* (pink). Samples were analyzed at 0, 60, 90, 120 and 150 min. Error bars indicate the standard deviation of three replicates. **e.** Cell-cell fusion error for mutants *dig1Δ* in red, *dig2Δ* in green and *fus3Δ* in pink was calculated in the following manner:  $1 - [(\text{fraction mutant fused})/(\text{fraction wild-type fused})]$ .



Figure 8 a

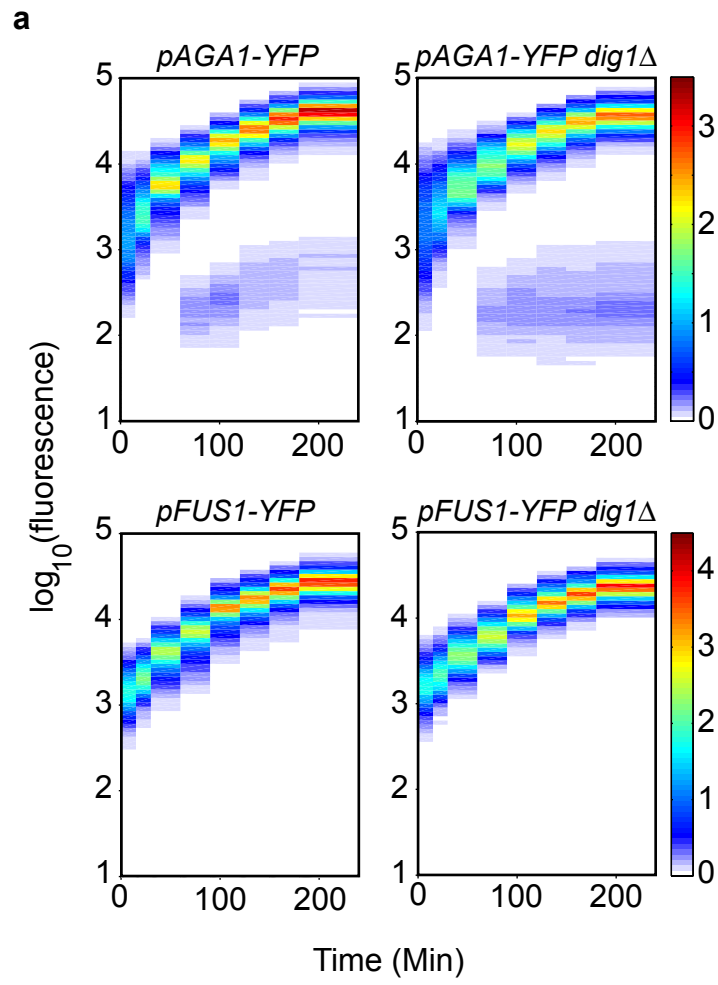
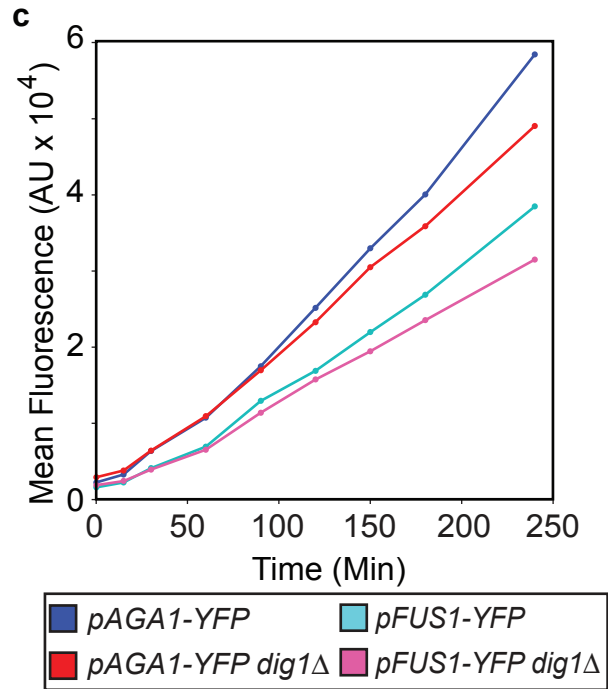
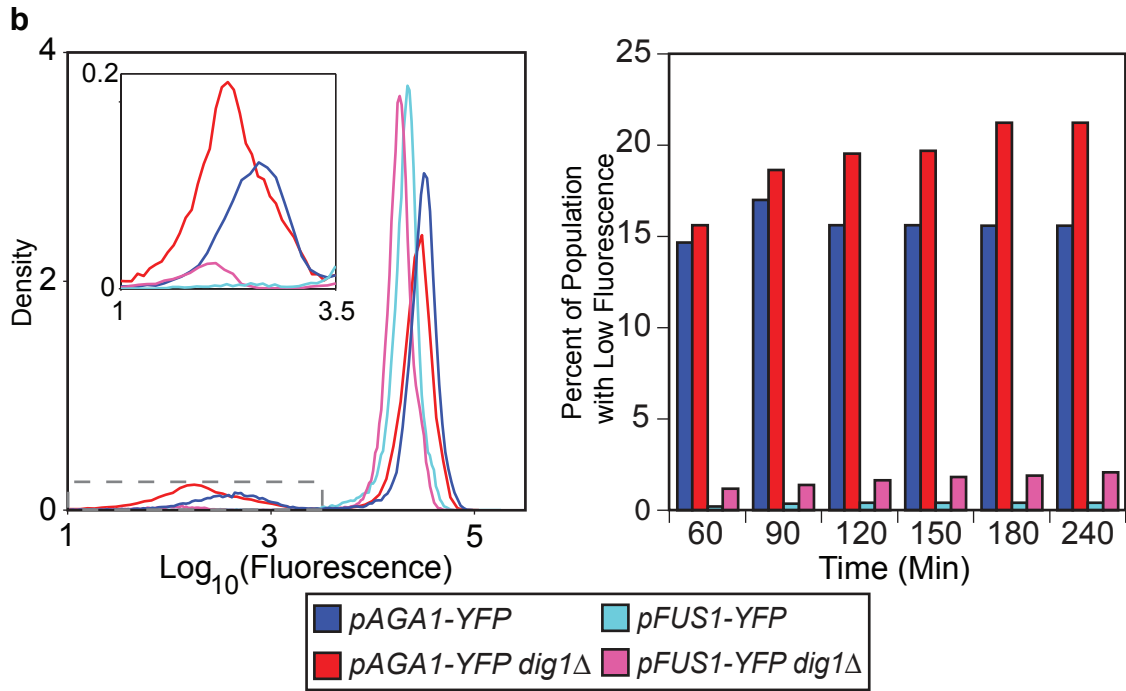
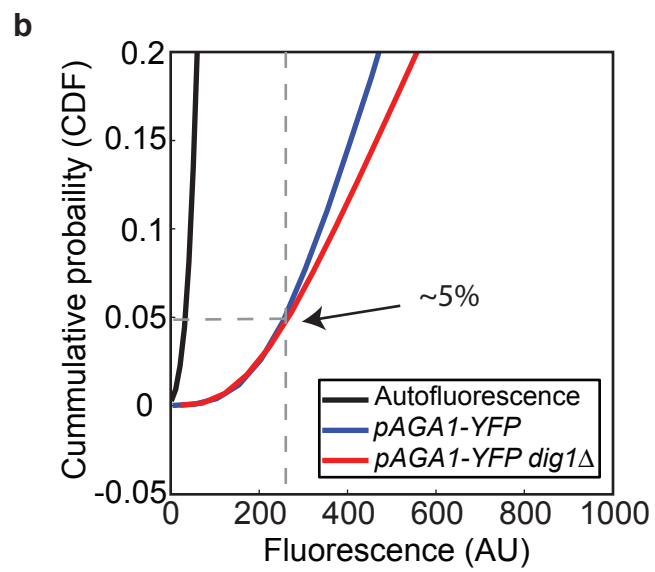
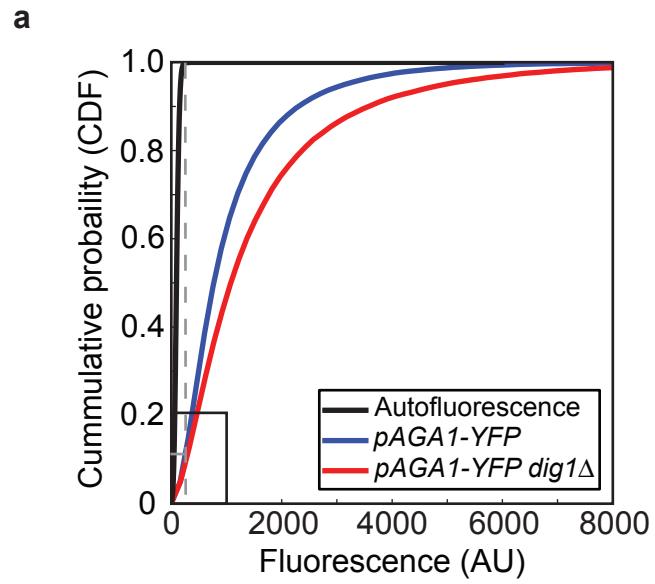


Figure 8 b,c



**Figure 8:** Time course of induction of *pAGA1-YFP* and *pFUS1-YFP* after treatment with pheromone. **a.** Heat map of induction of *pAGA1-YFP* (left) and *pFUS1-YFP* (right) in wild-type and *dig1Δ* cells. Samples were analyzed at 0, 15, 30, 60, 90, 120, 150, 180 and 240 min. **b. left:** Probability density functions for 150 min time point of *pAGA1-YFP* (dark blue), *pAGA1-YFP dig1Δ* (dark red), *pFUS1-YFP* (light blue) and *pFUS1-YFP dig1Δ* (pink). The inset is a blow-up of the area marked by the grey-dashed line. **right:** The percentage of cells in the low fluorescence population versus time. **c.** Mean fluorescence of the transcriptionally induced populations in part **a** versus time. Transcriptionally induced and un-induced populations (see **a**) were separated and the means of the high expressing populations were calculated for each time point. The colours are as in part **b**. **a-c.** Data shown are from a single representative experiment, but results have been replicated in three separate experiments.

Supplementary Figure S1 a,b



Supplementary Figure S1 c,d

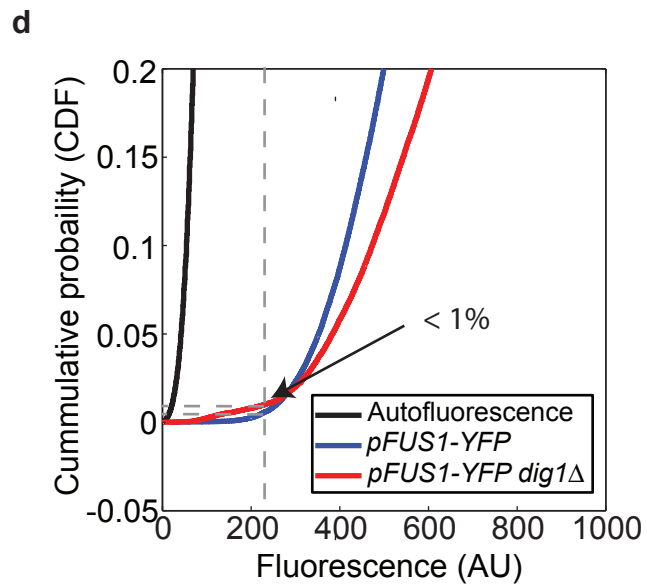
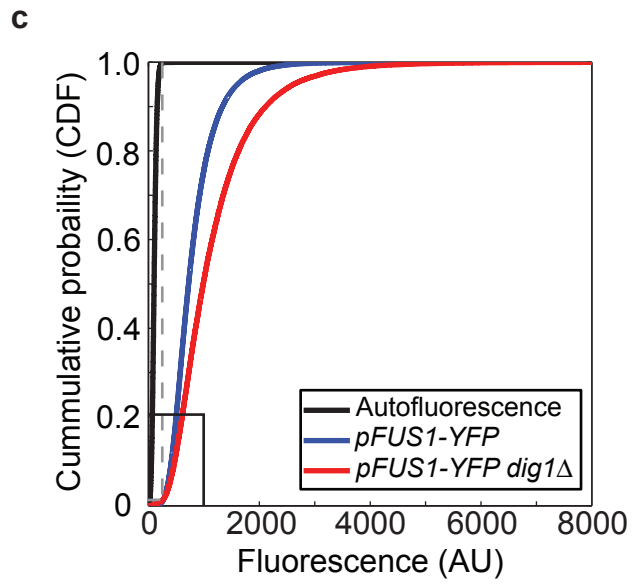


**Figure S1:** Cumulative probability density functions (CDFs) to measure overlap of fluorescent populations and autofluorescence. **a.** CDFs for non-fluorescent strain (black), *pAGA1-YFP* (blue), *pAGA1 dig1Δ* (red). **b.** Magnification of black box in **(a)**. **c.** CDFs for non-fluorescent strain (black), *pFUS1-YFP* (blue) and *pFUS1 dig1Δ* (red). **d.** Magnification of black box in **(c)**. **a-d.** The gray dashed line indicates the maximum fluorescence value of non-fluorescent yeast (CDF=1.0). *pAGA1-YFP* wild-type and *dig1Δ* distributions have CDF values of ~0.05 for this fluorescence value (5% of distribution overlaps with autofluorescence). *pFUS1-YFP* wild type and *dig1Δ* distributions have CDF values of <0.01 at this fluorescence value.

Supplementary Figure S2

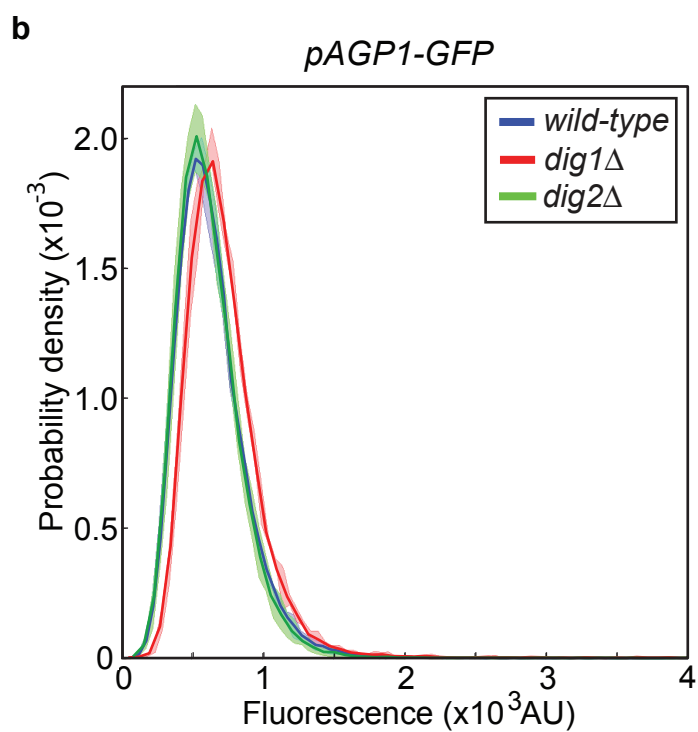
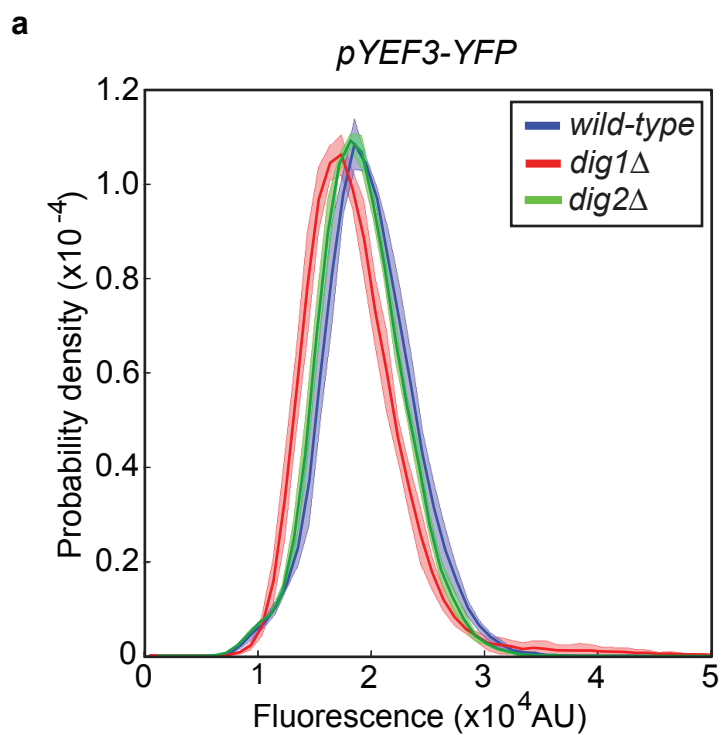
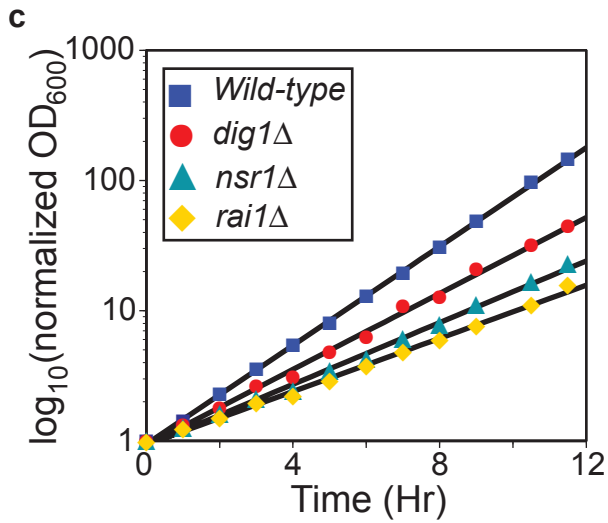
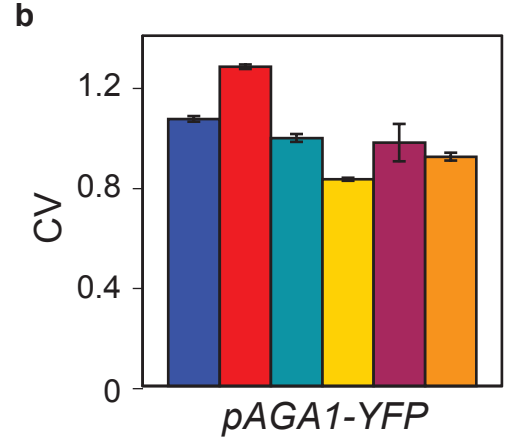
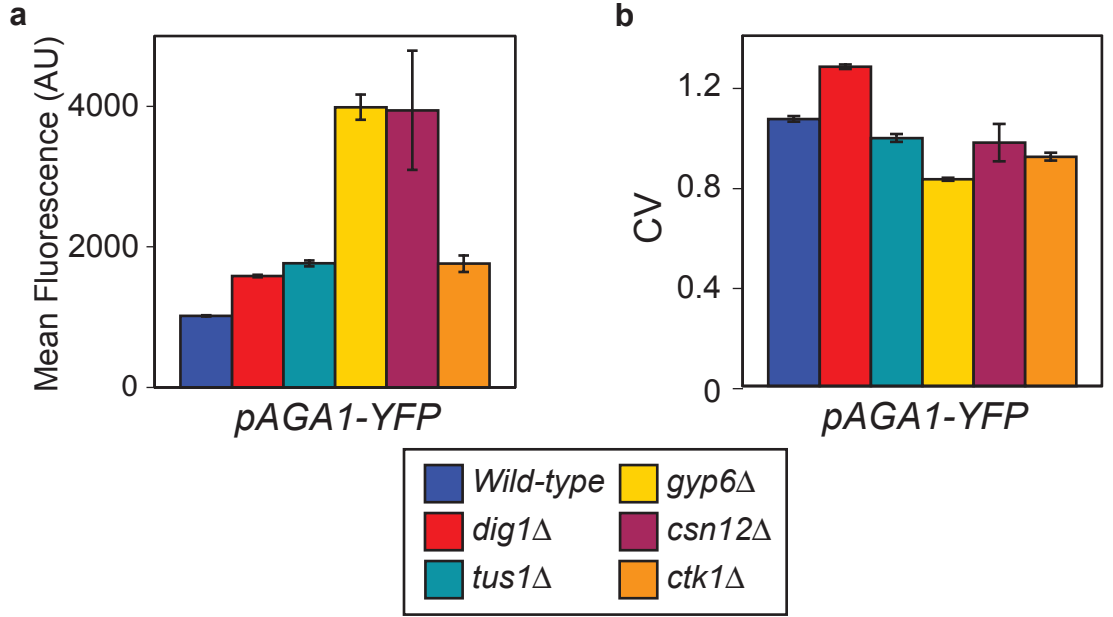


**Figure S2:** Probability density functions for two Ste12-independent promoters, **a.** *pYEF3* and **b.** *pAGP1*, driving YFP and GFP, respectively. Wild-type is in blue, *dig1Δ* is in red, and *dig2Δ* is in green. Solid line is the mean of three replicate experiments and the envelope reflects standard deviation of three replicates.



Supplementary Figure S3



| Strain       | Doubling Time (Hr) |
|--------------|--------------------|
| WT           | 1.6                |
| <i>dig1Δ</i> | 2.03               |
| <i>nsr1Δ</i> | 2.54               |
| <i>rai1Δ</i> | 2.95               |

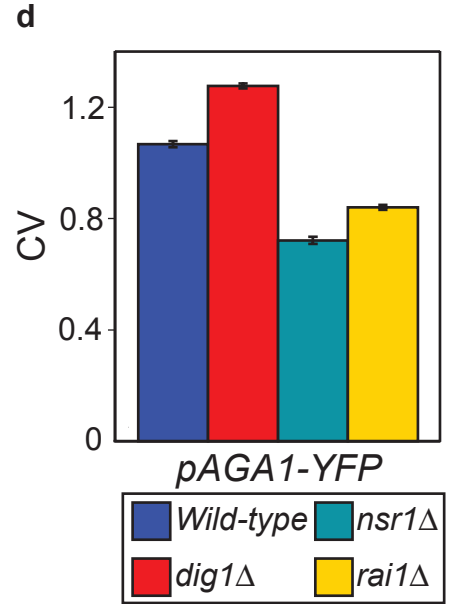
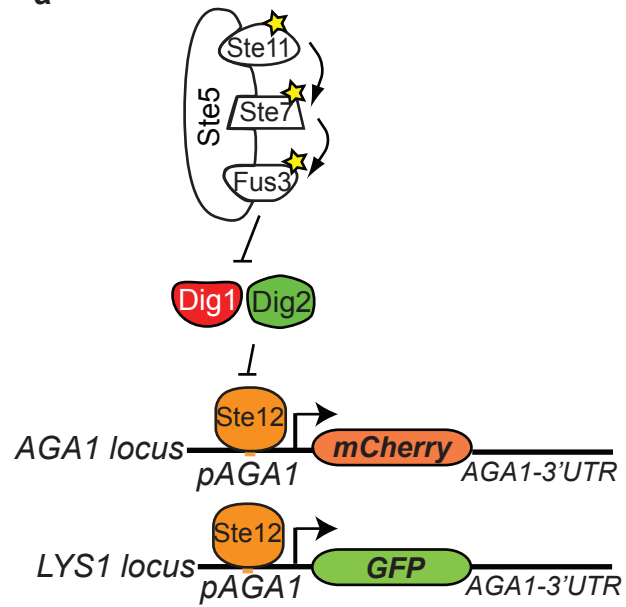


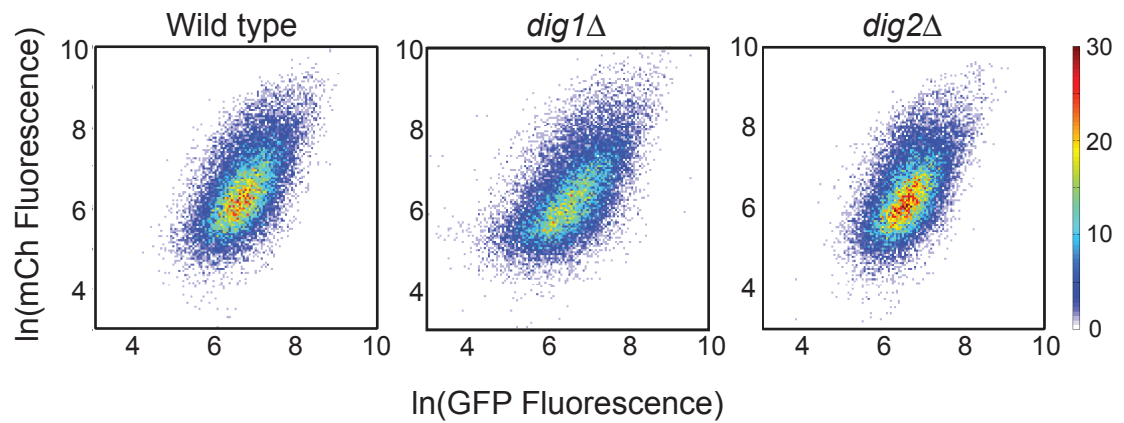
**Figure S3:** High mean and slow growth are not sufficient to cause increased noise in the output of the pheromone response pathway. **a.** Mean output of *pAGA1-YFP* in wild-type (blue), *dig1Δ* (red), *tus1Δ* (turquoise), *gyp6Δ* (yellow), *csn12Δ* (purple) and *ctk1Δ* (orange). Error bars represent the standard deviation of three replicates. **b.** CV of *pAGA1-YFP* output distributions. Strains are in same colour as in **a.** **c.** Normalized OD<sub>600</sub> versus time for wild-type (blue squares), *dig1Δ* (red circles), *nsr1Δ* (turquoise triangles) and *rai1Δ* (yellow diamonds). Doubling times were calculated and are listed in the table. **d.** CV of *pAGA1-YFP* output distributions of same strains as in **c.**

Supplementary Figure S4 a,b

**a**



**b**



Supplementary Figure S4 c-e

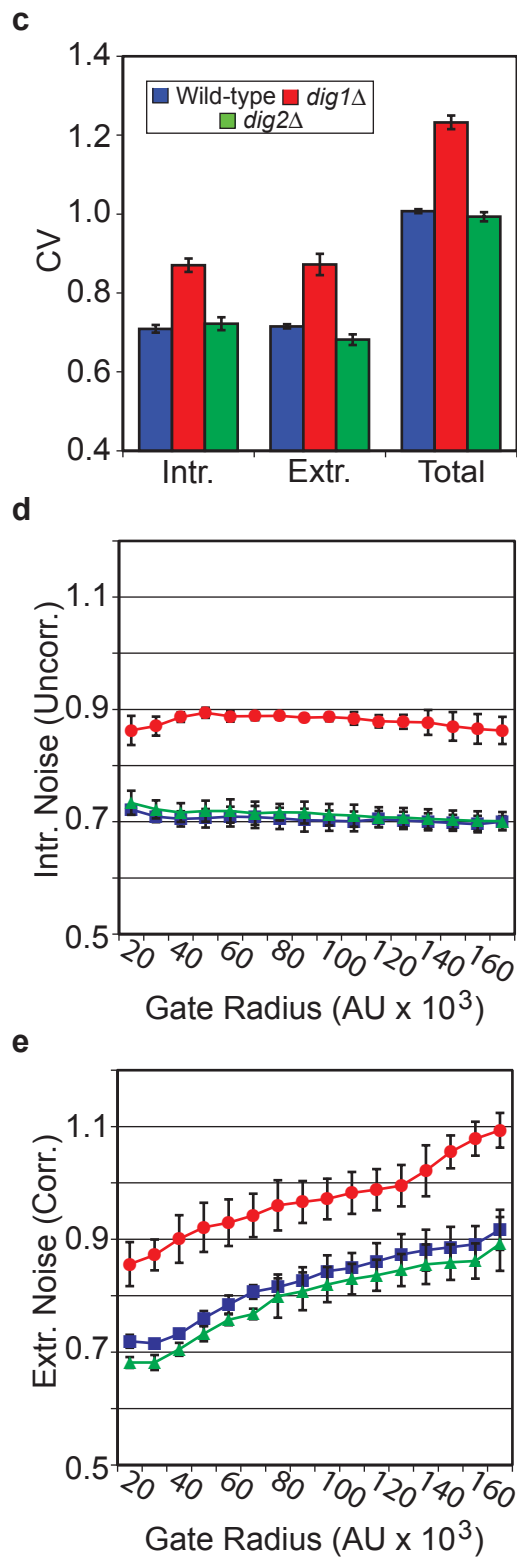
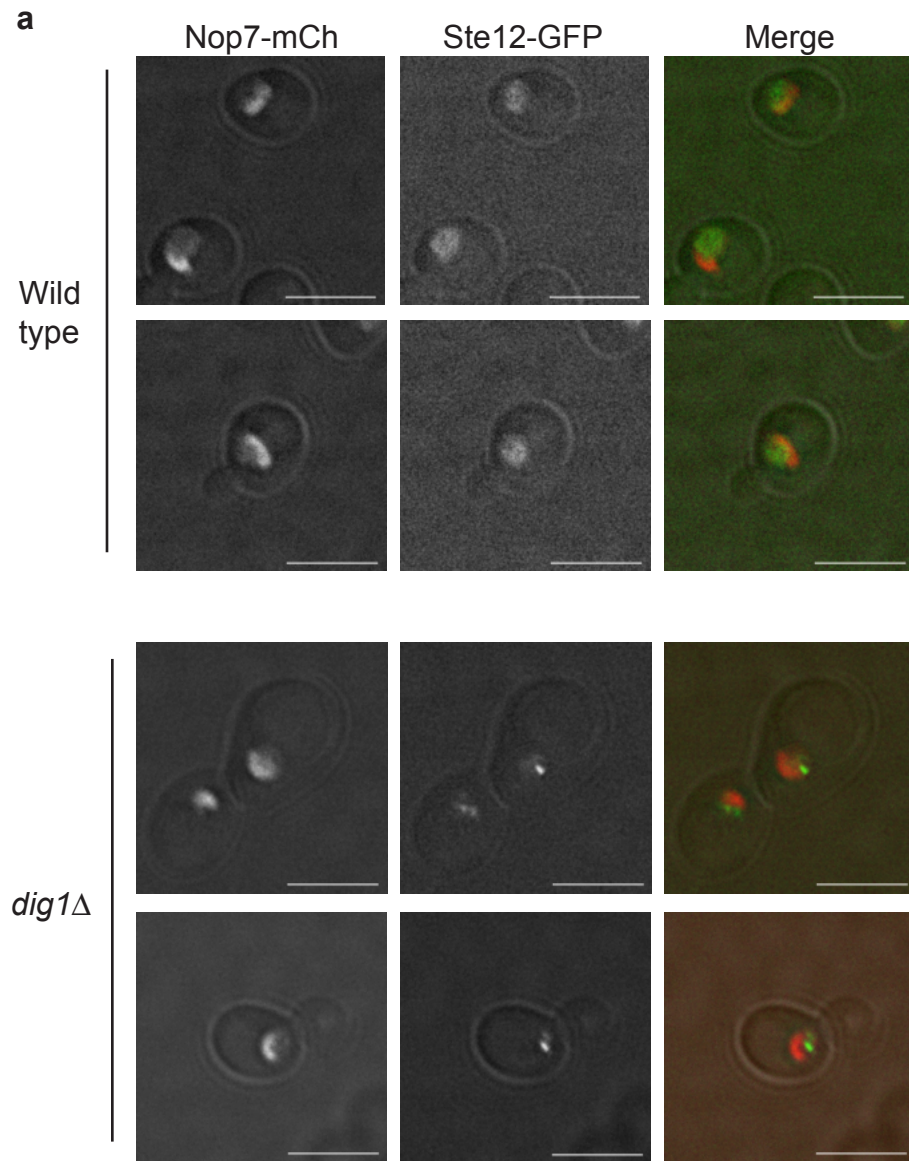


**Figure S4:** Two-colour experiment with the location of mCherry and GFP reversed. **a.** In this strain, mCherry was inserted in the endogenous *pAGA1* locus while *pAGA1-GFP-AGA1 3'UTR* was inserted in the *LYS1* locus. **b.** Density plots of mCherry vs. GFP fluorescence values for wild-type (left), *dig1Δ* (middle) and *dig2Δ* (right). **c.** CV vs. intrinsic, extrinsic and total noise. Wild-type in blue, *dig1Δ* in red, and *dig2Δ* in green. Total noise was calculated as in **Fig. 2c**. **d,e.** Intrinsic and extrinsic noise vs. gate radius (see Methods for exact gate radii). Wild-type is in blue, *dig1Δ* is in red and *dig2Δ* is in green.

Supplementary Figure S5 a



Supplementary Figure S5 b,c

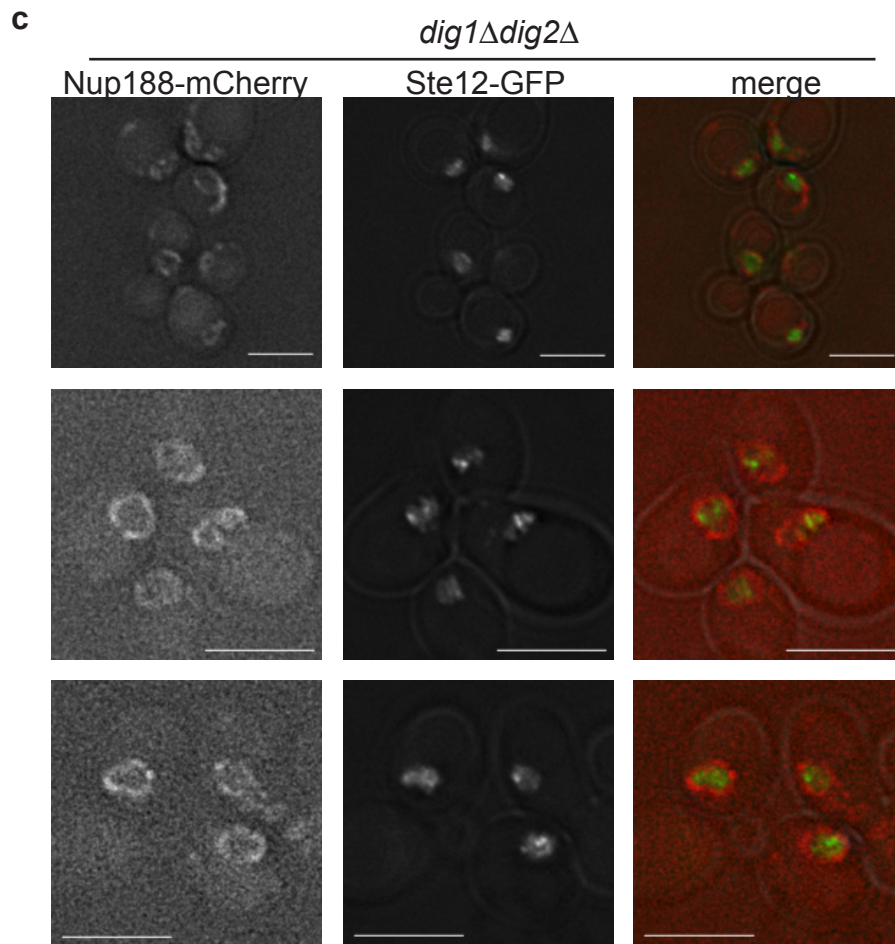
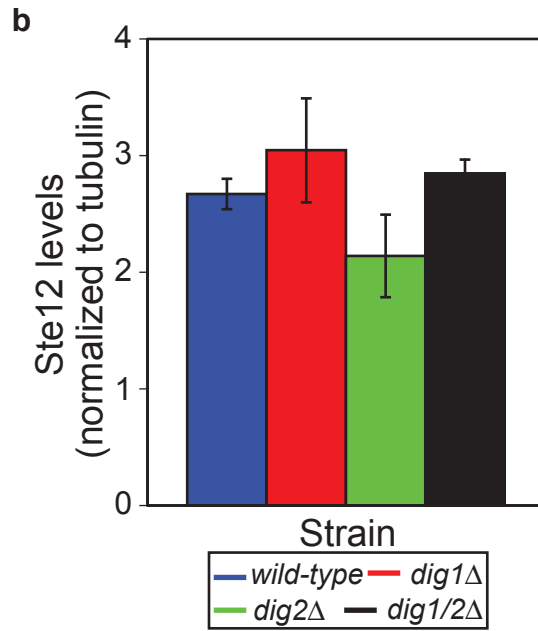


**Figure S5:** **a.** Ste12-GFP and Nop7-mCherry co-localization in wild-type (top two rows) and *dig1* $\Delta$  (bottom two rows) cells. Scale: 5  $\mu$ m. **b.** Ste12 levels normalized to tubulin in *wild-type* (blue), *dig1* $\Delta$  (red), *dig2* $\Delta$  (green) and *dig1* $\Delta$ *dig2* $\Delta$  (black) as measured by quantitative immunoblotting (see Methods). **c.** Ste12-GFP localization in *STE12-GFP dig1* $\Delta$ *dig2* $\Delta$  double mutant strains. Scale: 5  $\mu$ M.



Supplementary Figure S6

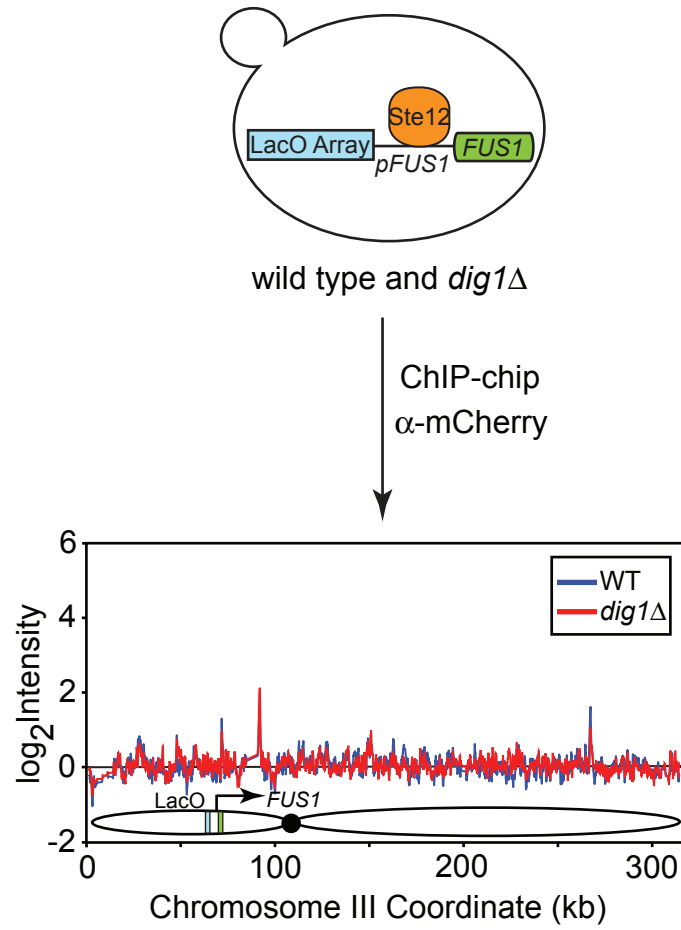
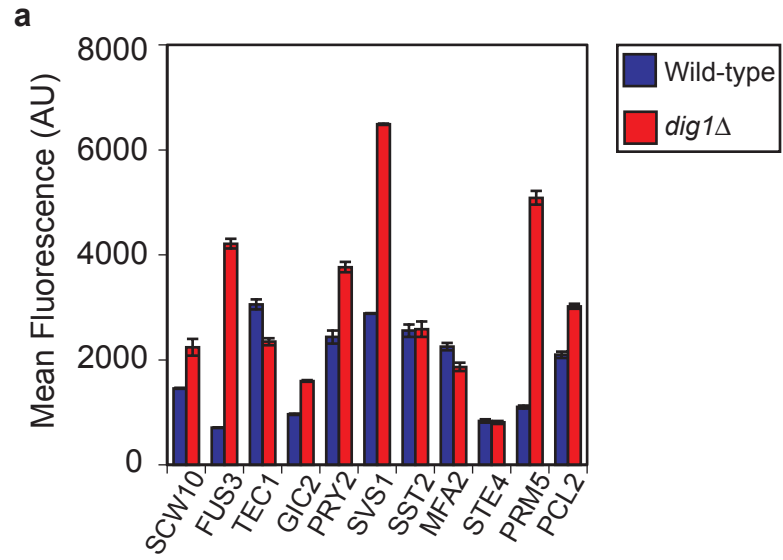


**Figure S6:** *FUS1* locus does not immunoprecipitate in absence of mCherry-LacI.

Supplementary Figure S7a



Supplementary Figure S7b

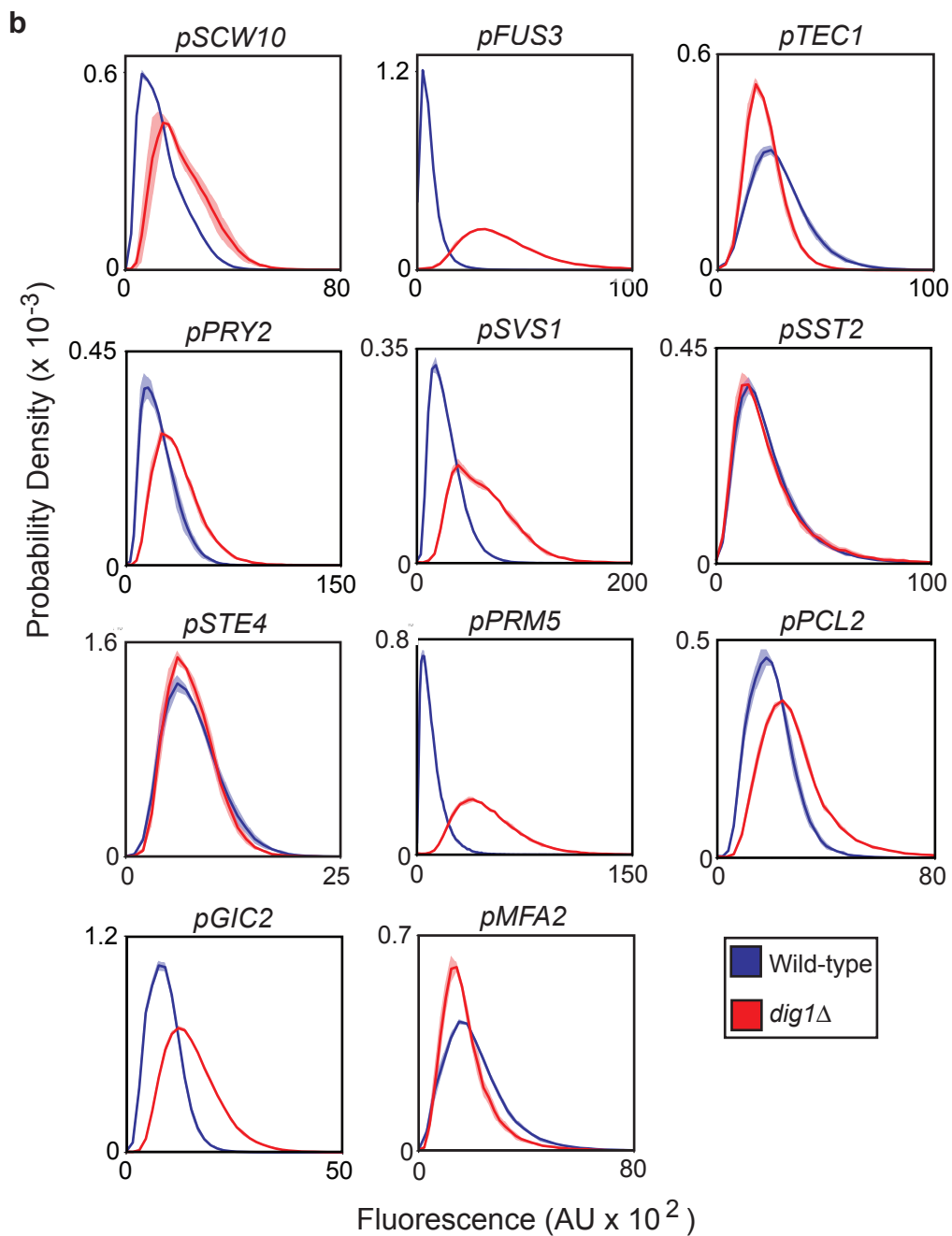


**Figure S7:** Mean expression and PDFs for 11 reporter strains whose promoters were found to interact with the *FUS1* locus. **a.** Mean fluorescence output for reporter strains in wild-type (blue) and *dig1* $\Delta$  (red) cells. **b.** PDFs of output distributions of 11 reporter strains. Wild-type is in blue, *dig1* $\Delta$  is in red.

Supplementary Figure S8

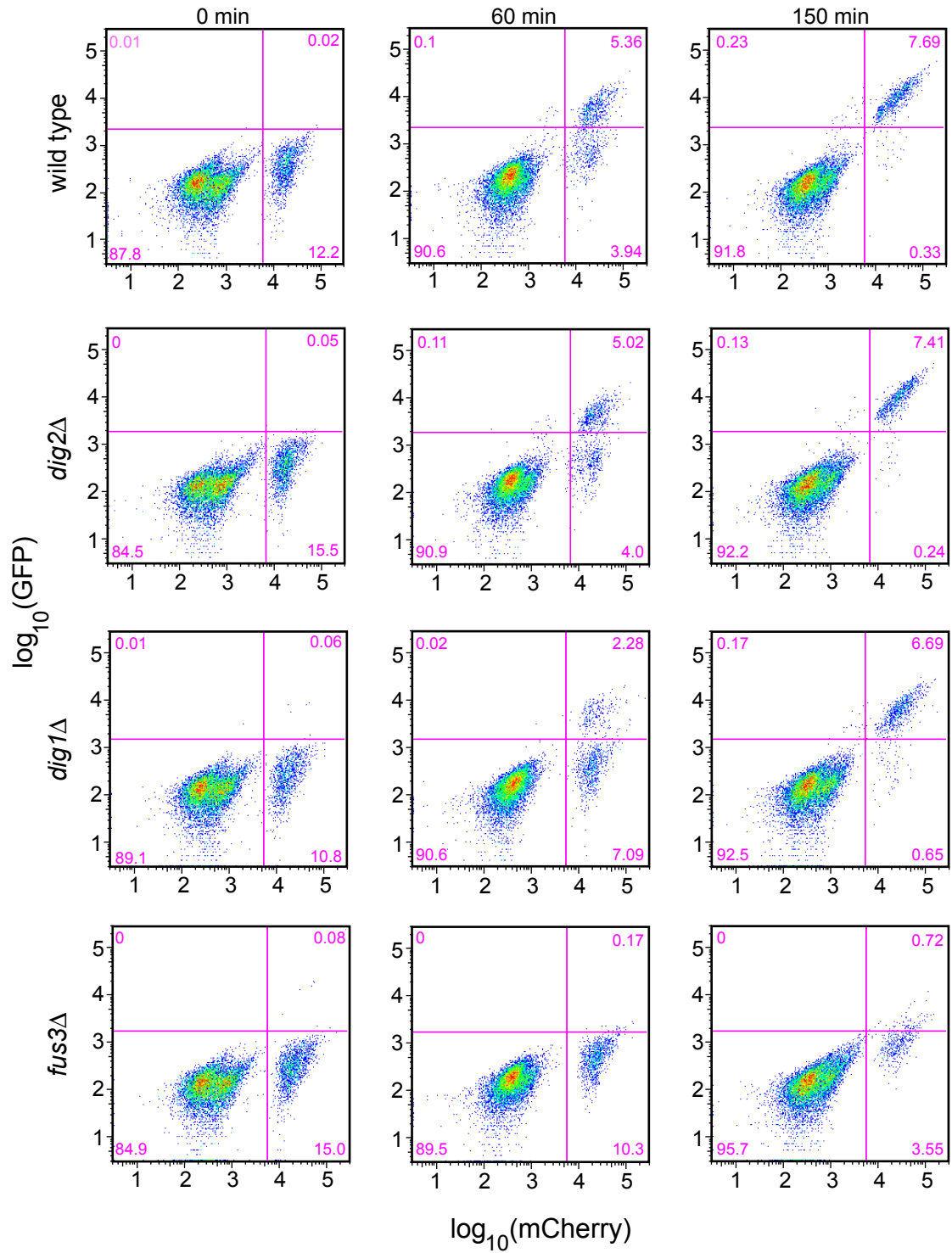


**Figure S8:** FACS scatter plots of the mating time course assay. GFP vs. mCherry data is plotted for each strain at three time points; 0 min, 60 min and 150 min. The quadrants in each plot separate wild-type unfused *MATa* GFP-/mCh- cells, unfused wild-type or mutant *MAT $\alpha$*  GFP-/mCh+ cells and fused GFP+/mCh+ cells. The percentage of cells in each quadrant is listed in pink.

**Table S1:** 5% of genes with largest differences in ChIP-chip signals

| <i>dig1Δ</i> - wild type |                  |
|--------------------------|------------------|
| Systematic Name          | Common Name      |
| YBL003C                  | <i>HTA2</i>      |
| YBL008W                  | <i>HIR1</i>      |
| YBL016W                  | <i>FUS3</i>      |
| YBL017C                  | <i>PEP1</i>      |
| YBL026W                  | <i>LSM2</i>      |
| YBL029W                  | <i>YBL029W</i>   |
| YBL067C                  | <i>UBP13</i>     |
| YBL086C                  | <i>YBL086C</i>   |
| YBR001C                  | <i>NTH2</i>      |
| YBR040W                  | <i>FIG1</i>      |
| YBR058C                  | <i>UBP14</i>     |
| YBR082C                  | <i>UBC4</i>      |
| YBR083W                  | <i>TEC1</i>      |
| YBR088C                  | <i>POL30</i>     |
| YBR095C                  | <i>RXT2</i>      |
| YBR096W                  | <i>YBR096W</i>   |
| YBR123C                  | <i>TFC1</i>      |
| YBR153W                  | <i>RIB7</i>      |
| YBR168W                  | <i>PEX32</i>     |
| YBR211C                  | <i>AME1</i>      |
| YBR233W-A                | <i>DAD3</i>      |
| YBR250W                  | <i>SPO23</i>     |
| YBR291C                  | <i>CTP1</i>      |
| YCR095W-A                | <i>YCR095W-A</i> |
| YDL013W                  | <i>SLX5</i>      |
| YDL076C                  | <i>RXT3</i>      |
| YDL102W                  | <i>POL3</i>      |
| YDL103C                  | <i>QRI1</i>      |
| YDL127W                  | <i>PCL2</i>      |
| YDL133C-A                | <i>RPL41B</i>    |
| YDL133W                  | <i>YDL133W</i>   |
| YDL155W                  | <i>CLB3</i>      |
| YDL165W                  | <i>CDC36</i>     |
| YDL166C                  | <i>FAP7</i>      |
| YDL176W                  | <i>YDL176W</i>   |
| YDL179W                  | <i>PCL9</i>      |
| YDR060W                  | <i>MAK21</i>     |
| YDR100W                  | <i>TVP15</i>     |
| YDR162C                  | <i>NBP2</i>      |
| YDR169C-A                | <i>YDR169C-A</i> |

| <i>dig1Δste12Δ</i> - wild type |                  |
|--------------------------------|------------------|
| Systematic Name                | Common Name      |
| YAL064W                        | <i>YAL064W</i>   |
| YAL067C                        | <i>SEO1</i>      |
| YAR003W                        | <i>SWD1</i>      |
| YBL009W                        | <i>ALK2</i>      |
| YBL010C                        | <i>YBL010C</i>   |
| YBL097W                        | <i>BRN1</i>      |
| YBR005W                        | <i>RCR1</i>      |
| YBR018C                        | <i>GAL7</i>      |
| YBR019C                        | <i>GAL10</i>     |
| YBR028C                        | <i>YBR028C</i>   |
| YBR058C                        | <i>UBP14</i>     |
| YBR123C                        | <i>TFC1</i>      |
| YBR129C                        | <i>OPY1</i>      |
| YBR148W                        | <i>YSW1</i>      |
| YBR164C                        | <i>ARL1</i>      |
| YBR166C                        | <i>TYR1</i>      |
| YBR167C                        | <i>POP7</i>      |
| YBR168W                        | <i>PEX32</i>     |
| YBR170C                        | <i>NPL4</i>      |
| YBR211C                        | <i>AME1</i>      |
| YBR212W                        | <i>NGR1</i>      |
| YBR216C                        | <i>YBP1</i>      |
| YBR217W                        | <i>ATG12</i>     |
| YBR245C                        | <i>ISW1</i>      |
| YBR246W                        | <i>YBR246W</i>   |
| YBR247C                        | <i>ENP1</i>      |
| YBR254C                        | <i>TRS20</i>     |
| YBR258C                        | <i>SHG1</i>      |
| YBR275C                        | <i>RIF1</i>      |
| YCR018C                        | <i>SRD1</i>      |
| YCR042C                        | <i>TAF2</i>      |
| YCR095W-A                      | <i>YCR095W-A</i> |
| YDL008W                        | <i>APC11</i>     |
| YDL036C                        | <i>PUS9</i>      |
| YDL065C                        | <i>PEX19</i>     |
| YDL084W                        | <i>SUB2</i>      |
| YDL102W                        | <i>POL3</i>      |
| YDL103C                        | <i>QRI1</i>      |
| YDL146W                        | <i>LDB17</i>     |
| YDL147W                        | <i>RPN5</i>      |



|           |                  |
|-----------|------------------|
| YDR177W   | <i>UBC1</i>      |
| YDR179C   | <i>CSN9</i>      |
| YDR179W-A | <i>YDR179W-A</i> |
| YDR181C   | <i>SAS4</i>      |
| YDR204W   | <i>COQ4</i>      |
| YDR217C   | <i>RAD9</i>      |
| YDR275W   | <i>BSC2</i>      |
| YDR309C   | <i>GIC2</i>      |
| YDR336W   | <i>YDR336W</i>   |
| YDR395W   | <i>SXM1</i>      |
| YDR415C   | <i>YDR415C</i>   |
| YDR416W   | <i>SYF1</i>      |
| YDR439W   | <i>LRS4</i>      |
| YDR459C   | <i>PFA5</i>      |
| YDR460W   | <i>TFB3</i>      |
| YDR464W   | <i>SPP41</i>     |
| YDR465C   | <i>RMT2</i>      |
| YDR466W   | <i>PKH3</i>      |
| YDR468C   | <i>TLG1</i>      |
| YDR496C   | <i>PUF6</i>      |
| YDR504C   | <i>SPG3</i>      |
| YDR507C   | <i>GIN4</i>      |
| YDR522C   | <i>SPS2</i>      |
| YDR532C   | <i>YDR532C</i>   |
| YEL001C   | <i>IRC22</i>     |
| YEL042W   | <i>GDA1</i>      |
| YER051W   | <i>JHD1</i>      |
| YER056C   | <i>FCY2</i>      |
| YER062C   | <i>HOR2</i>      |
| YER065C   | <i>ICL1</i>      |
| YER069W   | <i>ARG5,6</i>    |
| YER071C   | <i>YER071C</i>   |
| YER072W   | <i>VTC1</i>      |
| YER122C   | <i>GLO3</i>      |
| YER123W   | <i>YER123W</i>   |
| YER139C   | <i>RTR1</i>      |
| YER140W   | <i>YER140W</i>   |
| YER166W   | <i>DNF1</i>      |
| YER168C   | <i>CCA1</i>      |
| YFL003C   | <i>MSH4</i>      |
| YFL010C   | <i>WWM1</i>      |
| YFR002W   | <i>NIC96</i>     |
| YFR037C   | <i>RSC8</i>      |
| YFR038W   | <i>IRC5</i>      |
| YGL001C   | <i>ERG26</i>     |
| YGL017W   | <i>ATE1</i>      |
| YGL045W   | <i>RIM8</i>      |

|         |                |
|---------|----------------|
| YDL148C | <i>NOP14</i>   |
| YDL156W | <i>CMR1</i>    |
| YDL165W | <i>CDC36</i>   |
| YDL218W | <i>YDL218W</i> |
| YDR012W | <i>RPL4B</i>   |
| YDR014W | <i>RAD61</i>   |
| YDR026C | <i>YDR026C</i> |
| YDR060W | <i>MAK21</i>   |
| YDR070C | <i>FMP16</i>   |
| YDR081C | <i>PDC2</i>    |
| YDR140W | <i>MTQ2</i>    |
| YDR160W | <i>SSY1</i>    |
| YDR177W | <i>UBC1</i>    |
| YDR183W | <i>PLP1</i>    |
| YDR184C | <i>ATC1</i>    |
| YDR204W | <i>COQ4</i>    |
| YDR221W | <i>GTB1</i>    |
| YDR244W | <i>PEX5</i>    |
| YDR245W | <i>MNN10</i>   |
| YDR247W | <i>VHS1</i>    |
| YDR273W | <i>DON1</i>    |
| YDR283C | <i>GCN2</i>    |
| YDR315C | <i>IPK1</i>    |
| YDR318W | <i>MCM21</i>   |
| YDR320C | <i>SWA2</i>    |
| YDR321W | <i>ASP1</i>    |
| YDR369C | <i>XRS2</i>    |
| YDR370C | <i>YDR370C</i> |
| YDR371W | <i>CTS2</i>    |
| YDR374C | <i>YDR374C</i> |
| YDR414C | <i>ERD1</i>    |
| YDR416W | <i>SYF1</i>    |
| YDR439W | <i>LRS4</i>    |
| YDR468C | <i>TLG1</i>    |
| YDR469W | <i>SDC1</i>    |
| YDR484W | <i>VPS52</i>   |
| YDR503C | <i>LPP1</i>    |
| YDR523C | <i>SPS1</i>    |
| YEL042W | <i>GDA1</i>    |
| YER054C | <i>GIP2</i>    |
| YER107C | <i>GLE2</i>    |
| YER115C | <i>SPR6</i>    |
| YER134C | <i>YER134C</i> |
| YER139C | <i>RTR1</i>    |
| YER173W | <i>RAD24</i>   |
| YFL004W | <i>VTC2</i>    |
| YFL049W | <i>SWP82</i>   |

|           |                  |
|-----------|------------------|
| YGL067W   | <i>NPY1</i>      |
| YGL081W   | <i>YGL081W</i>   |
| YGL178W   | <i>MPT5</i>      |
| YGR005C   | <i>TFG2</i>      |
| YGR006W   | <i>PRP18</i>     |
| YGR014W   | <i>MSB2</i>      |
| YGR040W   | <i>KSS1</i>      |
| YGR071C   | <i>YGR071C</i>   |
| YGR074W   | <i>SMD1</i>      |
| YGR076C   | <i>MRPL25</i>    |
| YGR162W   | <i>TIF4631</i>   |
| YGR188C   | <i>BUB1</i>      |
| YGR194C   | <i>XKS1</i>      |
| YGR201C   | <i>YGR201C</i>   |
| YGR236C   | <i>SPG1</i>      |
| YGR253C   | <i>PUP2</i>      |
| YGR279C   | <i>SCW4</i>      |
| YHR016C   | <i>YHR016C</i>   |
| YHR017W   | <i>YHR017W</i>   |
| YHR082C   | <i>KSP1</i>      |
| YHR084W   | <i>STE12</i>     |
| YHR086W-A | <i>YHR086W-A</i> |
| YHR110W   | <i>ERP5</i>      |
| YHR122W   | <i>YHR122W</i>   |
| YHR128W   | <i>FUR1</i>      |
| YHR184W   | <i>SSP1</i>      |
| YHR201C   | <i>PPX1</i>      |
| YIL053W   | <i>RHR2</i>      |
| YIL104C   | <i>SHQ1</i>      |
| YIL117C   | <i>PRM5</i>      |
| YIL119C   | <i>RPI1</i>      |
| YIL123W   | <i>SIM1</i>      |
| YIL130W   | <i>ASG1</i>      |
| YIL131C   | <i>FKH1</i>      |
| YIL139C   | <i>REV7</i>      |
| YIL146C   | <i>ECM37</i>     |
| YIL147C   | <i>SLN1</i>      |
| YIL158W   | <i>AIM20</i>     |
| YJL049W   | <i>YJL049W</i>   |
| YJL130C   | <i>URA2</i>      |
| YJL134W   | <i>LCB3</i>      |
| YJL136C   | <i>RPS21B</i>    |
| YJL179W   | <i>PFD1</i>      |
| YJL180C   | <i>ATP12</i>     |
| YJR010C-A | <i>SPC1</i>      |
| YJR010W   | <i>MET3</i>      |
| YJR025C   | <i>BNA1</i>      |

|           |                |
|-----------|----------------|
| YFL050C   | <i>ALR2</i>    |
| YGL016W   | <i>KAP122</i>  |
| YGL059W   | <i>PKP2</i>    |
| YGL095C   | <i>VPS45</i>   |
| YGL171W   | <i>ROK1</i>    |
| YGL213C   | <i>SKI8</i>    |
| YGL232W   | <i>TAN1</i>    |
| YGR001C   | <i>AML1</i>    |
| YGR059W   | <i>SPR3</i>    |
| YGR169C   | <i>PUS6</i>    |
| YGR229C   | <i>SMI1</i>    |
| YHL012W   | <i>YHL012W</i> |
| YHL013C   | <i>OTU2</i>    |
| YHL046C   | <i>PAU13</i>   |
| YHR060W   | <i>VMA22</i>   |
| YHR111W   | <i>UBA4</i>    |
| YHR129C   | <i>ARP1</i>    |
| YHR177W   | <i>YHR177W</i> |
| YHR191C   | <i>CTF8</i>    |
| YHR197W   | <i>RIX1</i>    |
| YIL084C   | <i>SDS3</i>    |
| YIL104C   | <i>SHQ1</i>    |
| YIL120W   | <i>QDR1</i>    |
| YIL128W   | <i>MET18</i>   |
| YIL129C   | <i>TAO3</i>    |
| YIL130W   | <i>ASG1</i>    |
| YIL131C   | <i>FKH1</i>    |
| YIL139C   | <i>REV7</i>    |
| YIL146C   | <i>ECM37</i>   |
| YJL046W   | <i>AIM22</i>   |
| YJL047C   | <i>RTT101</i>  |
| YJL049W   | <i>YJL049W</i> |
| YJL085W   | <i>EXO70</i>   |
| YJL087C   | <i>TRL1</i>    |
| YJL091C   | <i>GWT1</i>    |
| YJL097W   | <i>PHS1</i>    |
| YJL204C   | <i>RCY1</i>    |
| YJL205C   | <i>NCE101</i>  |
| YJR010C-A | <i>SPC1</i>    |
| YJR025C   | <i>BNA1</i>    |
| YJR107W   | <i>YJR107W</i> |
| YKL001C   | <i>MET14</i>   |
| YKL002W   | <i>DID4</i>    |
| YKL011C   | <i>CCE1</i>    |
| YKL040C   | <i>NFU1</i>    |
| YKL090W   | <i>CUE2</i>    |
| YKL105C   | <i>YKL105C</i> |

|           |           |
|-----------|-----------|
| YJR154W   | YJR154W   |
| YKL042W   | SPC42     |
| YKL060C   | FBA1      |
| YKL084W   | HOT13     |
| YKL096W-A | CWP2      |
| YKL104C   | GFA1      |
| YKL138C-A | HSK3      |
| YKL183W   | LOT5      |
| YKL207W   | LRC3      |
| YKR004C   | ECM9      |
| YKR010C   | TOF2      |
| YKR011C   | YKR011C   |
| YKR013W   | PRY2      |
| YKR039W   | GAP1      |
| YKR041W   | YKR041W   |
| YKR091W   | SRL3      |
| YKR095W-A | PCC1      |
| YKR096W   | ESL2      |
| YKR103W   | NFT1      |
| YLL042C   | ATG10     |
| YLL056C   | YLL056C   |
| YLR018C   | POM34     |
| YLR040C   | YLR040C   |
| YLR042C   | YLR042C   |
| YLR044C   | PDC1      |
| YLR046C   | YLR046C   |
| YLR128W   | DCN1      |
| YLR129W   | DIP2      |
| YLR165C   | PUS5      |
| YLR172C   | DPH5      |
| YLR173W   | YLR173W   |
| YLR209C   | PNP1      |
| YLR210W   | CLB4      |
| YLR240W   | VPS34     |
| YLR248W   | RCK2      |
| YLR251W   | SYM1      |
| YLR264W   | RPS28B    |
| YLR268W   | SEC22     |
| YLR271W   | YLR271W   |
| YLR305C   | STT4      |
| YLR306W   | UBC12     |
| YLR309C   | IMH1      |
| YLR353W   | BUD8      |
| YLR362W   | STE11     |
| YLR369W   | SSQ1      |
| YLR412C-A | YLR412C-A |
| YLR421C   | RPN13     |

|         |         |
|---------|---------|
| YKL108W | SLD2    |
| YKL144C | RPC25   |
| YKL166C | TPK3    |
| YKL194C | MST1    |
| YKL206C | ADD66   |
| YKR004C | ECM9    |
| YKR010C | TOF2    |
| YKR051W | YKR051W |
| YKR084C | HBS1    |
| YKR098C | UBP11   |
| YKR103W | NFT1    |
| YLL042C | ATG10   |
| YLR021W | IRC25   |
| YLR083C | EMP70   |
| YLR102C | APC9    |
| YLR127C | APC2    |
| YLR128W | DCN1    |
| YLR134W | PDC5    |
| YLR165C | PUS5    |
| YLR166C | SEC10   |
| YLR172C | DPH5    |
| YLR173W | YLR173W |
| YLR188W | MDL1    |
| YLR195C | NMT1    |
| YLR201C | COQ9    |
| YLR207W | HRD3    |
| YLR209C | PNP1    |
| YLR210W | CLB4    |
| YLR234W | TOP3    |
| YLR238W | FAR10   |
| YLR251W | SYM1    |
| YLR284C | ECI1    |
| YLR292C | SEC72   |
| YLR293C | GSP1    |
| YLR305C | STT4    |
| YLR325C | RPL38   |
| YLR329W | REC102  |
| YLR360W | VPS38   |
| YLR361C | DCR2    |
| YLR362W | STE11   |
| YLR398C | SKI2    |
| YLR411W | CTR3    |
| YLR424W | SPP382  |
| YLR440C | SEC39   |
| YLR442C | SIR3    |
| YML017W | PSP2    |
| YML018C | YML018C |

|           |           |
|-----------|-----------|
| YLR433C   | CNA1      |
| YLR443W   | ECM7      |
| YLR452C   | SST2      |
| YML018C   | YML018C   |
| YML043C   | RRN11     |
| YML056C   | IMD4      |
| YML092C   | PRE8      |
| YMR001C   | CDC5      |
| YMR016C   | SOK2      |
| YMR038C   | CCS1      |
| YMR077C   | VPS20     |
| YMR100W   | MUB1      |
| YMR115W   | MGR3      |
| YMR144W   | YMR144W   |
| YMR192W   | GYL1      |
| YMR231W   | PEP5      |
| YMR234W   | RNH1      |
| YMR274C   | RCE1      |
| YMR293C   | HER2      |
| YMR305C   | SCW10     |
| YMR306W   | FKS3      |
| YNL024C-A | YNL024C-A |
| YNL038W   | GPI15     |
| YNL051W   | COG5      |
| YNL072W   | RNH201    |
| YNL087W   | TCB2      |
| YNL113W   | RPC19     |
| YNL141W   | AAH1      |
| YNL145W   | MFA2      |
| YNL146C-A | YNL146C-A |
| YNL154C   | YNL154C   |
| YNL163C   | RIA1      |
| YNL191W   | DUG3      |
| YNL216W   | RAP1      |
| YNL246W   | VPS75     |
| YNL283C   | WSC2      |
| YNL289W   | PCL1      |
| YNR010W   | CSE2      |
| YOL017W   | ESC8      |
| YOL018C   | TLG2      |
| YOL023W   | IFM1      |
| YOL070C   | NBA1      |
| YOL089C   | HAL9      |
| YOL159C-A | YOL159C-A |
| YOR046C   | DBP5      |
| YOR060C   | YOR060C   |
| YOR081C   | TGL5      |

|           |           |
|-----------|-----------|
| YML056C   | IMD4      |
| YML108W   | YML108W   |
| YML109W   | ZDS2      |
| YML110C   | COQ5      |
| YMR059W   | SEN15     |
| YMR060C   | SAM37     |
| YMR061W   | RNA14     |
| YMR078C   | CTF18     |
| YMR084W   | YMR084W   |
| YMR097C   | MTG1      |
| YMR106C   | YKU80     |
| YMR140W   | SIP5      |
| YMR180C   | CTL1      |
| YMR233W   | TRI1      |
| YMR234W   | RNH1      |
| YNL024C-A | YNL024C-A |
| YNL025C   | SSN8      |
| YNL119W   | NCS2      |
| YNL121C   | TOM70     |
| YNL122C   | YNL122C   |
| YNL158W   | PGA1      |
| YNL168C   | FMP41     |
| YNL191W   | DUG3      |
| YNL246W   | VPS75     |
| YNL249C   | MPA43     |
| YNL259C   | ATX1      |
| YNL260C   | YNL260C   |
| YNL265C   | IST1      |
| YNL308C   | KRI1      |
| YNR010W   | CSE2      |
| YNR048W   | YNR048W   |
| YNR055C   | HOL1      |
| YNR061C   | YNR061C   |
| YNR063W   | YNR063W   |
| YOL017W   | ESC8      |
| YOL018C   | TLG2      |
| YOL023W   | IFM1      |
| YOL024W   | YOL024W   |
| YOL102C   | TPT1      |
| YOL137W   | BSC6      |
| YOR046C   | DBP5      |
| YOR068C   | VAM10     |
| YOR115C   | TRS33     |
| YOR116C   | RPO31     |
| YOR150W   | MRPL23    |
| YOR156C   | NFI1      |
| YOR177C   | MPC54     |

|         |                |
|---------|----------------|
| YOR083W | <i>WHI5</i>    |
| YOR128C | <i>ADE2</i>    |
| YOR137C | <i>SIA1</i>    |
| YOR141C | <i>ARP8</i>    |
| YOR142W | <i>LSC1</i>    |
| YOR156C | <i>NFI1</i>    |
| YOR175C | <i>ALE1</i>    |
| YOR212W | <i>STE4</i>    |
| YOR221C | <i>MCT1</i>    |
| YOR239W | <i>ABP140</i>  |
| YOR246C | <i>YOR246C</i> |
| YOR247W | <i>SRL1</i>    |
| YOR291W | <i>YOR291W</i> |
| YPL016W | <i>SWI1</i>    |
| YPL050C | <i>MNN9</i>    |
| YPL054W | <i>LEE1</i>    |
| YPL055C | <i>LGE1</i>    |
| YPL070W | <i>MUK1</i>    |
| YPL071C | <i>YPL071C</i> |
| YPL117C | <i>IDI1</i>    |
| YPL135W | <i>ISU1</i>    |
| YPL137C | <i>GIP3</i>    |
| YPL141C | <i>YPL141C</i> |
| YPL163C | <i>SVS1</i>    |
| YPL179W | <i>PPQ1</i>    |
| YPL184C | <i>MRN1</i>    |
| YPL191C | <i>YPL191C</i> |
| YPL195W | <i>APL5</i>    |
| YPL210C | <i>SRP72</i>   |
| YPL270W | <i>MDL2</i>    |
| YPR035W | <i>GLN1</i>    |
| YPR047W | <i>MSF1</i>    |
| YPR104C | <i>FHL1</i>    |
| YPR137W | <i>RRP9</i>    |
| YPR152C | <i>URN1</i>    |
| YPR153W | <i>YPR153W</i> |
| YPR155C | <i>NCA2</i>    |
| YPR156C | <i>TPO3</i>    |
| YPR176C | <i>BET2</i>    |
| YPR178W | <i>PRP4</i>    |
| YPR180W | <i>AOS1</i>    |

|         |                   |
|---------|-------------------|
| YOR188W | <i>MSB1</i>       |
| YOR212W | <i>STE4</i>       |
| YOR214C | <i>YOR214C</i>    |
| YOR239W | <i>ABP140</i>     |
| YOR270C | <i>VPH1</i>       |
| YOR280C | <i>FSH3</i>       |
| YOR281C | <i>PLP2</i>       |
| YOR284W | <i>HUA2</i>       |
| YOR287C | <i>YOR287C</i>    |
| YOR350C | <i>MNE1</i>       |
| YOR356W | <i>YOR356W</i>    |
| YOR363C | <i>PIP2</i>       |
| YPL027W | <i>SMA1</i>       |
| YPL054W | <i>LEE1</i>       |
| YPL092W | <i>SSU1</i>       |
| YPL109C | <i>YPL109C</i>    |
| YPL119C | <i>DBP1</i>       |
| YPL125W | <i>KAP120</i>     |
| YPL167C | <i>REV3</i>       |
| YPL168W | <i>YPL168W</i>    |
| YPL169C | <i>MEX67</i>      |
| YPL180W | <i>TCO89</i>      |
| YPL184C | <i>MRN1</i>       |
| YPL187W | <i>MF(ALPHA)1</i> |
| YPL195W | <i>APL5</i>       |
| YPL225W | <i>YPL225W</i>    |
| YPL232W | <i>SSO1</i>       |
| YPL266W | <i>DIM1</i>       |
| YPR009W | <i>SUT2</i>       |
| YPR027C | <i>YPR027C</i>    |
| YPR057W | <i>BRR1</i>       |
| YPR068C | <i>HOS1</i>       |
| YPR073C | <i>LTP1</i>       |
| YPR084W | <i>YPR084W</i>    |
| YPR117W | <i>YPR117W</i>    |
| YPR122W | <i>AXL1</i>       |
| YPR176C | <i>BET2</i>       |
| YPR178W | <i>PRP4</i>       |
| YPR187W | <i>RPO26</i>      |
| YPR188C | <i>MLC2</i>       |
| YPR189W | <i>SKI3</i>       |

**Table S2: List of strains used in this study**

| Strain # | Genotype  | Source     |
|----------|---|------------|
| YM1731   | <i>MATa ura3Δ0 his3Δ1 leu2Δ0 lys2Δ0 met15Δ0</i>   |            |
| YM1953   | <i>MATa ura3Δ0 his3Δ1 leu2Δ0 lys2Δ0 met15Δ0 bar1::NatMX4</i>  | This study |
| YM1968   | YM1953 <i>aga1::YFP</i>   | This study |
| YM2091   | YM1953 <i>fus1::YFP</i>   | This study |
| YM2100   | YM2091 <i>dig1::KanMX4</i>  | This study |
| YM2101   | YM1953 <i>dig1::KanMX6</i>  | This study |
| YM2102   | YM2101 <i>dig2::HisMX6</i>  | This study |
| YM2105   | YM1968 <i>dig1::KanMX4</i>  | This study |
| YM2109   | YM2105 <i>dig2::HisMX6</i>  | This study |
| YM2112   | YM2100 <i>dig2::HisMX6</i>  | This study |
| YM2248   | <i>MATa can1::pSTE2-S.p.HIS5 lyp1Δ his3Δ1 leu2Δ0 ura3Δ0 met15Δ0 LYS2+ bar1::NatMX4 hygMX-pAGA1-YFP-3'AGA1-C.g.LEU2</i>                    | This study |
| YM2315   | YM1953 <i>dig2::HisMX6</i>  | This study |
| YM2636   | <i>MATa ura3Δ0 his3Δ1 leu2Δ0 lys2Δ0 bar1::NatMX4 aga1::eGFP lys1::pAGA1-mCherry-3'UTR AGA1</i>  | This study |
| YM2637   | <i>MATa ura3Δ0 his3Δ1 leu2Δ0 lys2Δ0 bar1::NatMX4 aga1::mCherry lys1::pAGA1-eGFP-3'UTR AGA1</i>  | This study |
| YM2643   | YM1953 <i>dig1::KanMX6 ste12::His3MX6</i>   | This study |
| YM2871   | YM2636 <i>dig1::KanMX6</i>  | This study |
| YM2872   | YM2637 <i>dig2::KanMX6</i>  | This study |
| YM2875   | YM2637 <i>dig1::KanMX6</i>  | This study |
| YM2876   | YM2636 <i>dig2::KanMX6</i>  | This study |
| YM2901   | <i>MATa ura3Δ0 his3Δ1 leu2Δ0 lys2Δ0 eGFP(aa1-158)-TRP1-NatMX4</i> (eGFP fragment from W. Lim)   | This study |
| YM2903   | <i>MATα ura3Δ0 his3Δ1 leu2Δ0 lys2Δ0 eGFP(aa159-240)-LEU2 lys1::KanMX6-pTEF2-mCherry</i> (eGFP fragment from W. Lim)                       | This study |
| YM2910   | <i>MATa ura3Δ0 his3Δ1 leu2Δ0 met15Δ0 STE12-eGFP-HIS3MX6 NUP188-mCherry-URA3MX</i>   | This study |
| YM3085   | YM2903 <i>fus3::NatMX4</i>  | This study |
| YM3086   | YM2903 <i>dig2::NatMX4</i>  | This study |
| YM3087   | YM2903 <i>dig1::NatMX4</i>  | This study |
| YM3099   | YM1968 <i>dig2::HIS3MX6</i>   | This study |
| YM3101   | YM2091 <i>dig2::HIS3MX6</i>   | This study |
| YM3102   | YM2910 <i>dig1::KanMX6</i>  | This study |
| YM3103   | YM2910 <i>dig2::KanMX6</i>  | This study |
| YM3104   | YM3102 <i>dig2::NatMX4</i>  | This study |
| YM3105   | YM1968 <i>pSTE12::pEAF3</i> (-530bp to ATG removed upstream of <i>STE12</i> and replaced with intergenic region upstream of <i>EAF3</i> ) | This study |
| YM3106   | YM1968 <i>pSTE12::pTAF4</i> (-530bp to ATG removed upstream of <i>STE12</i> and replaced with intergenic region upstream of <i>TAF4</i> ) | This study |
| YM3108   | YM3105 <i>dig1::KanMX6</i>  | This study |
| YM3109   | YM3105 <i>dig2::KanMX6</i>  | This study |
| YM3110   | YM3106 <i>dig1::KanMX6</i>  | This study |
| YM3111   | YM3106 <i>dig2::KanMX6</i>  | This study |
| YM3132   | YM2871 <i>dig2::HIS3MX6</i>   | This study |
| YM3133   | YM2875 <i>dig2::HIS3MX6</i>   | This study |
| YM3545   | <i>MATa ura3Δ0 his3Δ1 leu2Δ0 lys2Δ0 met15Δ0 bar1::NatMX4 lys1::pYEF3-YFP-3'UTR YEF3</i>   | This study |
| YM3546   | YM3545 <i>dig1::KanMX6</i>  | This study |

|        |  |            |
|--------|--|------------|
| YM3547 | YM3545 <i>dig2::HIS3MX6</i>  | This study |
| YM3550 | YM1953 <i>pmp1::GFP-HIS3MX</i>   | This study |
| YM3552 | YM1953 <i>agp1::GFP-HIS3MX</i>   | This study |
| YM3587 | <i>MATa ura3Δ0 his3Δ1 leu2Δ0 met15Δ0 STE12-eGFP-Hyg3MX LacO-HIS3MX6-pFUS1 pRS316-mCherry-LacI</i> (LacO from pLAU43 and LacI from JH2129)          | This study |
| YM3588 | YM3587 <i>dig1::KanMX6</i>   | This study |
| YM3593 | YM3550 <i>dig1::KanMX</i>  | This study |
| YM3594 | YM3550 <i>dig2::KanMX6</i>   | This study |
| YM3595 | YM3552 <i>dig1::KanMX6</i>   | This study |
| YM3596 | YM3552 <i>dig2::KanMX6</i>   | This study |
| YM3612 | YM3593 <i>dig2::Hyg3MX</i>   | This study |
| YM3628 | YM3550 <i>lys1::pPMP1-mCherry-URA3MX</i>   | This study |
| YM3629 | YM3628 <i>dig1::KanMX6</i>   | This study |
| YM3630 | YM3628 <i>dig2::KanMX6</i>   | This study |
| YM3631 | YM3629 <i>dig2::Hyg3MX6</i>  | This study |
| YM3639 | <i>MATa ura3Δ0 his3Δ1 leu2Δ0 met15Δ0 LacO-HIS3MX6-pFUS1</i> (LacO from pLAU43)   | This study |
| YM3640 | <i>MATa ura3Δ0 his3Δ1 leu2Δ0 met15Δ0 LacO-HIS3MX6-pFUS1 dig1::KanMX6</i> (LacO from pLAU43)  | This study |
| YM3687 | <i>MATa ura3Δ0 his3Δ1 leu2Δ0 met15Δ0 ste12::NatMX4 LacO-HIS3MX6-pFUS1 dig1::KanMX6 pRS316-mCherry-LacI</i> (LacO from pLAU43 and LacI from JH2129) | This study |
| YM3722 | <i>MATa ura3Δ0 his3Δ1 leu2Δ0 met15Δ0 REB1-eGFP-HIS3MX6 NUP188-mCherry-URA3MX</i>   | This study |
| YM3723 | YM3722 <i>dig1::KanMX6</i>   | This study |
| YM3724 | YM3722 <i>dig2::KanMX6</i>   | This study |
| YM3747 | <i>MATa ura3Δ0 his3Δ1 leu2Δ0 met15Δ0 DIG1-eGFP-HIS3MX6 NUP188-mCherry-URA3MX</i>   | This study |
| YM3760 | <i>MATa ura3Δ0 his3Δ1 leu2Δ0 met15Δ0 lys1::pSST2-YFP-3'SST2</i>  | This study |
| YM3762 | <i>MATa ura3Δ0 his3Δ1 leu2Δ0 met15Δ0 lys1::pTEC1-YFP-3'TEC1</i>  | This study |
| YM3763 | <i>MATa ura3Δ0 his3Δ1 leu2Δ0 met15Δ0 lys1::pGIC2-YFP-3'GIC2</i>  | This study |
| YM3764 | <i>MATa ura3Δ0 his3Δ1 leu2Δ0 met15Δ0 lys1::pFUS3-YFP-3'FUS3</i>  | This study |
| YM3766 | <i>MATa ura3Δ0 his3Δ1 leu2Δ0 met15Δ0 lys1::pPRY2-YFP-3'PRY2</i>  | This study |
| YM3767 | <i>MATa ura3Δ0 his3Δ1 leu2Δ0 met15Δ0 lys1::pSVS1-YFP-3'SVS1</i>  | This study |
| YM3769 | <i>MATa ura3Δ0 his3Δ1 leu2Δ0 met15Δ0 lys1::pSTE4-YFP-3'STE4</i>  | This study |
| YM3770 | <i>MATa ura3Δ0 his3Δ1 leu2Δ0 met15Δ0 lys1::pPRM5-YFP-3'PRM5</i>  | This study |
| YM3771 | <i>MATa ura3Δ0 his3Δ1 leu2Δ0 met15Δ0 lys1::pPCL2-YFP-3'PCL2</i>  | This study |
| YM3772 | <i>MATa ura3Δ0 his3Δ1 leu2Δ0 met15Δ0 lys1::pPCL1-YFP-3'PCL1</i>  | This study |
| YM3773 | <i>MATa ura3Δ0 his3Δ1 leu2Δ0 met15Δ0 lys1::pMFA2-YFP-3'MFA2</i>  | This study |
| YM3774 | <i>MATa ura3Δ0 his3Δ1 leu2Δ0 met15Δ0 STE12-eGFP-HIS3MX6 NOP7-mCherry-URA3MX</i>  | This study |
| YM3775 | <i>MATa ura3Δ0 his3Δ1 leu2Δ0 met15Δ0 STE12-eGFP-HIS3MX6 NOP7-mCherry-URA3MX dig1::KanMX6</i>   | This study |
| YM3776 | <i>MATa can1::pSTE2-S.p.HIS5 lyp1Δ his3Δ1 leu2Δ0 ura3Δ0 met15Δ0 LYS2+ bar1::NatMX4 hygMX-pAGA1-YFP-3'AGA1-C.g.LEU2 dig1::KanMX6</i>                | This study |
| YM3777 | <i>MATa can1::pSTE2-S.p.HIS5 lyp1Δ his3Δ1 leu2Δ0 ura3Δ0 met15Δ0 LYS2+ bar1::NatMX4 hygMX-pAGA1-YFP-3'AGA1-C.g.LEU2 nsr1::KanMX6</i>                | This study |
| YM3778 | <i>MATa can1::pSTE2-S.p.HIS5 lyp1Δ his3Δ1 leu2Δ0 ura3Δ0 met15Δ0 LYS2+ bar1::NatMX4 hygMX-pAGA1-YFP-3'AGA1-C.g.LEU2 rai1::KanMX6</i>                | This study |
| YM3779 | <i>MATa can1::pSTE2-S.p.HIS5 lyp1Δ his3Δ1 leu2Δ0 ura3Δ0 met15Δ0 LYS2+ bar1::NatMX4 hygMX-pAGA1-YFP-3'AGA1-C.g.LEU2 tus1::KanMX6</i>                | This study |
| YM3780 | <i>MATa can1::pSTE2-S.p.HIS5 lyp1Δ his3Δ1 leu2Δ0 ura3Δ0 met15Δ0 LYS2+ bar1::NatMX4 hygMX-pAGA1-YFP-3'AGA1-C.g.LEU2 gyp6::KanMX6</i>                | This study |

|        |  |            |
|--------|--|------------|
| YM3781 | <i>MATa can1::pSTE2-S.p.HIS5 lyp1Δ his3Δ1 leu2Δ0 ura3Δ0 met15Δ0 LYS2+ bar1::NatMX4 hygMX-pAGA1-YFP-3'AGA1-C.g.LEU2 csn12::KanMX6</i> | This study |
| YM3782 | <i>MATa can1::pSTE2-S.p.HIS5 lyp1Δ his3Δ1 leu2Δ0 ura3Δ0 met15Δ0 LYS2+ bar1::NatMX4 hygMX-pAGA1-YFP-3'AGA1-C.g.LEU2 ctk1::KanMX6</i>  | This study |
| YM3804 | <i>MATa ura3Δ0 his3Δ1 leu2Δ0 met15Δ0 lys1::pSST2-YFP-3'SST2 dig1::KanMX6</i>   | This study |
| YM3805 | <i>MATa ura3Δ0 his3Δ1 leu2Δ0 met15Δ0 lys1::pTEC1-YFP-3'TEC1 dig1::HIS3MX6</i>  | This study |
| YM3806 | <i>MATa ura3Δ0 his3Δ1 leu2Δ0 met15Δ0 lys1::pGIC2-YFP-3'GIC2 dig1::KanMX6</i>   | This study |
| YM3807 | <i>MATa ura3Δ0 his3Δ1 leu2Δ0 met15Δ0 lys1::pFUS3-YFP-3'FUS3 dig1::HIS3MX6</i>  | This study |
| YM3808 | <i>MATa ura3Δ0 his3Δ1 leu2Δ0 met15Δ0 lys1::pPRY2-YFP-3'PRY2 dig1::KanMX6</i>   | This study |
| YM3809 | <i>MATa ura3Δ0 his3Δ1 leu2Δ0 met15Δ0 lys1::pSVS1-YFP-3'SVS1 dig1::KanMX6</i>   | This study |
| YM3810 | <i>MATa ura3Δ0 his3Δ1 leu2Δ0 met15Δ0 lys1::pSTE4-YFP-3'STE4 dig1::HIS3MX6</i>  | This study |
| YM3811 | <i>MATa ura3Δ0 his3Δ1 leu2Δ0 met15Δ0 lys1::pPRM5-YFP-3'PRM5 dig1::KanMX6</i>   | This study |
| YM3812 | <i>MATa ura3Δ0 his3Δ1 leu2Δ0 met15Δ0 lys1::pPCL2-YFP-3'PCL2 dig1::KanMX6</i>   | This study |
| YM3813 | <i>MATa ura3Δ0 his3Δ1 leu2Δ0 met15Δ0 lys1::pPCL1-YFP-3'PCL1 dig1::HIS3MX6</i>  | This study |
| YM3814 | <i>MATa ura3Δ0 his3Δ1 leu2Δ0 met15Δ0 lys1::pMFA2-YFP-3'MFA2 dig1::KanMX6</i>   | This study |



## **CHAPTER 3**

### **Not all quiet on the noise front**

## **Abstract**

Phenotypic diversity exists even within isogenic populations of cells. Such nongenetic individuality may have wide implications for our understanding of many biological processes. The field of study concerned with the investigation of nongenetic individuality, also known as the 'biology of noise', is ripe with exciting scientific opportunities and challenges.

## **Commentary**

Cells are microscopic reactors where multitudes of chemical transformations occur simultaneously. Small numbers of molecular species may be involved, making such intracellular reactions particularly vulnerable to thermal fluctuations. Biochemical reactions are therefore probabilistic collision events between randomly moving molecules, with each event resulting in the increment or decrement of molecular species by integer amounts<sup>1,2</sup>. The amplified effect of fluctuations in the number of a molecular reactant or the compounded effects of fluctuations across many molecular reactants (which is referred to as 'molecular noise') often accumulate as an observable phenotype, endowing the cell with individuality and generating nongenetic cell-to-cell variability in a population (Fig. 1).

Observations of nongenetic variation in bacteria date back to the 1940s, when researchers observed that bacterial cultures were not completely killed by antibiotic treatment—a small fraction of cells “persist”<sup>3</sup>. The insensitivity to antibiotics exhibited by these persister cells was nonheritable<sup>4</sup>, and persister

cells spontaneously switched back to the nonpersistent state, regaining sensitivity to antibiotics. Today, single-cell measurement methods such as fluorescent reporters, flow cytometry and microscopy give revealing snapshots of this individuality. For example, when observed at the single-cell level, steady state tumbling frequencies and adaptation times among chemotaxing *Escherichia coli* cells grown in a homogeneous environment are variable<sup>5</sup>. This variability is strongly influenced by the fluctuations in the relative amount of the methyltransferase CheR, which is present in low molecular numbers within the cell<sup>6</sup>. Behavioral variation is elegantly linked with molecular noise—a link that is being unraveled by increasingly sophisticated single-cell measurement techniques.

### **Noise in gene expression**

'Biological noise', or nongenetic individuality, is commonly thought to arise from mechanisms that are susceptible to (or that exploit) the stochasticity of related biochemical reactions. Cell-to-cell variability in gene expression<sup>1,7,8</sup> has been investigated in recent years as a representative of biological noise. Gene expression noise is thought to arise in part from small numbers of molecules, such as mRNAs in yeast cells, half of which are present at a copy number of 10 per cell or less<sup>9</sup>. Additionally, theoretical modeling of gene expression in nondividing cells suggests that both the number of mRNAs and protein molecules, as well as the kinetics of the individual steps in gene expression (Fig. 2), contribute to variability in protein output<sup>10</sup>.

Variability in gene expression, which is quantitatively captured by the coefficient of variation (defined as the standard deviation of the protein abundance distribution divided by its mean), is predicted to depend on promoter dynamics and the rates of transcription and translation, as well as the half-lives of the mRNA and proteins<sup>1,10</sup>. Simple models indicate that increasing the transcription or translation rates or stabilizing the proteins and mRNA increases the average protein level while simultaneously decreasing the coefficient of variation<sup>10</sup> (Fig. 2). The intuitive interpretation is that removal or addition of a single molecule has a substantial effect in small systems and less of an effect in larger systems. However, the numerous regulation points in gene expression allow this variability to be tuned independently of the average expression level—for example by simultaneously manipulating mRNA turnover and transcription rate (Fig. 2). Measurements of gene expression noise for large numbers of genes in yeast showed that, in general, the most abundant proteins have the least variable expression<sup>11</sup>. However, the exceptions to this relationship point toward regulation of noise that is independent of expression level. These exceptions, notably stress responses, should be valuable in evaluating the functional requirements imposed on these noisy genes and the mechanistic details involved in modulating their variability.

### **Local noise, global noise and noise propagation**

Biochemical reactions generate their own local variability, but they are also subjected to variability from reactions that share substrates, enzymes or

molecular machinery. This subjugation can be nested and scaled, propagating molecular variability through the cell. The susceptibility of reactions to this local or global noise depends on genetic logic, reaction dynamics and feedback.

A key breakthrough in decomposing variability into local and global components came from studies by Elowitz *et al.*<sup>7</sup>, who devised a two-color reporter gene assay for distinguishing different origins of noise. The two different green fluorescent protein color variants were co-expressed in cells with identical promoters. Uncorrelated variation between intensities of the two reporter genes in the same cell, termed 'intrinsic noise', reports differences in the output due to stochastic events particular to the gene's expression. The variation between different cells, termed 'extrinsic noise', reflects differences in cellular state<sup>7</sup>. A study in budding yeast that used this experimental technique in conjunction with mathematical models found that the presence of an extrinsic noise floor in exponentially growing yeast cells resulted from the steady state structure (for example, cell size, shape, age, metabolic state) of the population<sup>12</sup>. However, differences in population structure could not completely account for extrinsic variability, and it was speculated that the additional variability resulted from fluctuations in an upstream regulator<sup>12</sup>. This further highlighted the fact that, in addition to variability stemming from global differences in cellular states, fluctuations propagated from circuit components or crosstalk with other circuits can be a major force in shaping noise in important pathway outputs.

### **Biological consequences of nongenetic variability**

Nongenetic variation can cause different cells in a population to exhibit all-or-none expression of certain genes and to exist in different defined states, such as persistence or competence<sup>13-15</sup>. Nongenetic variability can also generate a continuum of phenotypes, such as in the chemotactic behavior of *E. coli*<sup>6</sup>. In all cases, such heterogeneous phenotypes in a population have biological consequences. In unicellular organisms, special attention has been devoted to cell-to-cell variability generated by gene expression noise in stress response-related genes<sup>11</sup>. Stress genes were shown to be 'noisy' compared with the rest of the yeast genome. These data have been used to lend support to the hypothesis that variability in protein content among cells might confer a selective advantage to the population. Gene expression noise could broaden the range of stress resistance across the population and hence the likelihood that some cells within the population are better able to endure environmental assaults<sup>16</sup>. Many of these scenarios have been invoked to suggest bet-hedging strategies where a fraction of the cells in a population enters into a phenotypic state of reduced fitness in anticipation of future environmental stresses, therefore forfeiting the immediate fitness of the population on average in favor of spreading risk.

In contrast, many cellular functions require that cells transform information about their external environment into regulation of internal states to develop and maintain cellular homeostasis. This often demands accurate environmental sensing and faithful transduction and propagation of signals to make appropriate regulatory decisions. Thus, mechanisms to reduce variability in these signaling components may be necessary. A particularly compelling example is light-

dependent cell hyperpolarization in the retina. Here, the basis for reproducible responses to single photons<sup>17</sup> through signal-dependent multisite phosphorylation of rhodopsin and phosphodependent binding of the inhibitor arrestin plays a central role in reducing variability by inhibiting longer durations of rhodopsin activity characteristic of an exponential distribution. The multisite nature of the inhibition is key, because it averages stochastic variations in the shut-off process. Therefore, buffering mechanisms that reduce either the magnitude of noise in cellular networks or the phenotypic impact of such noise may exist. The existence of regulatory mechanisms that switch these buffering mechanisms 'on' when they are needed (for example, when a population is well adapted to its environment) or 'off' when they are less useful (for example, when environmental shifts occur) is an exciting prospect to consider.

### **Biological noise at UCSF**

The issues of nongenetic individuality were recently the subject of a minicourse offered through the Integrative Program in Quantitative Biology (iPQB) at the University of California, San Francisco. In this minicourse, a group of students with diverse scientific backgrounds surveyed and debated topics in the field of noise biology. In the final days of the class, we paused to contemplate what understanding was palpably missing from the field and to reflect on the road ahead. Our discussions resulted in three selforganized categories: basic science questions, the role of noise in the study of disease and drug discovery, and technology development. These are not exhaustive of the

opportunities within the field. Instead, they reflect our biases and preferences and should be further tested for statistical significance—the discussion involved 11 people and is therefore in the noisy small numbers regime.

### **Understanding nongenetic individuality: questions for the basic scientist**

**Is it noise, or an artifact of complexity?** Aside from simple examples, our understanding of how variability is modulated by topology and biochemical parameters of cellular networks remains incomplete. Such an understanding is essential for our ability to distinguish between phenotypic variations that result from noise and those that are due to other uncharacterized portions of complex processes. Deterministic and stochastic dynamics have intricate and interlocking roles in shaping phenotype. Unraveling these roles will require the combination of high-resolution measurements in a controlled cellular environment with techniques for modulating the input of a biological system in subtle and precise ways.

Overall, to determine the accurate manifestations of nongenetic individuality, many challenges remain. Can we use technologies such as microfluidic devices to adjust the local cellular environment and abolish potential effects of local cellular microenvironments? Can we eliminate confounding effects by establishing assays that control for cell size and age? Can we measure multiple network nodes simultaneously and dynamically in single cells? Can we organize this high-dimensional information into predictive computational frameworks that extract salient principles and generalizable rules about how a



cell modulates its internal fluctuations and responds to its environment?

**Are there common themes for nongenetic individuality in unicellular organisms and multicellular structures?** Researchers of ecology have described bet-hedging within a population as a method of survival through phenotypic variation<sup>18</sup>. A classic example can be found in the larval hatching behavior of the desert bee *Perdita portalis*. As part of its life cycle, *P. portalis* enters a hibernationlike diapause state in order to survive the arid conditions. Emergence from diapause is triggered by rainfall, but not all larvae emerge during a single rainy season. Instead, *P. portalis* hedges its bets by staggering larval emergence over several rainy seasons, allowing a fraction of the population to survive should disaster strike in any given year<sup>19</sup>.

Altruistic bet-hedging is perceived as a strategy in which individuals act in a manner that may not benefit themselves but profits the greater population<sup>20</sup>. Nongenetic variability can be used to signal genetically identical cells to engage in bet-hedging behavior. In *Bacillus subtilis*, this mechanism is used in biofilm formation. A small number of cells are stochastically designated as biofilm producers due to a bimodal distribution of SinI expression in the population. These cells take a substantial reduction in their own individual survival potential but increase the safety of the entire population in the event of a significant stress<sup>20</sup>. While it is understood that the bimodal distribution of SinI expression designates biofilm producers, it is unclear how the weight of this distribution (what percentage of cells are in one population or the other) is determined. The

ability to tune the weight of the distribution during various levels of stress is an appealing idea and could provide broad insights ranging from fractional killing of 'persister' cells during antibiotic treatment to the evolution of stress responses.

Given that bet-hedging strategies have been described in populations of unicellular organisms and in the communal behavior of multicellular organisms, it is intriguing to consider whether these strategies are also at play on the scale of tissue and organ development and maintenance. If this is the case, these bet-hedging tactics may have implications for differential drug and disease susceptibility in mammalian tissues.

In understanding the molecular mechanisms driving collective community behaviors of unicellular and multicellular individuals, several key questions remain unanswered. What is the exact quantitative relationship between bet-hedging and biochemical noise? What are the timescales for switching between phenotypic states? Are the molecular bases of bet-hedging in unicellular organisms applicable to multicellular organisms? Does bet-hedging drive evolution or vice versa? Do identical cells within tissues hedge their bets in development and disease? Is there any synergy between bet-hedging strategies and those that involve stochastic rearrangement of genetic material?

**How about 'extremes'?** Noise in cellular processes reflects the effects of random thermal fluctuations on molecular events such as diffusion, catalysis and binding. Thus, variability in 'extreme' organisms could provide a tool to measure the role of thermal fluctuations in biological noise. Investigations of cell-to-cell

variability have focused on mesophilic organisms that have adapted to life at moderate temperatures (20–42 °C); there are no biological noise studies of psychrophiles or thermophiles—organisms that live under extreme temperature conditions (<15 °C and >45 °C, respectively). Studies in such organisms have yielded insights into protein folding and enzymology, and have enabled development and optimization of technologies such as PCR. Analyzing variability in gene expression in thermophiles and psychrophiles could therefore reveal new mechanisms of noise regulation and/ or tolerance, and may pinpoint which steps in the process (transcription, mRNA processing, translation) are most susceptible to the effects of noise as temperature changes. Studies and comparisons of regulatory networks in these extremophiles could indicate whether different patterns of thermal fluctuations lead to the evolution of new architectures to dampen or exploit noise and could also reveal new methods of noise regulation in cellular processes. For example, biofilm formation and sporulation processes in which cell-to-cell variability plays a role have been observed in thermophiles found in industrial dairy and paper production<sup>21</sup>. Do thermophiles exploit noise levels differently than mesophiles during these processes? If noise levels differ in these processes in thermophiles and mesophiles, are these levels tuned particularly for survival in the two ranges of temperature?

## **Diseases, drugs and health**

### **How do cells, tissues and organs shape the variability in their**

**environment, and how are they shaped by it?** Understanding how variability affects cells within tissues in multicellular organisms and vice versa could be vital to decoding mechanisms that regulate cell fate. Environmental signals influence cellular processes in profound ways. In multicellular organisms, cell-to-cell signaling, architecture and topology influence stem cell maintenance and differentiation<sup>22</sup> and the overall tissue architecture. Moreover, the cellular environment has been shown to affect the development of certain cancers<sup>23</sup>. To understand the complex interactions between a cell and its environment, it is necessary to understand how cells respond to and create environmental variability and how stochastic fluctuations within a cell propagate to its neighbors (Fig. 3). This becomes especially important in contexts where chemical gradients set by collections of cells hold crucial, but noisy, positional information. For example, in *Drosophila melanogaster* wing disk development, the morphogen Dpp is secreted into the cellular microenvironment to establish a precise gradient that determines the architectural features and boundaries of the tissue<sup>24</sup>. A cell needs to decipher and filter this noisy signal in order to precisely orient itself. Understanding how much and what frequencies of noise cellular processes can afford should unravel key regulation mechanisms controlling cell fate. It should also illuminate mechanisms by which cells achieve exquisite signal processing and discrimination capabilities that enable tissue and organ homeostasis. How does intercellular signaling discern between environmental noise and relevant stimuli from other cells? In what circumstances and how do cells actively regulate their environment's chemical and electrical variability? Can we explore

how cells adapt to and exploit environmental noise using artificial tissue engineering?

**Do we need to personalize medicine to individual noise levels?** The completion of the Human Genome Project, along with everincreasing knowledge of genes responsible for complex human diseases, has prompted the advent of pharmacogenomics—a shift away from generalized health toward individualized medicine. Such a paradigm shift was propelled by the discovery that genetic differences strongly influence disease susceptibility and response to drugs. Recent studies have revealed yet another layer of complexity: nongenetic cell-to-cell variability also affects drug efficacy<sup>25,26</sup>. For example, the pro-apoptotic drug TRAIL kills only 22% to 78% of clonal cells depending on their cell type due to cell-to-cell variability in levels of regulatory proteins involved in receptor-mediated apoptosis<sup>25</sup>. These observations underscore the need for rigorous single-cell studies that increase our understanding of how nongenetic variability influences drug efficacy.

Specifically, a system-wide approach to understanding variability in cellular processes might be vital for improving individualized healthcare and facilitating the development of more efficient drugs. How can we extrapolate this understanding to improve drug efficacies? Are there ‘quiet’ signaling steps or pathways that could be more effective drug targets than ‘noisier’ steps and pathways? Can we increase drug efficacy by combining drugs whose target pathways have complementary dynamics or noise? These approaches would

require the development of tools to efficiently measure noise *in vivo*.

**Is aging a noise-susceptible process?** Recent studies show that aging is accompanied by an increase in cell-to-cell variability in gene expression across a population<sup>27-29</sup>. However, it is unclear whether aging results in increased variability or whether variability causes aging through the asynchrony of vital pathways. Several theories have been proposed to explain the relationship between increased variability and aging. The ‘disposable soma’ theory predicts that aging in metazoans results from accumulation of unrepaired somatic DNA damage, the random nature of which may infuse the aging process with the observed stochasticity<sup>30</sup>. Another theory postulates that genes that act in the postreproductive life stage experience less natural selection and therefore may be less tightly regulated than genes whose activity is required in the developmental and reproductive phases of life<sup>29</sup>. Modeling efforts also suggest that aging might preferentially attack regulatory genes that are important for network stability<sup>31</sup>. One or more of these theories could account for increased variability in aging. However, solid evidence for a causal relationship is absent: is the change in variability a product of aging or is the change in variability driving the aging process? It is reasonable to speculate that increased variability could promote aging. For example, an increase in gene expression noise could cause a cell to digress from its normal functional state, fail to respond to external cues correctly or fail to coordinate with its neighboring cells in the context of a tissue.

The involvement of noise and nongenetic variability adds a new dimension

and new questions to aging research. What is the contribution of nongenetic variability to aging in unicellular and multicellular organisms? Are there specific genes that control aging by influencing noise? Are aging rates or lifespans dependent on patterns of variability? Can the rate of aging be manipulated by modulating noise?

### **The road ahead**

Above, we have proposed an incomplete but still daunting list of questions. Answering these questions will require the development and maturation of many technologies. We believe that two areas are crucially important for furthering our understanding of noise in biological systems: the ability to quantitatively tune nongenetic individuality and the ability to measure its manifestations in currently 'hidden' variables.

The ability to manipulate variability—to be able to tune noise—will create new avenues for noise research. Three applications would benefit from such an effort. First, a toolkit of 'noise modulators' would allow us to (i) investigate the robustness of biological networks with respect to fluctuations, (ii) delineate topologies that are most resistant to the effects of noise and (iii) determine the limits of their functionality. Second, noise modulators would enable the use of variability as a tool for network inference. By inserting noise into cellular networks and observing its propagation, we could investigate the topology of these networks in a manner that mirrors system identification in manmade systems. Third, noise tuning might lead to the development of new therapeutics.

For example, it might provide a solution to the antibiotic fractional killing problem<sup>15</sup>. If antibiotic treatment is coupled to a drug that alters the frequency of switching of the bacterium to and from a persistent state, killing the entire bacterial population might be possible.

Several approaches exist for developing the necessary technology to modulate noise by changing the total number of molecules. One scenario relevant to drug action is to control the number of active molecules available for a given reaction. This can be achieved either by regulating the sequestration or the release of proteins in their active forms or by altering the stoichiometry of complex formation. The independence of events in stochastic processes can also be disrupted to affect variability within a system. For example, substituting processive events for independent events should affect noise. The number of noise-generating processes in a system could itself be altered by fusing together otherwise separate proteins or by splitting a protein into two pieces that must come together to be active. Breakthroughs and developments in synthetic biology will certainly empower these efforts.

Because our understanding of the dynamics of complex biological networks is incomplete, it remains difficult to predict how perturbations in the environment or system components will percolate through the network topology on their way to becoming a phenotype. Therefore, it is possible that processes appear to be stochastic when in fact they are determined by pre-existing hidden variables. Currently, most measurements of variability in gene expression focus on quantifying differences in protein levels using fluorescent protein reporters.



Although there has been some effort to directly quantify the number of mRNA molecules present in single cells<sup>8,32</sup>, few studies address how intermediate steps of gene expression (such as DNA states, mRNA processing and export, and protein folding) contribute to gene expression noise. These processes remain 'hidden variables', and quantification of their contribution to variability awaits the development of appropriate technologies.

A good starting point may be to expand current technologies. For example, methods that measure promoter DNA unwinding in real time *in vitro* would quantify noise in DNA transitions during transcription initiation if they could be applied *in vivo*<sup>33</sup>. Similarly, techniques used to visualize single mRNA molecules in fixed cells<sup>32</sup> could be applied to measure noise in mRNA processing pathways such as splicing and polyadenylation by designing several fluorescent *in situ* hybridization (FISH) probes that bind to specific sequences within the mRNA. Moreover, developing a multicolor reporter system with this technology may allow one to tease apart the relative contributions of intrinsic and extrinsic noise to mRNA processing. Although FISH does not allow for tracking mRNA processing in single cells over time, several other real-time mRNA visualization techniques exist<sup>8,34</sup> and could be used to study noise in mRNA export. Perhaps the hardest problem is to quantify intermediate states of protein folding, and radically new techniques might be needed.

Beyond gene expression, protein targeting/localization and post-translational modifications also affect variability. Technologies need to be developed to precisely quantify protein localization and post-translational

modification states in single cells in real time. This will be crucial for moving beyond gene expression to investigate variability and fidelity in complex signaling networks.

### **Final synopsis**

Nongenetic individuality is a quantitative cellular phenotype that is increasingly being implicated in many biological phenomena. In this commentary, we have presented a broad set of concepts and examples arguing that an understanding of nongenetic individuality can significantly influence our understanding of biological processes. While we recognize that we have put forth numerous daunting tasks that may not be fully answerable, we contend that such directions are necessary to push the 'biology of noise' field forward.

### **Acknowledgements**

We thank J. Steward-Ornstein for his comments on this commentary. This work was supported by the University of California, San Francisco Program for Breakthrough Biomedical Research and by a US National Institutes of Health grant (GM086379) to H.E.-S.

### **References**

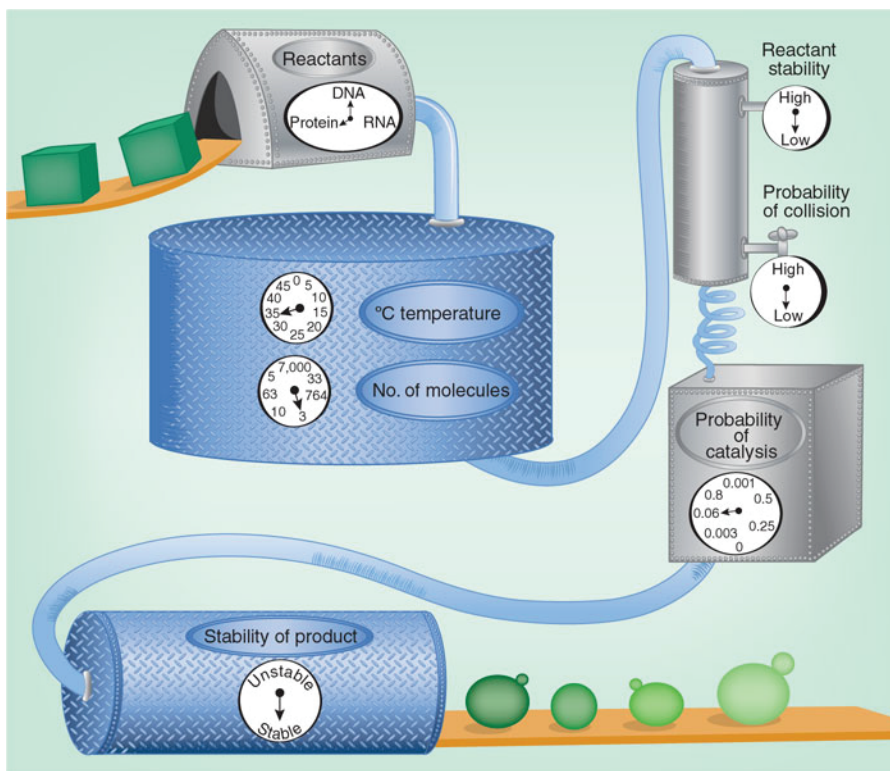
1. Raser, J.M. & O'Shea, E.K. Control of stochasticity in eukaryotic gene expression. *Science* 304, 1811-4 (2004).
2. McAdams, H.H. & Arkin, A. Stochastic mechanisms in gene expression. *Proc Natl Acad Sci U S A* 94, 814-9 (1997).
3. Bigger, J.W. Treatment of staphylococcal infections with penicillin by intermittent sterilization. *Lancet* 1944, 497-500 (1944).

4. Moyed, H.S. & Broderick, S.H. Molecular cloning and expression of hipA, a gene of *Escherichia coli* K-12 that affects frequency of persistence after inhibition of murein synthesis. *J Bacteriol* 166, 399-403 (1986).
5. Spudich, J.L. & Koshland, D.E., Jr. Non-genetic individuality: chance in the single cell. *Nature* 262, 467-71 (1976).
6. Korobkova, E., Emonet, T., Vilar, J.M., Shimizu, T.S. & Cluzel, P. From molecular noise to behavioural variability in a single bacterium. *Nature* 428, 574-8 (2004).
7. Elowitz, M.B., Levine, A.J., Siggia, E.D. & Swain, P.S. Stochastic gene expression in a single cell. *Science* 297, 1183-6 (2002).
8. Golding, I., Paulsson, J., Zawilski, S.M. & Cox, E.C. Real-time kinetics of gene activity in individual bacteria. *Cell* 123, 1025-36 (2005).
9. Velculescu, V.E. et al. Characterization of the yeast transcriptome. *Cell* 88, 243-51 (1997).
10. Thattai, M. & van Oudenaarden, A. Intrinsic noise in gene regulatory networks. *Proc Natl Acad Sci U S A* 98, 8614-9 (2001).
11. Newman, J.R. et al. Single-cell proteomic analysis of *S. cerevisiae* reveals the architecture of biological noise. *Nature* 441, 840-6 (2006).
12. Volfson, D. et al. Origins of extrinsic variability in eukaryotic gene expression. *Nature* 439, 861-4 (2006).
13. Novick, A. & Weiner, M. Enzyme Induction as an All-or-None Phenomenon. *Proc Natl Acad Sci U S A* 43, 553-66 (1957).
14. Suel, G.M., Garcia-Ojalvo, J., Liberman, L.M. & Elowitz, M.B. An excitable gene regulatory circuit induces transient cellular differentiation. *Nature* 440, 545-50 (2006).
15. Balaban, N.Q., Merrin, J., Chait, R., Kowalik, L. & Leibler, S. Bacterial persistence as a phenotypic switch. *Science* 305, 1622-5 (2004).
16. Avery, S.V. Microbial cell individuality and the underlying sources of heterogeneity. *Nat Rev Microbiol* 4, 577-87 (2006).
17. Hamer, R.D., Nicholas, S.C., Tranchina, D., Lamb, T.D. & Jarvinen, J.L. Toward a unified model of vertebrate rod phototransduction. *Vis Neurosci* 22, 417-36 (2005).
18. Cohen, D. Optimizing reproduction in a randomly varying environment when a correlation may exist between the conditions at the time a choice has to be made and the subsequent outcome. *J Theor Biol* 16, 1-14 (1967).
19. Danforth, B.N. Emergence dynamics and bet hedging in a desert bee, *Perdita portalis*. *Proc. R. Soc. Lond.* 266, 1985-1994 (1999).
20. Chai, Y., Chu, F., Kolter, R. & Losick, R. Bistability and biofilm formation in *Bacillus subtilis*. *Mol Microbiol* 67, 254-63 (2008).
21. Scott, S.A., Brooks, J.D., Rakonjac, J., Walker, K.M.R., Flint, S.H. The formation of thermophilic spores during the manufacture of whole milk powder. *International Journal of Dairy Technology* 60, 109-117 (2007).
22. Li, L. & Xie, T. Stem cell niche: structure and function. *Annu Rev Cell Dev Biol* 21, 605-31 (2005).

23. Iwasaki, H. & Suda, T. Cancer stem cells and their niche. *Cancer Sci* 100, 1166-72 (2009).
24. Bollenbach, T. et al. Precision of the Dpp gradient. *Development* 135, 1137-46 (2008).
25. Spencer, S.L., Gaudet, S., Albeck, J.G., Burke, J.M. & Sorger, P.K. Non-genetic origins of cell-to-cell variability in TRAIL-induced apoptosis. *Nature* 459, 428-32 (2009).
26. Cohen, A.A. et al. Dynamic proteomics of individual cancer cells in response to a drug. *Science* 322, 1511-6 (2008).
27. Bahar, R. et al. Increased cell-to-cell variation in gene expression in ageing mouse heart. *Nature* 441, 1011-4 (2006).
28. Somel, M., Khaitovich, P., Bahn, S., Paabo, S. & Lachmann, M. Gene expression becomes heterogeneous with age. *Curr Biol* 16, R359-60 (2006).
29. Herndon, L.A. et al. Stochastic and genetic factors influence tissue-specific decline in ageing *C. elegans*. *Nature* 419, 808-14 (2002).
30. Kirkwood, T.B. Understanding the odd science of aging. *Cell* 120, 437-47 (2005).
31. Xue, H. et al. A modular network model of aging. *Mol Syst Biol* 3, 147 (2007).
32. Raj, A., van den Bogaard, P., Rifkin, S.A., van Oudenaarden, A. & Tyagi, S. Imaging individual mRNA molecules using multiple singly labeled probes. *Nat Methods* 5, 877-9 (2008).
33. Roy, S., Lim, H.M., Liu, M. & Adhya, S. Asynchronous basepair openings in transcription initiation: CRP enhances the rate-limiting step. *EMBO J* 23, 869-75 (2004).
34. Grunwald, D., Singer, R.H. & Czaplinski, K. Cell biology of mRNA decay. *Methods Enzymol* 448, 553-77 (2008).

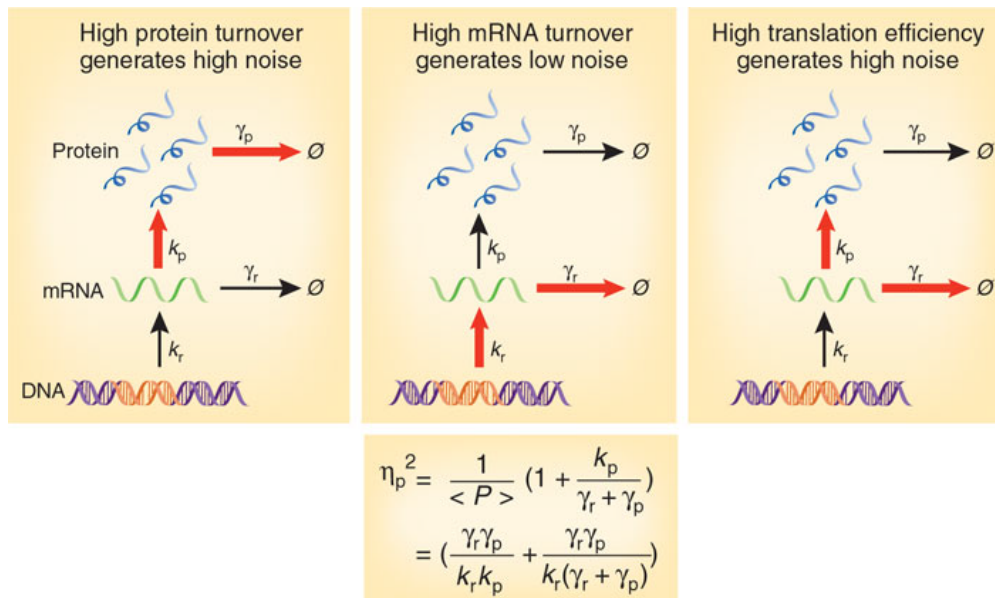
# Figures and Tables

Figure 1



**Figure 1:** Biochemical noise percolates to cellular phenotypes through complex networks, generating nongenetic individuality. As a result, individual genetically identical cells may have different sizes, shapes, states of their molecular constituents and responses to intracellular and extracellular cues.

Figure 2



$$\eta_p^2 = \frac{1}{\langle P \rangle} \left( 1 + \frac{k_p}{\gamma_r + \gamma_p} \right)$$

$$= \left( \frac{\gamma_r \gamma_p}{k_r k_p} + \frac{\gamma_r \gamma_p}{k_r (\gamma_r + \gamma_p)} \right)$$

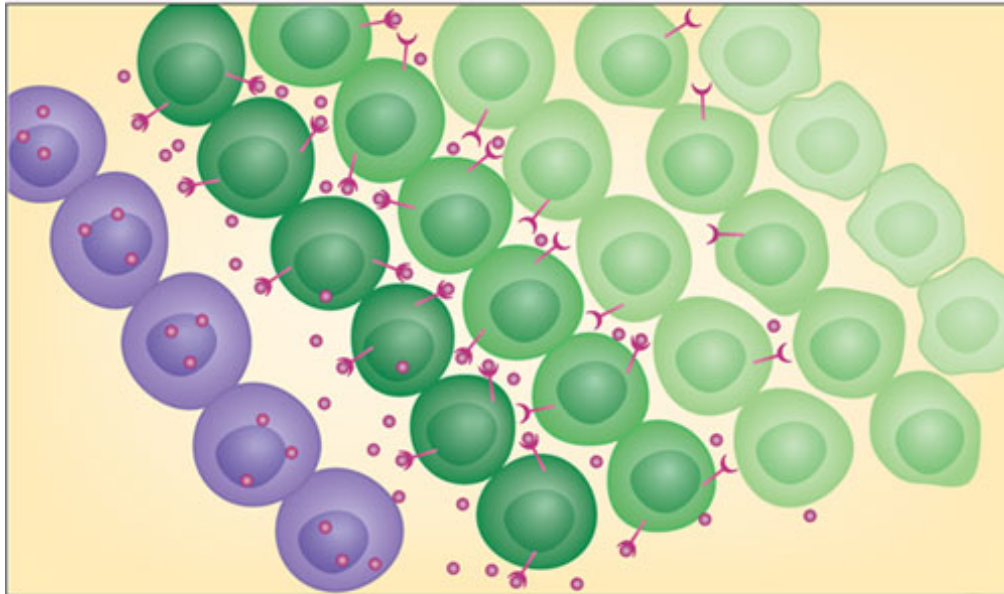
$\eta_p$ : Coefficient of variation of protein

**Figure 2:** Different steps in gene expression modulate protein variability.  $\langle P \rangle$ , mean number of protein molecules.

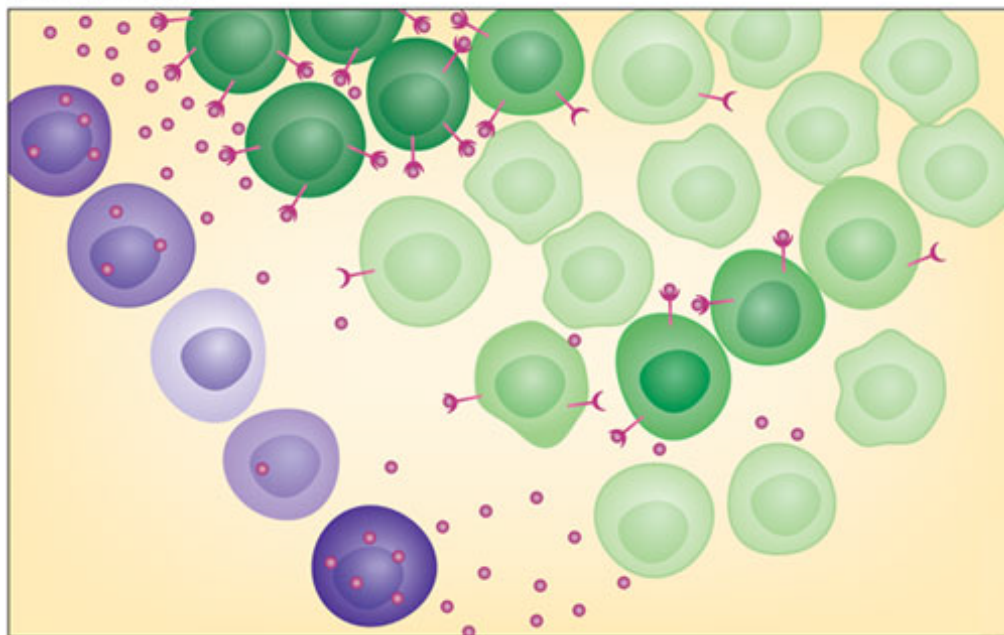


Figure 3

Quiet neighbors



Noisy neighbors



**Figure 3:** Nongenetic individuality can have important consequences for cell-cell communication and cellular fates in multicellular structures. Because decisions made by a cell are influenced by extracellular cues, propagation of noise from neighboring cells (when coupled to intrinsic cellular variability) can lead to widely heterogeneous responses across a tissue. Purple, signal-emitting cells; green, responding cells.

## **Appendix A: A genetic approach to understanding the mechanism of Ste12-focus formation in *dig1* $\Delta$ cells**

As discussed in Chapter 2, we found that Ste12 forms nuclear foci in *dig1* $\Delta$  cells. This is in contrast to the diffuse nucleoplasmic staining seen in wild type and *dig2* $\Delta$  cells. Both Dig1 and Dig2 are known to bind to Ste12. However, they bind to different regions; Dig1 to the activation domain and Dig2 to the DNA-binding domain. Given that Ste12 is known to bind to itself (1) as well as several to other proteins, we hypothesized that the removal of Dig1 from cells could expose a protein-protein interaction surface on Ste12. In the absence of Dig1, this surface could participate in long-range protein-protein interactions, thereby resulting in Ste12 focus formation.

To test this model genetically, we conducted a small-scale random mutagenesis screen to identify alleles of *STE12* that phenocopy the noise phenotype of *dig1* $\Delta$  cells (as discussed in Chapter 2) and form foci in *DIG1*<sup>+</sup> cells. *STE12* alleles were created using PCR mutagenesis with taq polymerase, which is estimated to create a mismatch every 10,000 bp (2). Using *in vivo* recombination, we generated a library of these *STE12* alleles (*STE12*<sup>\*</sup>) tagged with GFP and a selectable marker and flanked by homology to the *STE12* promoter and 3'UTR (Figure 1). This entire construct (*pSTE12-STE12*<sup>\*</sup>-*GFP-HIS3MX-3'STE12*) was excised from the plasmid and transformed into yeast containing *pAGA1-mCherry ste12::GSHU* (3). Single colonies were picked and arrayed into 11 96-well plates. In total, 907 mutants were isolated.

Single-cell measurements of *pAGA1-mCherry* fluorescence were conducted for each mutant as described in Chapter 2. The mean and coefficient of variation (CV) of the output distributions were calculated (Figure 2A). Most of the *STE12\** strains have output distributions whose mean and CV follow a similar relationship to that of wild-type. Approximately 12% of the mutants have output distributions that overlap with yeast autofluorescence, suggesting that the mutation in *STE12* created an early transcription termination signal. Inspection of the probability density functions (PDFs) of the *STE12\** mutant strains revealed 13 mutants that displayed either a bimodal distribution (indicative of a mixed population) or a distribution similar to that of the *dig1Δ* strain (Figure 2B). Six individual colonies were obtained from each of the 13 candidates and the output distributions were re-measured (Figure 3A,B). Ten mutants recapitulated the distributions from the original screen. The other three *STE12\** mutants (Plate 4 F9, Plate 4 H6 and Plate 5 B9) displayed more than one output distribution among the six isolates, indicating that those particular wells contain a mixed population of *STE12\** mutants. Isolate 1 for each mutant (see Figure 3) was sequenced. The resulting mutations are listed in Table 1.

Despite the increased noise in *pAGA1-mCherry* expression in our novel *STE12* mutants, none displayed Ste12-GFP nuclear foci. This small-scale mutagenesis screen was not saturating. Only 907 *STE12* mutants were analyzed and *STE12* is 2066 bp (688 amino acids) long. Additionally, in order to fully disrupt the Dig1-Ste12 interaction and form Ste12 foci, it may be necessary to mutate several residues simultaneously. Further mutagenesis and analysis

would need to be performed to identify additional mutants. Finally, it could be informative to combine the mutations from these *STE12* alleles into a single allele to see if Ste12 now forms nuclear foci.

## References

1. Y. L. Yuan, S. Fields, *Mol Cell Biol* **11**, 5910 (Dec, 1991).
2. K. A. Eckert, T. A. Kunkel, *PCR Methods Appl* **1**, 17 (Aug, 1991).
3. F. Storici, C. L. Durham, D. A. Gordenin, M. A. Resnick, *Proc Natl Acad Sci U S A* **100**, 14994 (Dec 9, 2003).

Figure 1

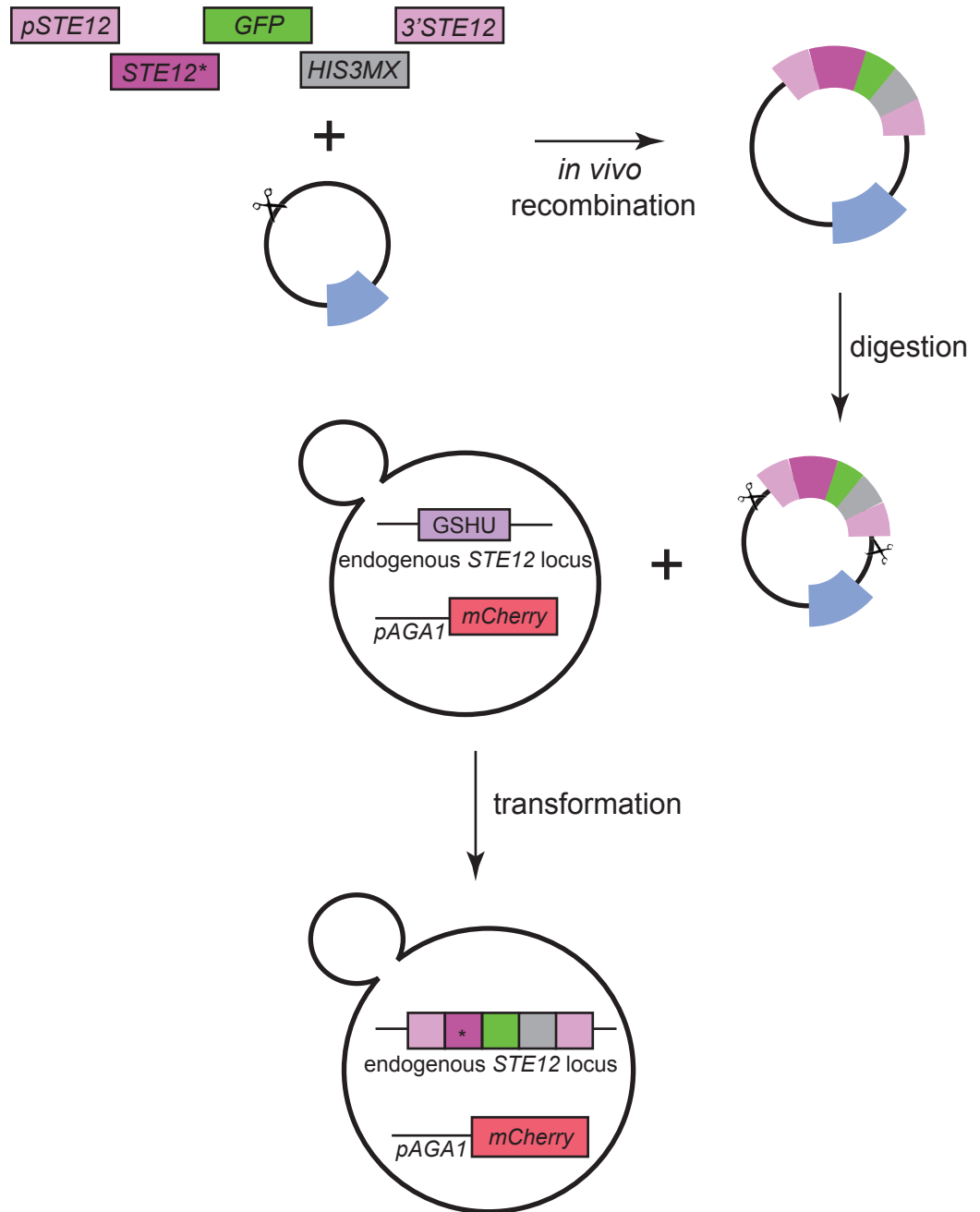


**Figure 1:** Outline of creation of *ste12* mutant alleles. 500 bp of *STE12* promoter, GFP, *HIS3MX* and 500 bp of *STE12* 3'UTR were amplified with the high fidelity polymerase Phu while *STE12* was amplified using taq polymerase. The individual pieces of DNA were transformed together with linearized pRS314 to create plasmids with mutant alleles of *ste12*. The entire construct was cut out of the plasmid and transformed into yeast.



Figure 2

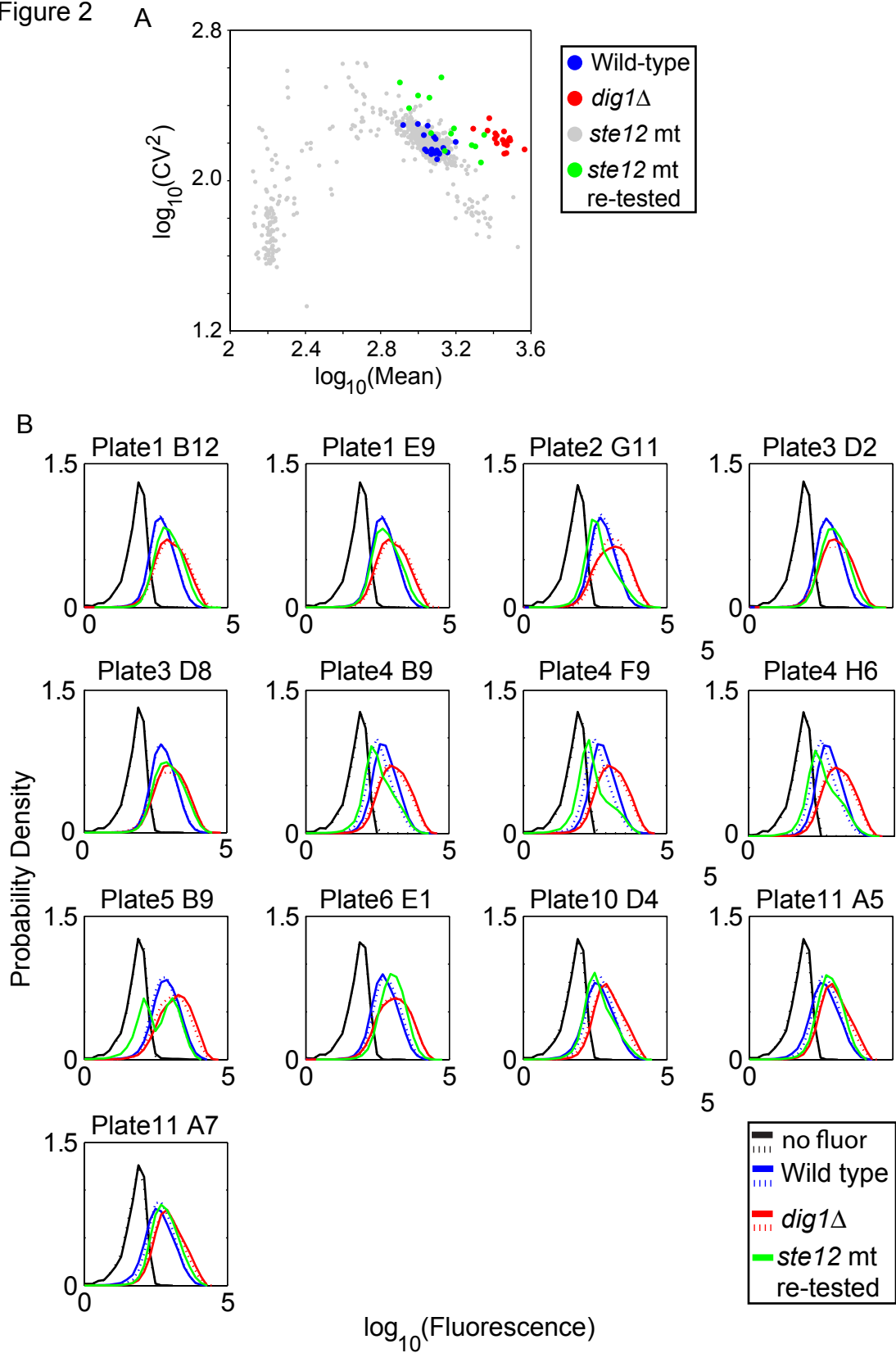


**Figure 2:** Results of the FACS-based screen. **A.** Plot of mean *pAGA1-mCherry* fluorescence vs  $CV^2$ . Replicates of wild type are in blue, *dig1* $\Delta$  is in red, *ste12* mutants are in gray and potentially interesting *ste12* mutants are in green. **B.** PDFs of *ste12* mutants in green from part **A.** No-fluor control is in black, wild type is in blue, *dig1* $\Delta$  is in red and the *ste12* mutant is in green. The dotted and solid lines represent independent replicates measured on the same day.

Figure 3 A

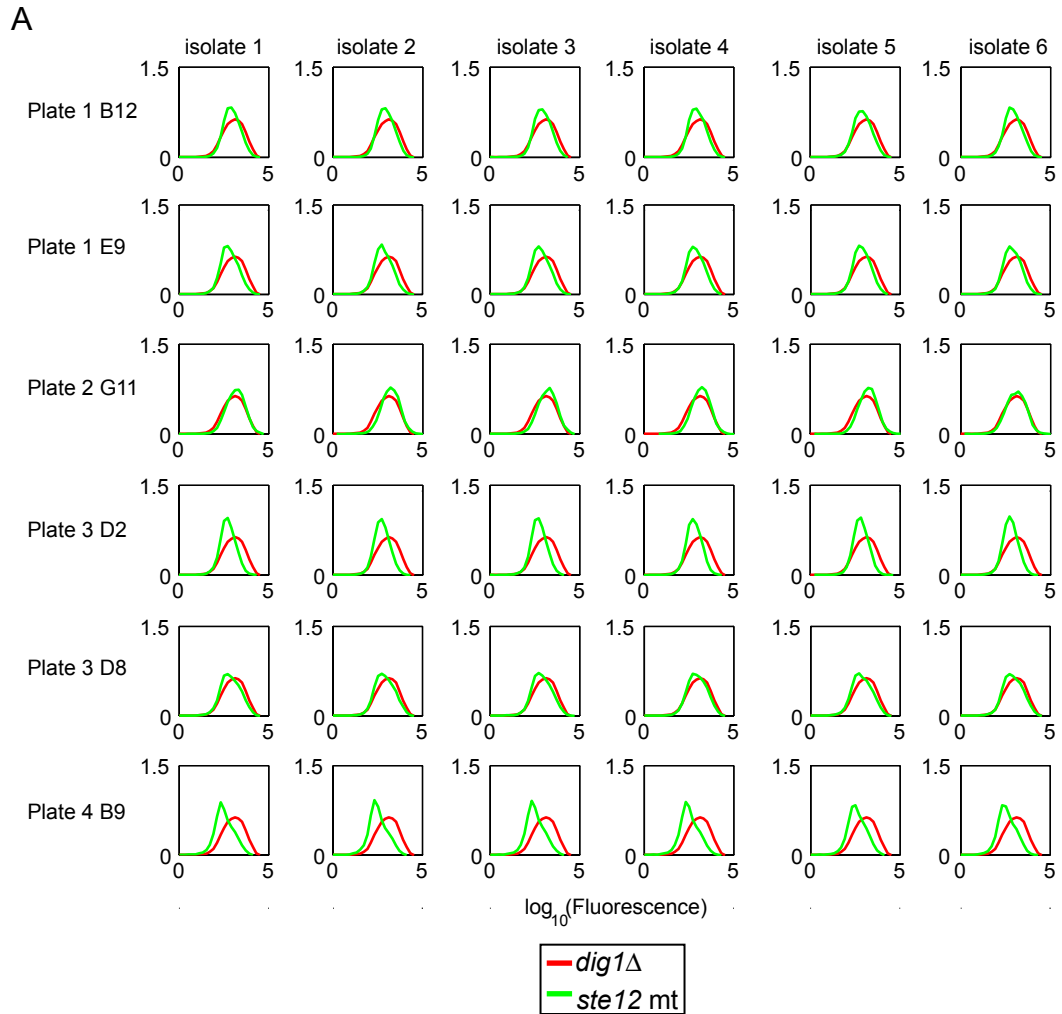
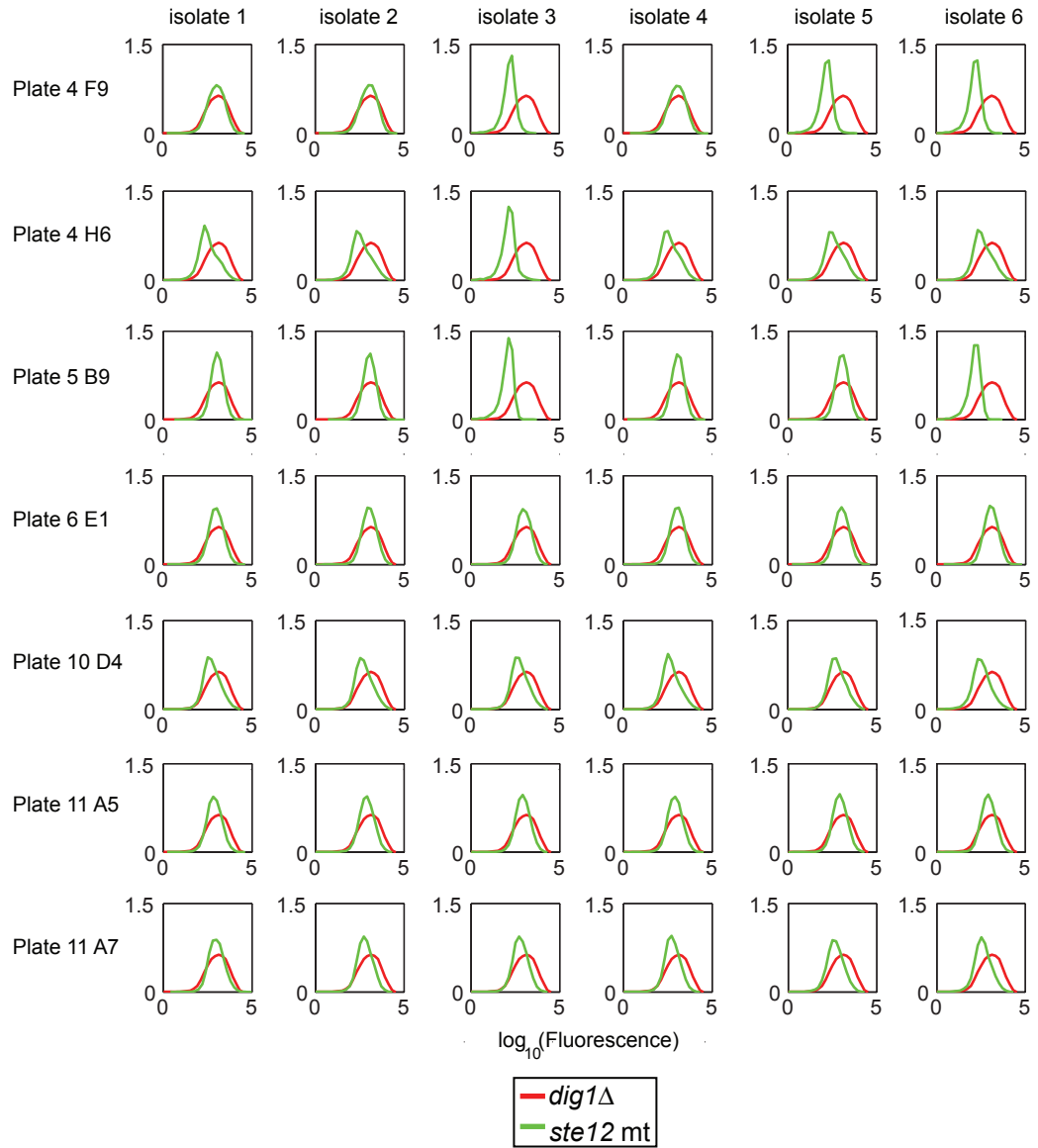


Figure 3 B

B



**Figure 3:** Re-tested *ste12* mutants were struck out to select for single colonies.

Six colonies were picked and *pAGA1-mCherry* fluorescence was measured.

**A,B.** PDFs for six isolates of the re-tested *ste12* mutants in Figure 2. *dig1Δ*

mutant is in red and the *ste12* mutant is in green.

Table 1

| Mutant      | <i>STE12</i> Alleles                   | A.A. Changes                     |
|-------------|--|----------------------------------|
| Plate 1 B12 | <i>A332G, A665G, A1045G</i>            | E11G, K222R, R349G               |
| Plate 1 E9  | <i>A356G</i>                           | N119S                            |
| Plate 2 G11 | <i>T993C</i>                           |                                  |
| Plate 3 D2  | <i>A170G, A1571G</i>                   | N57S, Y523C                      |
| Plate 3 D8  | <i>T98C, A914G</i>                     | D305G                            |
| Plate 4 B9  | <i>A690G, A1379G, C1742T, 1407G(?)</i> | Y460C, truncation at a.a.493 (?) |
| Plate 4 F9  | <i>A1798G</i>                          | K600E                            |
| Plate 4 H6  | <i>C497T, C1788T</i>                   | A166V, P596L                     |
| Plate 5 B9  | <i>A1320G, A1593G, A1659G, A1864G</i>  | K622E                            |
| Plate 6 E1  |  |                                  |
| Plate 10 D4 | <i>A180G</i>                           | I60M                             |
| Plate 11 A5 | <i>G1811A</i>                          | G604D                            |
| Plate 11 A7 | <i>2054ΔC</i>                          | P685Q, D686M, A687Q, T688P       |

**Table 1:** Mutations found in the *ste12* gene from re-tested mutant strains in Figure 2B.

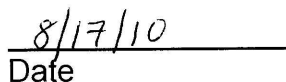
**Publishing Agreement**

*It is the policy of the University to encourage the distribution of all theses, dissertations, and manuscripts. Copies of all UCSF theses, dissertations and manuscripts will be routed to the library via the Graduate Division. The library will make all theses, dissertations and manuscripts accessible to the public and will preserve these to the best of their abilities, in perpetuity.*

**Please sign the following statement:**

*I hereby grant permission to the Graduate Division of the University of California, San Francisco to release copies of my thesis, in whole or in part, in perpetuity.*

  
Author Signature

  
Date